

**UNIVERSITY OF ALBERTA**

**Experimental Observations and Numerical Modeling of Gas Lifting in  
Small Diameter Pipes in View of Unloading Liquids from Wells with  
Low Reservoir Pressure**

By

**Javier Alfonso Becaria Valero**



A thesis  
submitted to the Faculty of Graduate Studies and Research  
in partial fulfillment of the requirements for the degree  
of Master of Science in

Petroleum Engineering

Department of Civil and Environmental Engineering

Edmonton, Alberta  
Fall, 2004



Library and  
Archives Canada

Bibliothèque et  
Archives Canada

Published Heritage  
Branch

Direction du  
Patrimoine de l'édition

395 Wellington Street  
Ottawa ON K1A 0N4  
Canada

395, rue Wellington  
Ottawa ON K1A 0N4  
Canada

*Your file* *Votre référence*  
*ISBN: 0-612-95706-3*  
*Our file* *Notre référence*  
*ISBN: 0-612-95706-3*

The author has granted a non-exclusive license allowing the Library and Archives Canada to reproduce, loan, distribute or sell copies of this thesis in microform, paper or electronic formats.

L'auteur a accordé une licence non exclusive permettant à la Bibliothèque et Archives Canada de reproduire, prêter, distribuer ou vendre des copies de cette thèse sous la forme de microfiche/film, de reproduction sur papier ou sur format électronique.

The author retains ownership of the copyright in this thesis. Neither the thesis nor substantial extracts from it may be printed or otherwise reproduced without the author's permission.

L'auteur conserve la propriété du droit d'auteur qui protège cette thèse. Ni la thèse ni des extraits substantiels de celle-ci ne doivent être imprimés ou autrement reproduits sans son autorisation.

---

In compliance with the Canadian Privacy Act some supporting forms may have been removed from this thesis.

Conformément à la loi canadienne sur la protection de la vie privée, quelques formulaires secondaires ont été enlevés de cette thèse.

While these forms may be included in the document page count, their removal does not represent any loss of content from the thesis.

Bien que ces formulaires aient inclus dans la pagination, il n'y aura aucun contenu manquant.

# Canada

## AKNOWLEDGEMENTS

I would like to express my sincere gratitude and appreciation to Dr. Peter Toma and Dr. Ergun Kuru for their unconditional support, advice, encouragement and guidance throughout the course of this study.

Thanks are also sincerely expressed to Mr. Sean Watt for his invaluable technical advice in the design and construction of the experimental set up.

I am also grateful to Dr. Tayfun Babadagli and Dr. Brian A. Fleck, members of the thesis committee, for the pertinent technical input and corrections.

I thank to IRAP – NRC-CNRC program and P R Toma Consulting Ltd. for the financial support received during the Summer 2003.

Finally, I would like to extend my deepest thank to my loving wife, mother and brothers for their patience and unconditional support during my studies.

## **DEDICATORY**

To my wife Teresa and unborn child  
Thomas who encouraged me to keep going  
during difficult times and have been my  
motivation and strong pillar to reach my  
goals.

## TABLE OF CONTENTS

### ABSTRACT

<b>1. CHAPTER 1: INTRODUCTION</b>	<b>1</b>
1.1 Overview	1
1.2 Statement of the problem	2
1.3 Objective and scope of the research	4
1.4 Structure of the thesis	6
<b>2. CHAPTER 2: LITERATURE REVIEW</b>	<b>7</b>
2.1 Unloading gas wells	7
2.1.1 Methods of sustaining natural flow	9
2.1.1.1 Alternate flow/shut in periods	9
2.1.1.2 Plunger lift	10
2.1.1.3 Swabbing	10
2.1.1.4 Small diameter production tubing	11
2.1.1.4 Foaming agents	11
2.1.2 Artificial lift	12
2.1.2.1 Sucker rod pumping	12
2.1.2.2 Gas lift	12
2.1.3 Combined methods	13
2.1.3.1 Gas lifting and small diameter pipes	13
2.1.3.2 Injection system used for gas lifting	14
2.2 Gas lift	15
2.2.1 Continuous and intermittent gas lift	16
2.2.2 Two-phase flow patterns in vertical pipes	17
2.2.2.1 Pipe size classification	19
2.2.2.2 Flow pattern transition maps for conventional vertical pipes	21
2.2.3 Two-phase flow patterns in vertical small diameter pipes	26
2.2.3.1 Flow pattern transition maps in small diameter pipes	27
2.2.4 Flow patterns in capillaries	29
2.2.4.1 Flow pattern transition maps for capillaries	30
2.3 Slug Flow and elongated bubble flow pattern	31
2.3.1 Slug flow pattern in vertical pipes	31
2.3.2 Elongated bubble pattern in vertical pipes	34
2.4 Previous experiments in small and conventional diameter pipes	37
2.4.1 Experiments with small diameter pipes	37
2.4.1.1 Experimental data (Kouremenos and Staïcos)	38
2.4.1.2 Experimental data (Reinemann et al.)	40
2.4.1.3 experimental data (Cachard and Delhaye)	41

2.4.2 Experiments with conventional diameter pipes	42
2.5 Modeling slug flow in conventional and small diameter pipes	43
2.5.1. Slug flow models in conventional and big diameter pipes	43
2.5.1.1 Hasan's model	44
2.5.1.2 Ansari's model	46
2.5.2 Slug flow model in small diameter pipe- Reinemann's model	49
2.6 Instabilities in small diameter pipes	53
<b>CHAPTER 3: EXPERIMENTAL PROGRAM</b>	<b>55</b>
3.1 Experimental set up	55
3.2 Calibrations	58
3.2.1 Pressure transducer calibration	58
3.2.2 Flowmeter calibration	61
3.2.3 Surface tension measurement (Fisher Surface Tensiomat Model 21)	63
3.2.4 Viscometer (Brookfield Viscosimeter Model DV-II)	66
3.3 Experimental procedure	66
3.3.1 Liquid preparation and physical properties	66
3.3.2 Experimental program	67
3.3.3 Rising bubble velocity	69
<b>CHAPTER 4: EXPERIMENTAL RESULTS AND OBSERVATIONS</b>	<b>70</b>
4.1 Experimental results Part 1: Water/Air System	70
4.1.1 Observations on flow patterns specifics	70
4.1.2 Lump Flow in small diameter pipes	72
4.1.3 The effect of tube diameter – liquid production and calculated efficiency	73
4.1.4 The effect of submergence	79
4.1.5 Superficial velocities and pattern transitions	82
4.1.5.1 Transition conditions	82
4.1.5.2 Superficial velocities for evaluating the system efficiency	83
4.2 Experimental results Part 2: Water-Methanol/Air System	85
4.2.1 Water-methanol mixture physical properties	85
4.2.2 Flow Patterns – visual observation	86
4.2.3 Flow instabilities	89
4.2.4 Surface tension effect	94
4.2.5 Submergence and tubing diameter effects	97
4.2.6 The upward T-D Bubble velocity	98

<b>CHAPTER 5: COMPARISON OF EXISTING NUMERICAL MODELS AND IN-HOUSE MODEL DEVELOPMENT</b>	<b>103</b>
5.1 Conventional pipe models – Validation at low-pressure systems	103
5.2 Experimental results versus existing model predictions-small diameters	106
5.3 Critical production condition model (CPC)	108
5.3.1 CPC model formulation	109
5.3.2 CPC model validation	112
5.3.3 CPC model - Field application	115
5.4 Small Diameter pipe model (SDP)	117
5.4.1 SDP model formulation	117
5.4.2 SDP model verification	122
5.4.3 SDP model predictions and instabilities	126
5.4.4 SDP model and liquid production	128
5.4.5 Limitations of the SDP model	129
<b>CHAPTER 6: CONCLUSIONS AND RECOMMENDATIONS</b>	<b>130</b>
6.1 Conclusions	130
6.2 Recommendations for future works	132
<b>REFERENCES</b>	<b>133</b>
<b>APPENDIX A: EXPERIMENTAL DATA FOR CONVENTIONAL DIAMETER PIPES</b>	<b>140</b>
<b>APPENDIX B: APPARATUS DESIGN</b>	<b>142</b>
<b>APPENDIX C: EXPERIMENTAL RESULTS FOR THE WATER/AIR GAS LIFT SYSTEM</b>	<b>148</b>
<b>APPENDIX D: COMPARATIVE EXPERIMENTAL RESULTS FOR THE WATER-AIR AND WATER/METHANOL -AIR GAS LIFT SYSTEMS</b>	<b>161</b>
<b>APPENDIX E: NUMERICAL MODELS FOR SLUG FLOW AND ELONGATED BUBBLE FLOW MOVING UPWARDS</b>	<b>166</b>

## LIST OF TABLES

<i>Table</i>		<i>Page</i>
3.1	Equivalent L/min flow rates for the F&P® read values	62
3.2	Liquid level and submergences used for the 4.0, 7.8 and 12 mm risers	67
3.3	Air flow rate used for 4.0, 7.8 and 12 mm riser	68
4.1	Average Repeatability (in percentage) of experimental measurements	74
4.2	Water/air ratios at maximum production conditions for 12mm, 7.8 mm, and 4 mm diameter pipes, 16.6% submergence	77
4.3	Submergence effect on the water/air ratio measured at the maximum production conditions for the 12, 7.8 and 4.0 mm riser	81
4.4	Minimum submergence required for initiating the liquid production for 4., 7.8, and 12mm diameter (L=3m) and for ref. [48] (D=30 mm L=1.0 m)	82
4.5	Physical properties of water, methanol and water-methanol 60:40 mixture	85
4.6	Liquid (water-methanol)/air ratio at maximum production conditions (MPC) with 7.8 and 12 mm risers at 12.5 and 20.1% submergence	98
4.7	Liquid film thickness and local void fractions evaluated using theoretical calculations for the rising velocity of T-D bubble and measured values	102
5.1	Void fraction comparisons using Fernandes' [50] experimental data against Hasan and Ansari's model predictions	104
A.1	Experimental data, Fernandes experiment for slug flow [50]	141
B.1	Data from Reinemann's model [42] in 3.18 mm, 6 mm, 9.53 mm and 25 mm risers	143
B.2	Calculations for the storage tank diameter	144

B.3	Bottom loop pipe selection - Frictional pressure losses for 4, 3 and 2 inches pipe diameter	144
B.4	Cross sectional area ( $A_s$ ) ratio used during the experiments	146
B.5	Calculations for determining the diameter of the separator	146
C.1	First repeatability data for 12 mm ID riser, submergence 20.1%	148
C.2	Percentage of repeatability for three sets of data for the 12 mm riser at 20.1% submergence	148
C.3	Third repeatability data for 12 mm ID riser, submergence 16.6%	149
C.4	Repeatability for three sets of data for the 12 mm riser at 16.6% submergence	149
C.5	Second repeatability set of data for 12 mm ID riser, submergence 12.5%	150
C.6	Repeatability for three sets of data for the 12 mm riser at 12.5% submergence	150
C.7	Fourth repeatability data for 7.8 mm ID riser, submergence 20.1%	151
C.8	Percentage of repeatability to obtain sets of data for the 7.8 mm riser at 20.1% submergence	151
C.9	Fourth repeatability data for 7.8 mm ID riser, submergence 16.6%	152
C.10	Repeatability for three sets of data for the 7.8 mm riser at 16.6% submergence	152
C.11	Fourth repeatability set of data for 7.8 mm ID riser, submergence 12.5%	153
C.12	Repeatability for three sets of data for the 7.8 mm riser at 12.5% submergence	153
C.13	Second repeatability set of data for 7.8 mm ID riser, submergence 8.3%	154
C.14	Repeatability for three sets of data for the 7.8 mm riser at 8.33% submergence	154

C.15	Second repeatability set of data for 7.8 mm ID riser, submergence 4.16%	155
C.16	Liquid production at 6.25% submergence in a 7.8 mm riser - % Variation in three sets of data	155
C.17	Percentage of repeatability for three sets of data for the 4.0 mm riser at 20.1% submergence	156
C.18	Percentage of repeatability for three sets of data for the 4.0 mm riser at 20.1% submergence	156
C.19	Third repeatability data for 4.0 mm ID riser, submergence 16.6%	157
C.20	Repeatability for three sets of data for the 4.0 mm riser at 16.6% submergence	157
C.21	Second repeatability set of data for 4.0 mm ID riser, submergence 12.5%	158
C.22	Repeatability for three sets of data for the 4.0 mm riser at 12.5% submergence	158
C.23	Second repeatability set of data for 4.0 mm ID riser, submergence 8.3%	159
C.24	Repeatability for three sets of data for the 4.0 mm riser at 8.33% submergence	159
C.25	Second repeatability set of data for 4.0 mm ID riser, submergence 4.16%	160
C.26	Liquid production at 4.16% submergence in a 4.0 mm riser - % Variation in three sets of data	160
D.1	Data for a 12 mm riser with 63.5 cm of water, submergence 20.1%	161
D.2	Data for a 12 mm riser with 38.1 cm of water, submergence 12.5%	162
D.3	Data for a 7.8 mm riser with 63.5 cm of water, submergence 20.1%	162
D.4	Data for a 7.8 mm riser with 38.1 cm of water, submergence 12.5%	163
D.5	Data 12.0 mm riser with 63.5 cm of water/methanol, submergence 20.1%	163

D.6	Data 12 mm riser with 38.1 cm of water/methanol, submergence 12.5%	164
D.7	Data 7.8 mm riser with 63.5 cm of water/methanol, submergence 20.1%	165
D.8	Data 7.8 mm riser with 38.1 cm of water/methanol, submergence 12.5%	165
E.1	Hassan's model spread sheet	166
E.2	Input data Ansari's model	167
E.3	Model calculations for a specific flowing condition. Punctual results	168
E.4	Ansari's model - Table of results	169
E.5	Reinemann's model spread sheet	169
E.6	CPC model spreadsheet	170
E.7	SPD Model – Void Fraction	171
E.8	SDP model spreadsheet	172

## LIST OF FIGURES

<i>Figure</i>		<i>Page</i>
2.1	Sketch of liquid loading-up stages	8
2.2	Gas lift. a) Intermittent gas lift; b) Continuous gas lift	17
2.3	Two-phase flow patterns in vertical pipe. (a) Disperse Bubble, (b) Bubble Flow, (c) Slug Flow, (d) Churn Flow, (e) Annular flow (idealized representations)	18
2.4	The effect of the Eötvös Number on the minimal mixture velocity required for establishment of dispersed bubble flow in terrestrial air-water systems [23]	20
2.5	Taitel-Dukler-Barnea flow pattern map for a vertical tube: 5.0 cm diameter, air-water at 25 °C, 10 N/cm <sup>2</sup> [19]	22
2.6	Flow patterns in small diameter pipe. (a) Bubble flow, (b) slug flow, (c) churn flow, (d) annular flow	27
2.7	Flow pattern map, upward vertical flow: air/water, 0.1 MPa, 25 °C. (a) For 12.3 mm pipe. (b) For 4 mm pipe [32]	28
2.8	Flow regime map for d=4.08 mm [22]	29
2.9	Flow regime map for d= 2.05 mm [22]	31
2.10	Slug flow pattern in conventional pipes [38]	32
2.11	Elongated bubble pattern in small diameter pipes [38]	34
2.12	Relationship between volumetric flow rate of water discharge and air supplied for D= 12.00 mm. [46]	38
2.13	Relationship between volumetric flow rate of water discharge and air supplied for D= 19.23 mm. [46]	39
2.14	Airlift pumping performance: experimental results vs. theoretical model predictions. [47]	41
2.15	Experimental apparatus - Reinemann et al. [42]	51
3.1	Experimental set up	55

3.2	Views of experimental apparatus	56
3.3	Detail of the gas injection (section #3)	57
3.4	Picture of the Validyne's pressure transducer and the control box	59
3.5	Picture of the Omega® DPI 610 pressure calibrator	59
3.6	Calibration curve for the 8.0 psi diaphragm	60
3.7	Calibration curve for the 8.0 psi diaphragm	60
3.8	F& P® and Matheson® flowmeters	61
3.9	Calibration curve for F& P® rotameter	62
3.10	Calibration data for the Matheson® air flowmeter	63
3.11	Picture of the Fisher Surface Tensiomat ® Model 21	64
4.1	(a) Bubble flow (0.2 L/min air injection rate) and (b-c-d) Elongated bubble flow pattern (1.0, 1.36 and 2.66 L/min air injection rate, respectively), 12 mm riser.	71
4.2	Picture of the elongated bubble flow pattern for a water/air flow in a 7.8 mm diameter riser; gas flow rate 1.36 L/min (0.47 m/s)	72
4.3	The effect of injected gas (air) on produced liquid (water) for three groups of experiments (12, 7.8 and 12 mm ID risers) and various.	75
4.4	Liquid production with 4, 7.8 and 12 mm risers at a simulated reservoir pressure of 50.8 cm water column (16.6% submergence); – recommended zones of use (laboratory data performed with 3 m risers)	76
4.5	Water production vs. Air injection flow rate in a 4mm riser for 20.1, 16.6,12.5,8.3, and 4.16% submergence	78
4.6	Water production with 4, 7.8 and 12 mm risers at a) 20.1%, b) 16.6 %, c) 8.33% submergence	80
4.7	Comparison of present experiments and similar data from literature – indicating the effect of length of tube -Water/air ratio versus submergence for 4, 7.8 and 12 mm and 3.05 m length risers; and 30 mm ID, 1.0m length riser (Lawniczak et al. [48])	81

4.8	Liquid superficial velocity versus gas superficial velocity for 4, 7.8 and 12 mm risers	83
4.9	Liquid superficial velocity versus gas superficial velocity for 4, 7.8 and 12 mm risers (at 16.6% submergence)	84
4.10	(a) Elongated bubble flow pattern in 12 mm riser water/air system. 20.1% submergence, 3.7L/min air flow rate. (b) Elongated bubble flow pattern in 12 mm riser water-methanol/air system. 20.1% submergence, 3.7 L/min air flow rate. (c) Elongated bubble flow pattern in a 7.8 mm riser water/air system. 20.1% submergence, 1.4 L/min air flow rate. (d) Elongated bubble flow pattern in 8.0 mm riser water-methanol/air system, 20.1% submergence, 0.6 L/min air flow rate	86
4.11	Elongated bubble pattern with grouped but un-coalesced bubbles forming a T-D bubble structure, water methanol mixture, 0.2 L/min air flow rate, 12 mm riser	88
4.12	(a) Picture of a T-D bubble capturing a small bubble just above it. (b) Picture of two consecutive T-D bubbles just after coalescing	90
4.13	RMS graph showing the maximum-maximorum (max-max), minimum-minimorum (min-min), and average value (i.e. Water 12 mm riser and 6.3 L/min air injection rate)	91
4.14	Extreme of BHP oscillations (envelopes) observed with a 12 mm riser in a water-methanol system – 20.1% submergence	92
4.15	Extreme of BHP oscillations (envelopes) observed with 12 mm riser in a water system – 20.1% submergence	92
4.16	Extreme of BHP oscillations (envelopes) observed with 7.8 mm riser in a water-methanol system – 20.1 % submergence	93
4.17	Extreme of BHP oscillations (envelopes) observed with 7.8 mm riser in a water system – 20.1% submergence	93
4.18	IFT Effect on Liquid production at 12.5 and 20% submergence with 12 mm riser	95
4.19	IFT Effect on Liquid production at 12.5 and 20% submergence with 7.8 mm riser	96

4.20	Superficial liquid velocity versus superficial gas velocity for water-methanol experiments conducted in 7.8 and 12 mm at 12.5 and 20% submergence	97
4.21	Measured and calculated rising velocity of T-D bubble (12 mm diameter riser, 20.1% and 12.5% submergence, 100% water)	99
4.22	Measured and calculated rising velocity of T-D bubble (12 mm diameter riser 20.1% and 12.5% submergence, 60:40 water/methanol)	99
4.23	Measured and calculated rising velocity of T-D bubble velocity (7.8 mm diameter riser, 20.1% and 12.5% submergence, 100% water)	100
4.24	Measured and calculated rising velocity of T-D bubble (7.8 mm diameter riser, 20.1% and 12.5% submergence, 60:40 water-methanol)	100
5.1	Comparison between experimental data (Fernandes [50]) and modeled void fraction (Hasan and Ansari) – conventional-diameters	105
5.2	Water versus air superficial velocities; experimental results from this work compared with calculations using the Ansari and the Reinemann models (12 mm ID riser, 20.1% submergence)	106
5.3	Water vs. air superficial velocities – this work experimental result and Ansari and Reinemann liquid flow predictions (7.8 mm ID riser, 20.1% submergence - 63.5 cm)	107
5.4	Calculated (CPC Model) critical depth ( $L_{CPC}$ ) versus critical depth measured at three variable reservoir pressures (7.8 mm diameter tubing – air injection rate corresponding to 0.234 m/s)	113
5.5	Calculated (CPC Model) critical depth ( $L_{CPC}$ ) versus critical depth measured at three variable reservoir pressures (12 mm diameter tubing - air injection rate corresponding to 0.326 m/s)	113
5.6	Calculated (CPC Model) critical depth ( $L_{CPC}$ ) versus critical depth measured at three variable reservoir pressures (7.8mm diameter tubing-air injection rate corresponding to 0.21 m/s - water-methanol/air system)	114

5.7	Calculated (CPC Model) critical depth ( $L_{CPC}$ ) versus critical depth measured at three variable reservoir pressures (12mm diameter tubing-air injection rate corresponding to 0.35 and 0.93 m/s- water-methanol/air system)	115
5.8	CPC model prediction of critical depth ( $L_{CPC}$ ) versus reservoir pressure (12 mm diameter tubing), extrapolation to field conditions	116
5.9	Evolution of the liquid slug while travels from point 1 (position i) to point 2 (position i+1)	118
5.10	Prediction (SDP and Ansari's models) of the riser's length (well depth) for a certain liquid production (laboratory measured) and injected gas flowrate (Note – the depth used in the laboratory is 3.04 m) for a 12 mm riser: 63.5 and 38.1 cm of water	123
5.11	Prediction (SDP Model) of the riser's length (well depth) for a certain liquid production (laboratory measured) and injected gas flowrate (Note – the depth used in the laboratory is 3.04 m) for a 7.8 mm riser: 63.5 and 38.1 cm of water	124
5.12	Prediction (SDP and Ansari's models) of the riser's length (well depth) for a certain liquid production (laboratory measured) and injected gas flowrate (Note – the depth used in the laboratory is 3.04 m) for a 12 mm riser: 63.5 and 38.1 cm of water/methanol	124
5.13	Prediction (SDP Model) of the riser's length (well depth) for a certain liquid production (laboratory measured) and injected gas flowrate (Note – the depth used in the laboratory is 3.04 m) for a 7.8 mm riser: 63.5 and 38.1 cm of water/methanol	125
5.14	SDP Model Length prediction for a 7.8 mm riser: 63.5 and 38.1 cm of water compared against its respective percentage of instability	127
5.15	Liquid production vs. gas injected, comparison between Ansari, Reinemann and SDP models and the Experimental data - 12 mm riser, 63.5 cm liquid level (20.1 % submergence)	128
A.1	Water rate as function of air flow rate [48]	140
B.1	Apparatus dimensions	142
B.2	The air injection section	145
B.3	Separator design: Angle applied to allow the liquid flow toward the storage tank	147

## NOMENCLATURE

### Symbol

<b><i>A</i></b>	Cross section area of the pipe, (m <sup>2</sup> )
<b><i>A<sub>o</sub></i></b>	Cross section area of the pipe, (m <sup>2</sup> ) [46]
<b><i>As</i></b>	Ratio (Nozzle OD) <sup>2</sup> /(Tubing ID) <sup>2</sup>
<b><i>BHP</i></b>	Bottom Hole Pressure, (KPa, psi)
<b><i>Ca</i></b>	Capillary Number (dimensionless)
<b><i>C<sub>o</sub></i></b>	Distribution coefficient. Usually Co=1.2
<b><i>CPC</i></b>	Critical Production Condition. (The minimum gas flowrate or gas superficial velocity to obtain the first drop of liquid production)
<b><i>D</i></b>	Internal tube diameter, (m)
<b><i>d</i></b>	Bubble diameter, (m, mm)
<b><i>dL</i></b>	Differential Length
<b><i>dP</i></b>	Differential pressure
$\left  \frac{dp}{dz} \right $	Absolute differential pressure with respect to the length (Pa/m)
<b><i>Eö</i></b>	Eötvös Number ( $\Delta\rho g D^2 / \sigma$ )
<b><i>F<sub>R</sub></i></b>	Froude Number (dimensionless)
<b><i>f</i></b>	Friction factor
<b><i>f<sub>M</sub></i></b>	Moody friction factor (Blasius Equation)
<b><i>g</i></b>	Acceleration of gravity, (m/s <sup>2</sup> )
<b><i>H</i></b>	Holdup (Ansari's model [51])
<b>"H"</b>	Harmathy Bubble.
<b><i>h</i></b>	Length of Liquid column measured from the gas injection point, (m)
<b><i>ID</i></b>	Internal tube diameter, (m)
<b><i>k</i></b>	Constant (0.68 for drops, 1.14 for bubbles)
<b><i>L</i></b>	Tubing Length, (m).
<b><i>Max-max</i></b>	Maximum-maximorum

<b><i>Min-Min</i></b>	Minimum-minimorum
<b><i>Mo</i></b>	Morton Number (dimensionless)
<b><i>MPC</i></b>	Maximum production condition (Gas injection rate at which the maximum liquid production is sustained)
<b><i>N<sub>L</sub></i></b>	Inverse viscosity number (dimensionless)
<b><i>OD</i></b>	External pipe diameter, (m, mm)
<b><i>P</i></b>	Pressure (Pa)
<b><i>Q</i></b>	Flow rate, (m <sup>3</sup> /s)
<b><i>Q'</i></b>	Dimensionless flow rate
<b><i>Re</i></b>	Reynolds Number (dimensionless)
<b><i>SDP</i></b>	Small Diameter Pipe model
<b><i>s</i></b>	Submergence.
<b><i>t</i></b>	Time, (s)
<b><i>T-D</i></b>	Taylor-Dumitrescu Bubble
<b><i>U</i></b>	Velocity, (m/s)
<b><i>U'</i></b>	Dimensionless velocity [42]
<b><i>V</i></b>	Volume, (m <sup>3</sup> )
<b><i>Z</i></b>	Length (m) – Reinemann et al [42]

### **Subscripts**

<b><i>a</i></b>	Air
<b><i>add</i></b>	Added volume
<b><i>ave</i></b>	Average
<b><i>calc</i></b>	Calculated value
<b><i>CPC</i></b>	Critical Production Condition
<b><i>cr</i></b>	Critical (i.e. Critical tube diameter D <sub>cr</sub> )
<b><i>crit.</i></b>	Critical (i.e. critical diameter d <sub>crit.</sub> )
<b><i>exp</i></b>	Experimental value

<b><i>FB</i></b>	Fall back
<b><i>fr</i></b>	Friction
<b><i>g</i></b>	Gas phase
<b><i>i</i></b>	Segment of tubing located at the “i” position
<b><i>i+1</i></b>	Segment of tubing located immediately above the “i” position
<b><i>in</i></b>	Inlet condition
<b><i>L</i></b>	Liquid phase (Ansari’s Model [51])
<b><i>LTD</i></b>	Liquid film in the T-D bubble
<b><i>LS</i></b>	Liquid slug section in the slug unit
<b><i>l</i></b>	Liquid phase
<b><i>m</i></b>	Mixture
<b><i>max</i></b>	Maximum
<b><i>out</i></b>	Outlet condition
<b><i>phase</i></b>	Gas or liquid phase
<b><i>Res</i></b>	Reservoir
<b><i>s</i></b>	Submergence
<b><i>st</i></b>	Static
<b><i>SU</i></b>	Slug unit
<b><i>T</i></b>	Total tubing length
<b><i>T-D</i></b>	Taylor – Dumitrescu bubble section in the slug unit
<b><i>T-D Nicklin</i></b>	Used to define the T-D bubble rising velocity using the Nicklin’s drift flux equation
<b><i>T-D<math>\infty</math></i></b>	Taylor – Dumitrescu bubble terminal velocity
<b><i>t<math>\infty</math></i></b>	Harmathy bubble terminal velocity
<b><i>U</i></b>	Slug unit
<b><i>w</i></b>	Water

**Superscripts**

<b><i>s</i></b>	Superficial
-----------------	-------------

### Greek Symbols

$\bar{\alpha}$	Average void fraction
$\alpha$	Void fraction
$\beta$	Submergence (According to Kouremenos and Staïcos [46])
$\beta$	Ratio between the liquid slug length and the slug unit length (Ansari and Hasan's model)
$\delta_L$	Film thickness, (m)
$\Delta$	Difference (i.e. Difference of density, pressure, etc.)
$\Sigma$	Inverse Eötvös Number (dimensionless)
$\varepsilon$	Rate of energy dissipation per unit mass
$\xi$	Ratio between the internal pipe diameter and the external diameter of the gas injection tube [46]
$\eta$	Airlift efficiency [42]
$\rho$	Density ( $\text{m}^3/\text{s}$ )
$\mu$	Viscosity (MPa.s)
$\sigma$	Surface tension, (N/m, Dyna/cm)

# CHAPTER 1

## INTRODUCTION

---

### 1.1 Overview

**Depleted gas reservoirs** are frequently facing problems of water or condensate accumulation at the bottom of the well. As gas reservoirs become mature and the gas pressure is not sufficiently high to transport the small quantities of liquid to the top, a production problem called “loading” appears.

A loading problem in gas wells occurs when a small amount of liquid (usually water resulted from an aquifer), normally carried by the gas stream, is no longer transported to the well head and therefore is accumulated at the bottom of the well. Most of the times, especially in depleted gas reservoirs, the static pressure exercised by a small column of liquid exceeds the reservoir pressure and impede the flow of gas. Gas wells around the world are facing not only the effect of depletion after several years of production but also the negative effect of the loading backpressure [1 – 2].

**Unconventional gas technologies** such as Coal Bed Methane (CBM) faced similar problems when the water coming from the coal bed is drained towards the well reducing the gas productivity [3]. Several methods have been used for unloading gas wells with limited success, among them: plunger lift, intermittent production cycles, rod pumps, gas lifting with or without foaming agents and swabbing [4].

A significant factor affecting the success of implementing one or another method for unloading gas wells is the reservoir pressure. For instance, a still “healthy” gas reservoir could sustain a natural production after shut in periods (intermittent), strategy enhanced by using plunger lifting.

On the other hand, a very depleted reservoir with loading problems will require more external energy, rod pumping or swabbing, because of the smaller column of liquid killing the well. Those solutions will require a continuous intervention or permanent liquid pumping to recover the gas production.

Under natural flowing conditions, **small diameter pipes** (pipe diameter less than 1.0 inch) are used to increase the gas superficial velocity by reducing the flow cross sectional area. Therefore, the gas velocity is kept above a critical value in order to avoid the liquid droplets transported in the gas stream fall and accumulate at the bottom of the well. The **critical gas velocity** was defined by Turner [5] as the minimum velocity at which the drag forces of the gas are balanced with the gravitational forces of a liquid droplet.

Artificial gas lifting in combination with small diameter pipes is used either to unload continuously the liquid from the well by keeping the gas velocity above its critical value or intermittently by using a convenient slug flow pattern.

The present work is focused on the cases where the reservoir pressure is extremely low and the available unloading technologies are not capable to economically restore the productivity of the well.

## **1.2 Statement of the problem**

### **Liquid Accumulation**

The liquid accumulated at the bottom hole level has two main sources: a. water produced from a nearby aquifer, b. condensate or oil entrained by gas.

Unloading gas wells is a long-term problem still looking for a practical and economical solution. Gas wells accumulate water and condensate when the reservoir pressure decreases under the value required to overcome the frictional and static pressure required for transportation of produced liquid (water and condensate) from the bottom hole to the

well head levels. A sudden increase of the liquid inflow will have a similar effect of stopping the continuous gas-liquid flow of the well.

The droplets of liquid when the gas flow rate is below the critical gas flowrate, are deposited at the bottom of the well and form a column of liquid that creates a backpressure effect on the reservoir. This loading prevents the gas from flowing freely to the well, reduces its production potential and, later on, stops the gas flow and kills the well.

### **Liquid removal**

Conventional methods for unloading gas wells such as conventional gas lifting and small diameter pipe with or without soap treatments have been designed and implemented to keep the gas velocity above its critical value. Although these methods have been applied with relative success, those are temporary solutions since the natural depletion of the reservoir will reach again a critical “abandonment” pressure. In this case, the unloading method should be re-visited.

When the height of the column of liquid killing the well is low, none of the mentioned unloading strategies have proven to be efficient. As a rule of thumb, gas lifting is applied to conventional diameter tubing (1.0 inch to 4.0 inches tubing) when the ratio between the length of the shut-in liquid column, measured from the gas injection level, to the length of the tubing (measured from the gas injection point up) should be in excess of 0.5. A sufficient liquid head is a general condition for efficient rod or submersible pump operation. The static pressure equivalent of the column of liquid above the perforation level, measured during the shut-in well (no flow), is a direct measure of the reservoir pressure and is an essential parameter considered for implementation of any gas lift operation.

Overcoming the conventional operational limits will help to extend the productive life of the well. In order to implement a new technology, both physical operation factors and economical aspects should be carefully considered.

Reducing the diameter of tubing under conventional values results in increasing the void fraction (relative volume occupied by gas during the up flow of gas-liquid). This will further reflect in reducing the contribution of static pressure to the total well flowing pressure drop (including static and frictional components). While this effect was observed and used for limited (industrial application) lifting heights, there is insufficient theoretical and experimental (field) evidence required for field application and design. Alteration of conventional flow pattern description and mapping is essential for developing mechanistic models and implementing proper calculation procedures of gas-liquid flowing pressure. An experimental and numerical study has been initiated to re-visit and improve the present knowledge in view of future field applications of gas lifting technologies using small-diameter tubing designs.

In concordance with this goal, the effectiveness of gas-liquid vertical transport in small diameter pipes was assessed using experimental results in a 3 m height gas lifting laboratory apparatus. Results obtained from the experiments are compared first with the existing (industry-accepted) mechanistic models. It was found that none of the available models for conventional pipes is suitable to assess the gas-liquid transport in small-diameter conditions.

A detailed description of the main factors controlling the gas-liquid transportation in small-diameter pipes and a simplified, but more realistic mechanistic flow model have been completed and can aid to further field-implementations strategies.

### **1.3 Objective and scope of the research**

The primary objective of this research is to assess potential application of small diameter pipes for unloading gas wells with very low reservoir pressure (equivalent to submergence values less than 0.2).

The second objective of this study is to develop a mechanistic model for predicting the maximum tubing length (well depth) to be considered for a potential gas-lifting strategy

with small-diameter pipes and validate this model using a broad range of laboratory experimental conditions. The model will be used to estimate limiting depth for potential field applications.

To achieve these research objectives the following tasks have been completed and are described in this dissertation:

- 1) Literature survey and discussion,
- 2) Model the gas lifting process using existing mechanistic models (initially developed for conventional gas-liquid gas lifting conditions) and numerically investigate the effect of reducing the pipe diameter; compare and discuss the results,
- 3) Design, construct and instrument a suitable gas-lifting apparatus for investigating the effect of small-pipe diameter to transport efficiency and flow pattern description,
- 4) Perform a large number of laboratory experiments using standard (pressure and temperature) conditions for air-water and air-water-methanol (surface tension modifiers) to assess the effect of gas-liquid-reservoir pressure on the gas-liquid transport efficiency,
- 5) Investigate the validity of existing (literature) numerical, mechanistic models (developed for conventional pipe diameters) for predicting laboratory measured results,
- 6) Describe the gas-liquid flow in small-diameter pipes and develop a numerical model to assess limiting flow conditions,
- 7) Validate the numerical model using laboratory data,
- 8) Use the model for assessing limitation and advantages of gas lifting with small diameter tubes.

## **1.4 Structure of the Thesis**

Chapter 1 presents a general outline of the problem of unloading gas wells with very small reservoir pressures. It includes, overview, statement of the problem, objectives and scope of the research.

Chapter 2 contains related concepts and literature review of methods for unloading gas wells, gas lifting in small and intermediate diameter pipes, previous works and models describing slug flow and semi-slug flow, effect of pipe diameter, superficial tension and instabilities on the liquid production.

Chapter 3 explains the experimental program. Includes the details of the experimental set up, calibration procedure for pressure transducer and flowmeters, and test procedures for water and water and methanol tests.

Chapter 4 presents the discussion of the experimental results and observations.

Chapter 5 provides the details of the model development for slug flow in small diameter pipes.

Chapter 6 presents the conclusions of the research as well as recommendations for future works.

## CHAPTER 2

### LITERATURE REVIEW

---

#### 2.1 Unloading gas wells

The liquid loading-up is a common problem in gas wells production from low-pressure (depleted) reservoirs. A depleted gas reservoir is usually indicated by low wellhead pressure, and increase in liquid production. As the reservoir pressure goes down, liquid may accumulate in the bottom hole region. The composition of liquid is water, hydrocarbon (i.e. such as condensate or oil) or a mix.

In the absence of adequate energy required for transport to wellhead level of produced liquid and gas, the liquid accumulation can cause serious problems. The problem can be attributed to a low gas production rate due to low bottom hole pressure or low gas relative permeability for given conditions [6]. This problem is called load-up and also could exist in gas wells with high liquid-gas ratios (i.e. CBM cases). In this type of wells the high liquid production rates cause increased pressure losses and liquid accumulation in the bottom, even if the reservoir pressure is high.

An adequate method to unload the well should consider the combined effect of reservoir pressure, well permeability, gas/liquid ratio (GLR), liquid physical and chemical properties, sand, wax or paraffin content, and economical aspects such as: existing equipment, cost of new equipment, operational cost, surface facilities and chemical additives.

Four identifiable [4] stages during the evolution of a loading-up process in a gas well are illustrated in Figure 2.1 as such:

**Stage 1:** Initially the reservoir produces liquid in the form of micro-droplets traveling with the gas along the pipe (i.e., mist flow). In this case the gas velocity is higher than

the critical gas velocity (required to effectively transport the droplets e.g. well in excess of free falling velocity of individual droplet) and the drag forces of the gas will carry the liquid.

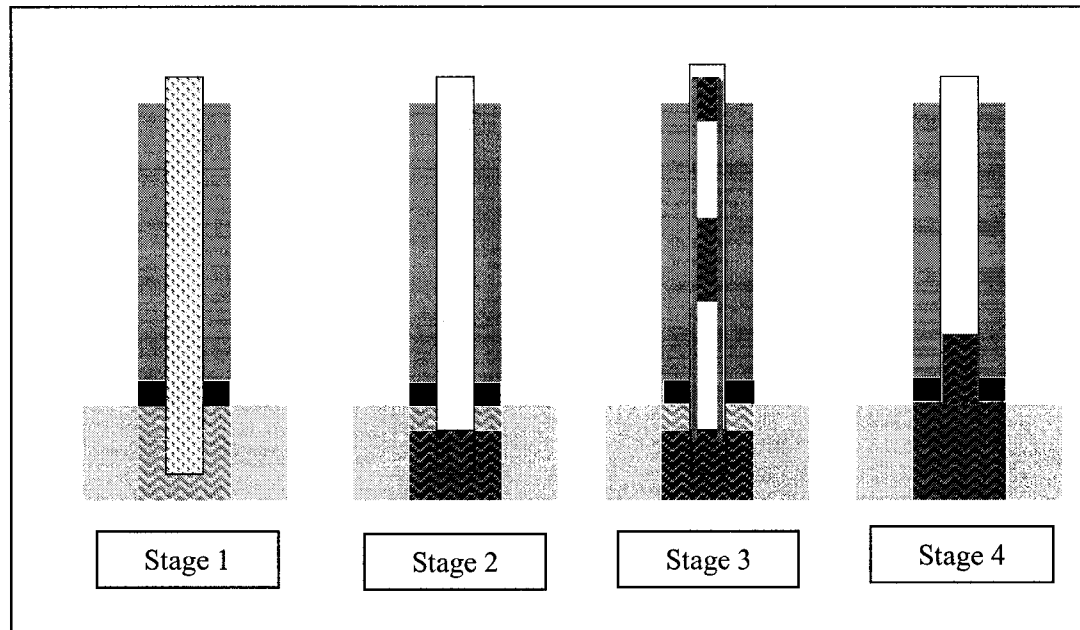


**Figure 2. 1** Sketch of liquid loading-up stages

**Stage 2:** As the reservoir pressure decreases, the gas flow rate also declines. Therefore, the gas velocity is no longer above the critical value and some liquid starts to accumulate at the bottom of the well. At this point the local pressure drop at the perforation level increases and, in addition, the accumulated liquid starts to apply a sizable backpressure on the reservoir.

**Stage 3:** As the time goes by, the accumulated liquid produces a blocking effect at the bottom of the well acting like a chock valve. If the reservoir energy is high enough to counterbalance the weight of the liquid column, accumulated reservoir energy will suddenly blow the liquid out of the pipe usually in the form of a liquid slug. The accumulation and removal will alternate in cycles.

**Stage 4:** Most of the time the liquid film left behind on the pipe wall is drained down to the bottom and the cycle begins again from stage 2. The time between one liquid blows

out and the next increases as the reservoir pressure goes down. After a certain period, the reservoir is no longer able to lift the liquid column and the well dies.

The applicability of remedial methods would largely depend of the actual stage of the reservoir. Three groups of unloading gas wells methods are identified according to the available energy of the reservoir: a. methods aiming at sustaining natural flow, b. methods using artificial lifting, and c. combined methods [4].

### **2.1.1 Methods of sustaining natural flow**

Natural flow refers directly to the well's capability of transporting produced gas and liquid to the surface using the available (flowing) bottom hole pressure.

When a gas reservoir has reached the second or third stage, the efficiency of gas production is limited by the liquid accumulation at the bottom. The following methods have been used in the industry to solve this problem.

#### ***2.1.1.1 Alternate flow/shut in periods***

Alternate Flow/shut-in periods may be performed manually, however, they are normally accomplished with the aid of a cyclic control system ("intermitted"). The gas pressure is built up in the reservoir as well as in the annulus (the space between the tubing and the casing). When the accumulated pressure is high enough to overcome the liquid column pressure, the control valve (intermitter) opens and the gas flow pass through the tubing producing the liquid to the top. The system is then shifted from high to low pressure environment. The cycle starts again when the valve (intermitter) shuts down after the pressure is released [4].

This is one of the most economical methods since the required equipment, an "intermitter" and a controller, and the modifications to existing facilities are minimum. However, the economical advantage of this cyclic production strategy diminishes with the reservoir pressure depletion, and a significant reduction in gas production. That is

why this method is just a temporary solution while the reservoir is able to overcome the backpressure applied by the liquid column.

#### ***2.1.1.2 Plunger lift***

Plunger Lift system was based on the same principle as the flow/shut in method. In this case, a free running plunger is used to act as a solid interface between the accumulated liquid and the lift gas. Most operators agree that plunger lift is the most suitable method for unloading low productivity gas wells with GLR's in excess of 5000 scf/bbl and liquid production rates less than 50 bpd [4].

This method also requires a controller, a shut-in valve ("intermitter") and, in addition, a plunger. It is considered to be one of the most economical methods applicable for unloading gas wells. The limiting factor is the reservoir pressure that should carry both the liquid and the plunger to the top and the delay introduced by the plunger fall down. For depleted reservoirs this method is not convenient.

#### ***2.1.1.3 Swabbing***

Swabbing fluids from a well consist of lowering a swabbing tool down the tubing and physically lifting the fluids to the surface. By reducing the liquid column length, the reservoir, at certain point, will overcome the pressure applied by the remaining column of liquid and the gas flow will be re-established.

The main problem associated with the swabbing method is the frequency of interventions that should be done to sustain the gas production.

As mentioned before, once the reservoir losses pressure, the liquid will be accumulated more frequently at the bottom and the column of liquid required to kill the well will be lower than before. The swabbing becomes more frequent and economically inapplicable.

#### ***2.1.1.4 Small diameter production tubing***

The objective of this method is to reduce (i.e. annular flow) the static pressure exercised by the liquid accumulated liquid under the value required for creating a continuous flow condition sustained by the flowing bottom hole pressure only.

In order to select an optimal diameter it is necessary to build a bottom hole pressure (BHP) vs. pipe diameter curve at constant GLR using one of the available models to predict the pressure drop along the pipe in multiphase flow. The depth of the well is another critical factor in implementation of this method. The dynamics of the reservoir pressure, and permeability of the reservoir (expected decline) should be also considered for implementing this technology.

In addition, the industry considers that the cost of the tubing compared with the revenue of the gas production is a main limiting factor for field implementation of this method.

#### ***2.1.1.5 Foaming agents***

Soap sticks or liquid surfactants are used to form stable homogeneous water and gas foam, produced (and broken) at the wellhead level. Foaming agents are used basically when the loading is caused by water. Condensates are non-polar liquids; therefore, the conventional surfactants have less foaming action on them.

Foams are also used to sustain the mist flow in the tubing. Surfactants at very low concentrations can reduce dramatically the surface tension of the water, which allows, under small turbulence conditions, the liquid to break in smaller droplets that could be carried to the top by the gas flowing at lower velocities. Researches about the effect of foaming agents on unloading gas wells revealed that annular flow is reached quickly when the liquid is treated with surfactants [8]. It means that the droplets could be carried by the dragging action of the gas in the core of an annular flow, while a thin liquid film is formed on the wall; depending on the gas-droplets velocity of core flow, the liquid film is entrained upwards or simply flows down (fallback).

Foaming agents are one of the cheapest methods that require minimum investment to be implemented. This method could be combined with artificial lifting such as gas lifting or small diameter pipes in order to improve its efficiency [9]. Sometimes the difficulties arising from emulsion breaking and fluid treatment and resulted environmental damage are overlooked.

### **2.1.2 Artificial Lift**

Artificial lifting methods are used when the reservoir pressure is no longer able to sustain the natural flow. An external source of energy complements the necessary forces to lift the liquids out of the well.

#### ***2.1.2.1 Sucker Rod Pumping***

The application of rod pumping to gas wells experiencing liquid loading problems is drawing a considerable amount of attention. The first real advantage is that the liquid unloading does not depend on the gas velocity, secondly, the external energy applied to the liquid can unload even smaller column of liquids, which means smaller submergence values. The liquid is sucked by the pump and delivered to the tubing that transported it to the top. The gas is produced freely in the annulus. This characteristic allows the well to be produced until the latest abandonment pressure or economic limit.

A remarkable disadvantage with respect to the other methods is the cost of the equipments and the possible interventions required for maintaining the down hole equipments and, the requirement of a sizable level of fluid above the upper part of the pump.

#### ***2.1.2.2 Gas Lift***

As a general concept, gas lift is an artificial lifting method that uses gas to light on the column of liquid in the well. The reduced density allows the two-phase mixture to travel to the top and produce the liquid that is recovered after a separation process.

Gas lifting is considered by some operators to be one of the most successful methods in keeping the productivity of gas wells with loading problems. The gas should be injected in the lowest possible level in order to produce maximum density reduction in the liquid column and therefore maximum relief in hydrostatic pressure.

The gas injection may be applied continuously [10] or intermittently [11]. Both cases have demonstrated to be economically viable if the facilities already exist in the field or if the equipments required, such as compressors, valves and tubing, do not overcome the window of profitability. This technology is conveniently applied after other methods have been discarded or they are not successful anymore [4].

### **2.1.3 Combined Methods**

A combined solution utilizing external and reservoir energies to produce the loading liquids is a logical and advantageous method that has showed better long-term results.

#### ***2.1.3.1 Gas lifting and small diameter pipes***

Gas lifting combined with small diameter pipes with [12] or without foaming agents showed economical solutions for terminal wells.

An intermittent gas lifting system with small diameter pipes was called “Air Pulse System” [11]. The gas was pumped through a  $\frac{3}{4}$  inch steel tubing in a down-hole pump chamber and the liquid and gas were returned through a 1.0 inch PVC pipe to the surface. A 3 HP air compressor was used in intermittent cycles to unload two wells. The authors concluded that the system could provide an economical solution for unloading gas wells. They worked in two wells with submergence values of 34% and 31%. The limiting conditions observed were depth of the wells that should be less than 600 m (~ 2000 ft), and the liquid production under 100 bpd.

Saleh and Al-Jamae’y [8] studied an unloading method that combined gas lifting, foaming agents and small diameter pipes. They worked with a 1.0-inch ID; 40 ft height

tubing that discharged the liquid in a small separator at the top. The liquid production was measured after separation. Liquid was recovered as foam in a continuous foamy phase.

They concluded that the effect of reducing the liquid surface tension from 72 to 33 Dyne/cm by adding surfactants was the reduction of the critical superficial gas transition velocity (from slug to annular flow pattern). Therefore, by reducing the surface tension, the transport of liquid as a core of droplets in an annular flow pattern becomes possible at smaller velocities. This effect agreed the Hinze's Splitting Theory [13] that predicted the break-up of a liquid drop will occur at a critical Weber Number ( $We=30$ ):

$$We_{crit} = \left( \frac{\tau D}{\sigma} \right)_{crit} \quad 2.1$$

Saleh and Al-Jamae'y are assuming a preferred annular flow pattern transport. For extremely low reservoir pressures, this assumption has to be re-visited altogether.

### ***2.1.3.2 Injection systems used for gas lifting***

To improve the gas-liquid transport efficiency, down-hole devices ("tools") such as vortex inducers [14] and gas lifting valves [15] have been used with a various degree of success.

The vortex device created a helical flow to unload liquids [14]. Laboratory experiments were conducted using a clear PVC tubing that simulates a 2" well of 125 ft (38 m). The experiments observed an enhanced liquid production. These observations are explained using the previous Mingaleeva's studies [16] who compared the power spent to overcome the hydraulic drag for raising an air column in a helical trajectory against the rising and the motion of an equivalent mass of air in a vertical trajectory. The studies concluded that the helical path was more favourable from an energy-use viewpoint.

The special gas-lifting valve called "Reber-Landry Tool" [15] was designed taking into consideration aspects such as: submergence, gas and liquid superficial velocity

correlations, liquid-gas slippage and pressure drop. The tool was tested in Grande-Prairie-Alberta and in Verlo Field – Saskatchewan [15].

Negative results (no production whatsoever) due to insufficient reservoir pressure (submergence) available for the well test performed in Grand Prairie clearly suggested the salient importance of reservoir pressure/submergence in any gas lifting operation and the relatively minor effect of a special injection valve; however, a production in excess of 300 CMD (water and oil) was demonstrated using the same valve design in Verlo field.

Again the most limiting factor for these technologies were the cost of utilizing external energy sources and high capital required for the surface compressor-separator equipment. Using the gas lifting for marginal (“stripper”) wells is a technical challenge and requires in-depth information on reservoir production-pressure history and a good knowledge of the gas-liquid flow patterns and pressure profile.

The present work proposes a combined technology exploiting the optimal injection ranges for minimizing the transport pressure (static and dynamic) through the use of small diameter pipes and the relatively inexpensive gas lifting technology.

A review the gas-liquid upward flow mechanisms is required to outline the particulars of small-diameter pipe transport.

## **2.2 Gas Lift**

According the Petroleum Engineering handbook [17]: “ Gas lift is the method of artificial lift that uses an external source of high-pressure gas for supplementing formation gas to lift the well fluids”. Gas lift is the only method of artificial lift that fully utilizes the energy in the formation to produce the liquid. This definition is perfectly suited for conventional production of gas and liquid, where reservoir pressure is suffice to sustain naturally a sizable fluid production. Any additional gas injected may lead to an increase of production. The science was required to determine the most suitable position of injection valves and to minimize the capital cost related to surface compressing-

separation equipment. For marginal reservoirs conditions, a conventional gas lifting is not necessary a solution for resurrecting the production, regardless of the capital invested in the equipment [15].

Gas lifting technologies have been continuously improved since later 18<sup>th</sup> century when mining industry used airlift to evacuate the water flooding in the coal and copper mines. Today gas lifting is seen as one of the most effective lifting methods to enhance the oil production either during or after natural flow [18].

### **2.2.1 Continuous and Intermittent Gas Lift**

The reservoir pressure, liquid production rates, depth of the well, gas availability and economics are important factors to be considered for proper design of a gas lifting operation. The two most popular gas lifting methods are: a. continuous and b. intermittent gas lift (Figure 2.2.)

**Continuous gas lift** was first implemented to enhance the production in naturally flowing wells and, then, to recover the liquid production in dead wells. A packer was installed in the lower well zone to allow for the gas injection through the annulus (Figure 2.2 b) and the liquid and gas injected to be produced through the tubing. Parallel tubing also was used to inject the gas [18]. The production was enhanced by reducing the bottom hole flowing pressure (BHFP) as a result of significant reduction of static and dynamic pressure across the depth of the gas-liquid flowing tube.

**Intermittent gas lift method** (Figure 2.2 a) is used when the reservoir produces small amounts of liquid and the reservoir pressure is not enough to sustain the production (Typical case for gas wells with loading-up problems). The gas is injected at high pressure at the bottom of the liquid column generating long slug units that pushes the liquid slug up to the top. A valve located at the lower part of the well is shut in and the well is allowed to fill the column of liquid again [18].

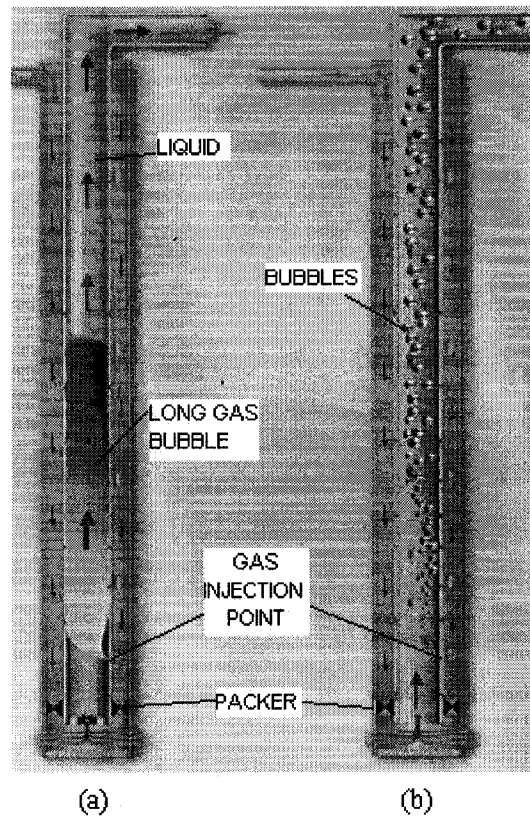


**Figure 2.2** Gas lift. a) Intermittent gas lift; b) Continuous gas lift [18]

This method generates significant reductions in the BHFP that is occasionally not supported by certain wells with unconsolidated sand problems [17]. Gas lifting systems work thanks to the interaction of multi phases in the pipe, water and gas, oil and gas, or water-oil and gas. The two phases structuring the system exhibit different patterns based on the liquid and gas flow rates. The appropriate working pattern should be decided in accordance with the GLR, reservoir pressure, and severity of the load-up problem.

### 2.2.2 Two-phase flow patterns in vertical pipes

Taitel and Barnea [19] defined five different flow patterns for an air-water system upward flowing through a vertical pipe: disperse bubble flow, bubble flow, slug flow,

churn flow and annular flow. Figure 2.3 shows, using an idealized schematic, the different characteristics of the patterns.

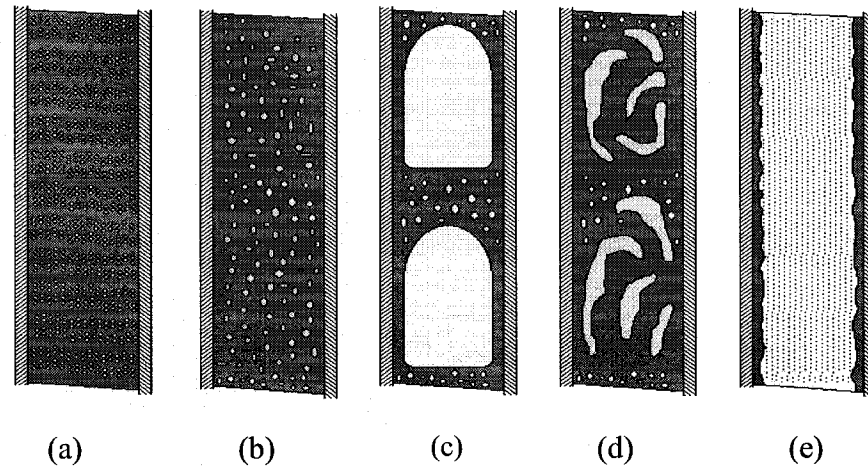


**Figure 2.3** Two-phase flow patterns in vertical pipe. (a) Disperse Bubble, (b) Bubble Flow, (c) Slug Flow, (d) Churn Flow, (e) Annular flow (idealized representations)

The slug flow, Figure 2.3(c), is one of the most common patterns observed in gas lifting with conventional pipe diameters. A long Taylor- Dumitrescu (TD) bubble zone and a liquid slug zone that contains some fraction of gas in form of small bubbles called “Harmathy” [21] bubbles characterized this pattern. A liquid film is bridging the T-D bubble and the internal pipe diameter. The thin liquid film surrounding the T-D bubble falls back.

The TD bubble, the liquid slug and the falling film form one slug unit that travels along the pipe to deliver the liquid at the wellhead. While the slug unit and the T-D bubble unit are raising at comparable speed, the liquid film is a separate entity that falls back at a considerable slip velocity with respect to the rising central bubbles.

For most of the conventional diameter calculation routines, the effect of the falling back film to the distribution of phases in the section is neglected. The TD bubble is a long bubble (in comparison with the pipe diameter) that is related to the main hydrostatic pressure reduction within the slug flow pattern.

The "organized" slug flow pattern disappears with increasing the gas flowrate/velocity above a critical level. This would cause the liquid to be re-distributed in an annulus where the central zone is occupied by gas and entrained liquid droplets flowing against the extremely disturbed (wavy) liquid film supported on the pipe wall. Figure 2.3(e). There is a transition flow pattern between the slug and annular flow. This flow pattern is called churn flow, Figure 2.3 (d). Distorted T-D bubbles coalescing and braking inside a relatively small amount of liquid characterize this pattern. This chaotic behavior negatively affects the liquid transportation and production.

Disperse bubble flow pattern, Figure 2.3 (a) is formed at high liquid flowrates when the turbulent liquid forces, overcome the interfacial tension forces in the gas bubbles, breaking the big bubbles into smaller, not coalescing ones. The liquid and gas travel at almost the same velocity in a well known homogeneous flow (where the gas-liquid slip velocity is usually neglected). The bubble flow, Figure 2.3 (b) appears at lower liquid and gas velocities where the liquid turbulence is less and the bubbles can coalesce easier. Characterized by the presence of "Harmathy's" bubble (similar to the bubble population found in the "slug" sub-region of the slug assemble flow pattern), the bubble flow pattern cannot be achieved practically with small-diameter pipes. The equivalent diameter of the wobbling "Harmathy" bubble is usually larger than the (small) diameter and this lead to fast coalescence induced by wall-bubble contact and disappearance of this typical bubble.

### **2.2.2.1 Pipe size classification**

Brauner [23], using air-water systems (Figure 2.4), calculated the minimum mixture velocity required for maintaining a statistically-stable population of dispersed bubble flow. In Figure 2.4, presenting the bubble-model transitions as function of total transport velocity ( $U_m$ ) and pipe internal diameter,  $D$  the minimum mixture transport velocity required for transition to dispersed bubble flow is also a function of Eötvös Number (uniquely related to pipe diameter for the same gas-liquid)

$$Eö = \frac{\Delta\rho g D^2}{8\sigma} \quad 2.2$$

According to Brauner's classification [23] tubes with  $E\ddot{o}$  less than 0.1 ( $D < 0.3$  cm also) are called "capillary tube". Brauner used Hinze model [13] predicts the minimum mixture velocity ( $U_m$ ) required for transition from bubble to dispersed bubble flow in capillary tubes. The prediction made by Hinze [13], considers the effect of the turbulence overcoming the surface tensional forces of the bubble. He also proposed the breaking of bubble into smaller, spherical, non-coalescing bubble, to occur at a critical Weber number ( $We=30$ ) (Equation 2.1).

Brauner [23] classified the pipes with  $E\ddot{o}$  greater than 100 ( $D > 10$  cm) as "Large diameter tube". She used Hughamark model [26], to determine the minimum mixture velocity ( $U_m$ ) for transition from bubble to disperse bubble flow in large diameter tubes. Hughamark [26] proposed to use the maximum bubble diameter calculated from the fluctuating turbulent velocity of the fluid.

Brauner [23] concluded the transition to disperse bubbles should be carefully up scaled specially in vertical pipes where the models showed the maximum variation, around  $E\ddot{o}=5$ . This Eötvös number corresponds to the small diameter pipe, approximately  $ID=2.0$  cm.

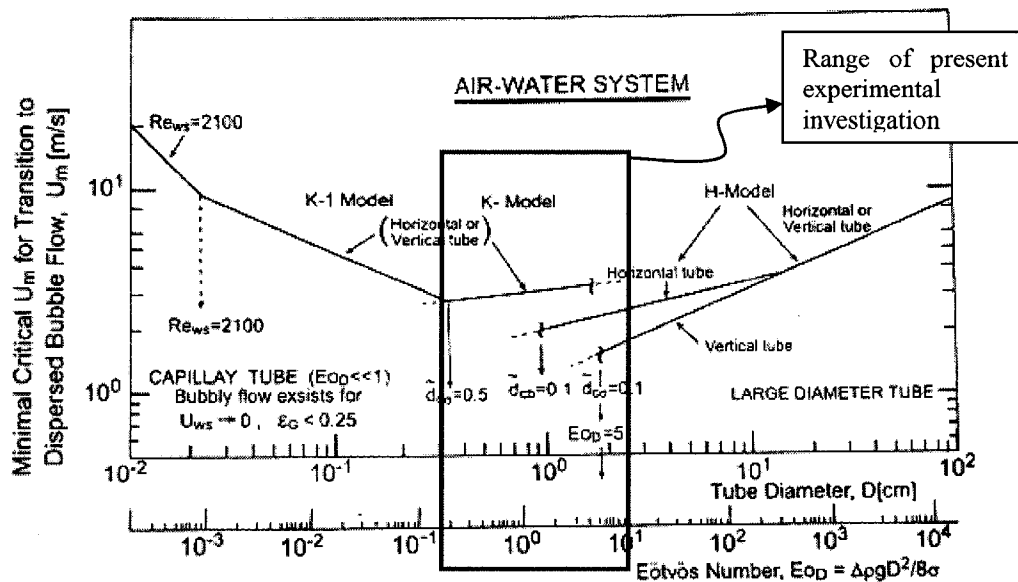


**Figure 2.4** The effect of the Eötvös Number on the minimal mixture velocity required for establishment of dispersed bubble flow in terrestrial air-water systems [23].

In this study, the tubing size classification suggested by Brauner [23] will be used with some modifications. By elaborating on the intermediate pipe diameter region, the following classification of pipe diameters will be adopted in this research:

Capillary tube:  $ID < 3.0$  mm

Small diameter tube:  $3.0 \text{ mm} < ID < 25$  mm

Conventional diameter tube:  $25\text{mm} < ID < 100\text{mm}$

Large diameter tube:  $ID > 100$  mm.

#### ***2.2.2.2 Flow pattern transition maps for conventional vertical pipes***

For a 50 mm ID riser (conventional diameter pipes  $25\text{mm} < ID < 100\text{mm}$ ) and using a number of mechanistic models suggested and validated for air-water at (close to) standard conditions, Taitel and Barnea [19], mapped the transitions boundaries and flow patterns zones (Figure 2.5). The flow pattern map uses the superficial velocities of the liquid and the gas as coordinates. For each pair of gas-liquid and local PVT properties, a new map has to be first obtained to define the specific, local flow pattern. Changing of pipe diameter and particularly deviation from vertical position requires a re-visited set of mechanistic models. Similar maps (using superficial velocities as co-ordinates to collect laboratory observations) have been initially suggested by Wallis [29], and Govier and Aziz [30]; however, Taitel and Barnea [19] have been pioneering the full use of mechanistic models and complete calculation procedures [65].

Dimensional maps as shown in Figure 2.5, ( $U_l^s$  versus  $U_g^s$ ) have been generalized by contemporary researchers and used as valuable tools for engineering design since they allow quick comparisons among various pipe diameters within the conventional-diameter region.

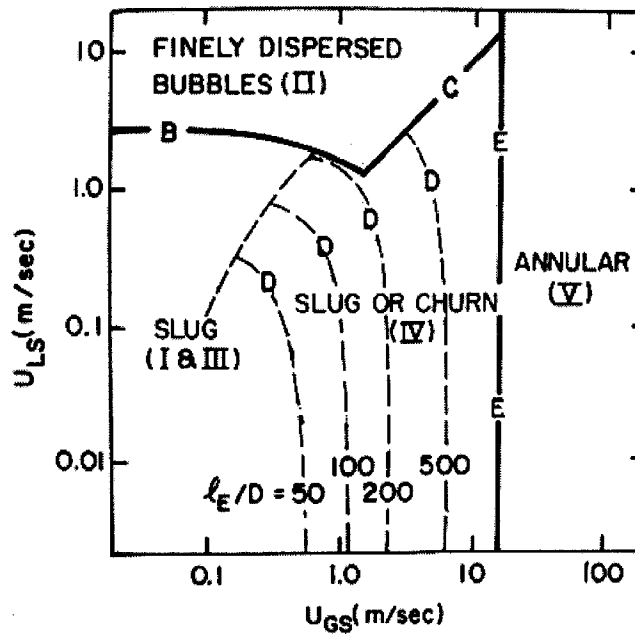


**Figure 2.5** Taitel-Dukler-Barnea flow pattern map for a vertical tube: 5.0 cm diameter, air-water at 25 °C, 10 N/cm<sup>2</sup> [19].

### Dispersed bubble (DB) – bubble (BB) transitions

The balance between turbulent and surface tension forces dominating the breaking and coalescence mechanism was used to develop calculation criteria used to determine the transition boundary between disperse bubble and bubble patterns (Curve B, Figure 2.5).

Hinze [13] proposed a critical Weber Number ( $We = 30$ ) to define the maximum stable bubble diameter ( $d_{max}$ ) under certain conditions of turbulence. His study led to the following relationship:

$$d_{max} = k \left( \frac{\sigma}{\rho_1} \right)^{\frac{3}{5}} (\varepsilon)^{-\frac{2}{5}} \quad 2.4$$

where  $\varepsilon$  is the rate of energy dissipation per unit mass,  $k$  is a constant that he calculated as 0.725 using experimental data from Clay [26]. Later on, Sevic and Park [27] developed theoretical values of  $k$ ;  $k = 0.68$  for drops (density of dispersed phase  $\gg$

density of continuous phase) and  $k=1.41$  for bubbles (density of dispersed phase  $\ll$  density of the continuous phase).

The rate of energy dissipation per unit mass for turbulent pipe flow,  $\varepsilon$ , is given as follows:

$$\varepsilon = \left| \frac{dp}{dz} \right| \frac{U_m}{\rho_m} \quad 2.5$$

$$\left| \frac{dp}{dz} \right| = \frac{f}{2D} \rho_m U_m^2 \quad 2.6$$

The equation 2.6 is indicating the frictional pressure loss through the pipe where  $D$  is internal diameter,  $f$  is the Moody friction factor;  $U_m$  is the mixture velocity calculated from the superficial velocities (Equation 2.7) and  $\rho_m$  is the density of the mixture.

$$U_m = U_g^s + U_l^s \quad 2.7$$

$$U_{\text{Phase}}^s = \frac{Q_{\text{phase}}}{A} \quad 2.8$$

$U_{\text{Phase}}^s$  is the superficial velocity of the phase (liquid or gas) calculated as the ratio of the flow rate,  $Q_{\text{phase}}$ , to the cross sectional area of the pipe,  $A$ .

The braking-coalescence equilibrium mechanism used to calculate the dispersed bubble domain is altered when the gas concentration in the liquid phase is high enough to promote coalescence of the bubbles and form a new transition border from disperse bubble to bubble flow. This is further avoided if the turbulence of the mixture contains enough energy to break the bubbles and create micro-spherical undistorted, very stable, micro- bubbles. Brodkey [28] defined this critical bubble size as:

$$d_{\text{crit}} = \left[ \frac{0.4\sigma}{(\rho_l - \rho_g)g} \right]^{\frac{1}{2}} \quad 2.9$$

When the  $d_{\text{max}}$  is less than  $d_{\text{crit}}$  the bubbles remain undistorted and spherical and travel without coalescing. This characteristic prevails up to a point where the fraction of gas in the mixture (void fraction  $\alpha$ ) is 0.52 considering as the maximum packing density. The curve C in Figure 2.5 represents the boundary disperse bubble (DB) –slug (S) and DB-Annular (A) describing this condition.

### **Bubble (BB) – slug (S) transition**

In the bubble-flow pattern, a population of deformable Harmathy [21] bubbles travels within the liquid describing a spiral path. If the gas fraction is increased, the bubbles will have not enough room to travel freely and coalesce in a bigger bubble. This process will continue until the void fraction is very close to 0.25 where the transition from bubble to slug flow begins (Curve B, Figure 2.5).

The transition from bubble to slug flow regime is accelerated when the diameter of the tubing is reduced. If the pipe diameter is smaller than certain critical value ( $D_{\text{crit}}$ ), the bubbles will be forced to coalesce prompting the transition to slug flow pattern. This critical pipe diameter is presented in Equation (2.6) [38].

$$D_{cr} = 19 \sqrt{\frac{\Delta\rho\sigma}{\rho_l^2 g}}, [\text{m}] \quad 2.10$$

Equation 2.10 demonstrated again that the diameter of the pipe is important when defining the transition boundary between bubble (BB) and slug (S) flow regime.

### The Drift Flux Velocity Concept

In the bubble flow, the liquid and gas travel at different velocities creating a “slip velocity” between the phases. Nicklin [31] using his drift flux model explained the gas velocity in the bubble flow pattern.

$$U_g = C_o U_m + U_{t\infty} \quad 2.11$$

$$U_{t\infty} = 1.53 \left[ \frac{\Delta\rho g \sigma}{\rho_l^2} \right]^{0.25} \quad 2.12$$

Where  $C_o$  is the distribution coefficient generally assumed to be equal to 1.2,  $U_m$  is the transport velocity [m/s],  $U_{t\infty}$  [m/s] is the terminal velocity of bubbles described by Harmathy [21],  $\rho$  is the density [Kg/m<sup>3</sup>],  $g$  is the acceleration of the gravity [m/s<sup>2</sup>], and  $\sigma$  is the liquid surface tension [N/m].

Harmathy [21], by using experimental data from different sources, found that in the range of  $E\ddot{o}$  between 1.0 and 13, the terminal velocity of a deformable bubble is a direct function of the liquid properties but not of the bubble equivalent diameter (Equation 2.12). When  $E\ddot{o}$  is less than 0.1, the bubble diameter is expected to be important. Equation 2.12, disregarding the effect of fluid viscosity could also cause unrealistic predictions of the terminal velocity.

### Slug (S)- annular (AN) transition

The slug (S) –Annular (AN) transition (curve E in Figure 2.5) is determined by the turbulence forces of the gas phase that breaks and atomizes the liquid film wavy interface. The entrainment of liquid droplets in the gas core will depend on the drag forces acting at the interface. Turner et al. [5] suggested that annular flow cannot exist, unless the gas velocity in the gas core is sufficient to lift the entrained droplets. When the gas rate is insufficient, the droplets fall back, accumulate, and form a bridge leading to a churn or slug flow. The critical gas transition velocity is given by:

$$U_g^s = 3.1 \left( \frac{\sigma g [\rho_l - \rho_g]^{1/4}}{\rho_g^{1/2}} \right) \text{ [m/s]} \quad 2.13$$

The superficial velocity  $U_g^s$  depends only on the local fluids properties and the acceleration due to gravity ( $g$ ). Because the value is independent of the flow rate and pipe diameter, the transition to annular flow will vary only if the fluid properties are altered. This may very well occur during the upflow transport of gas and liquid due to the salient effect of decreasing the gas density. At a certain level, the actual gas velocity surpasses the critical transition one.

### 2.2.3 Two-phase flow patterns in vertical small diameter pipes

The characteristics of the flow patterns observed in small diameter pipes are different than that familiar to conventional diameters. Depending of the fluids and diameters, several patterns descriptions are presented in the literature. Mishima and Hibiki [22] identified four patterns in experiments conducted in pipe diameters of 4 mm and smaller: ( ), bubbly flow, slug flow, churn flow and annular flow.

In bubbly flow, Figure 2.6(a), bubbles tend to concentrate along the tube axis. Smaller bubbles form a spiral train, while larger bubbles with the diameter comparable to line up right next to each other to form intermittent bubble trains, without coalescing. This train of bubbles was also identified with capillaries.

In slug flow, Figure 2.6(b), the TD bubbles are long with a more spherical nose than observed with conventional pipes. In the liquid slug, oscillating small bubbles (yet not similar to Harmathy [21] bubbles that was described for conventional diameter pipes) were observed. This pattern has been subdivided by other authors such as Barnea, Luninski and Taitel [32] into elongated bubble and slug patterns, both included into the intermittent flow regime.

In churn flow, Figure 2.6(c), long slug bubbles are deformed and do not have a spherical nose anymore, a number of tiny bubbles were observed moving rapidly in liquid slugs.

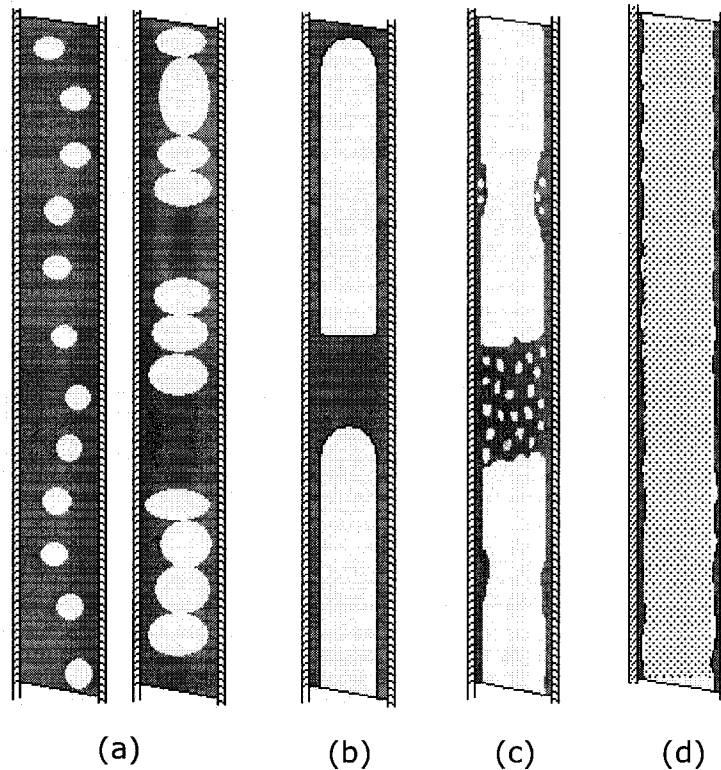


**Figure 2.6** Flow patterns in small diameter pipe. (a) Bubble flow, (b) slug flow, (c) churn flow, (d) annular flow.

The Annular flow, Figure 2.6(d), showed similar characteristics as observed in conventional diameter pipes, indicating a core containing a mist flow and an annulus formed by a liquid film moving upwards to the top.

### ***2.2.3.1 Flow pattern transition maps in small diameter pipes***

Barnea, Luninski and Taitel [32] studied the effect of the surface tension on the transitions boundaries for multiphase flow in small diameter pipes. They concluded that the boundaries for vertical small diameter pipes are in agreement with those proposed for Taitel and Barnea [19] for conventional diameter pipes. Later, Mishima and Hibiki [22] evaluated the flow transitions by using the Mishima-Ishii's model [33]. They concluded that if the differences in the definition of flow regimes are taken into consideration, the

results from Taitel-Barnea [19] and Mishima –Ishii’s [33] models agreed fairly well with each other. They also found the Mishima and Ishii’s model is applicable to capillary tubes with diameters between 1mm to 4 mm.

Figure 2.7 shows the transition maps presented by Barnea-Luninski and Taitel [33] for pipes with 4.0 and 12.3 mm. The open circles represent the elongated bubbled pattern corresponding to a train of bubbles separated by small liquid slugs. This is considered as a special pattern for small diameter pipes and it was included inside the generalized term of intermittent flow pattern (I). The black circles correspond to the slug flow that was also included in the intermittent region. The half black-half white circles identify the churn flow pattern region. The open triangles indicate the presence of annular flow (A). The black-downward triangles represent the disperse bubble pattern (DB).

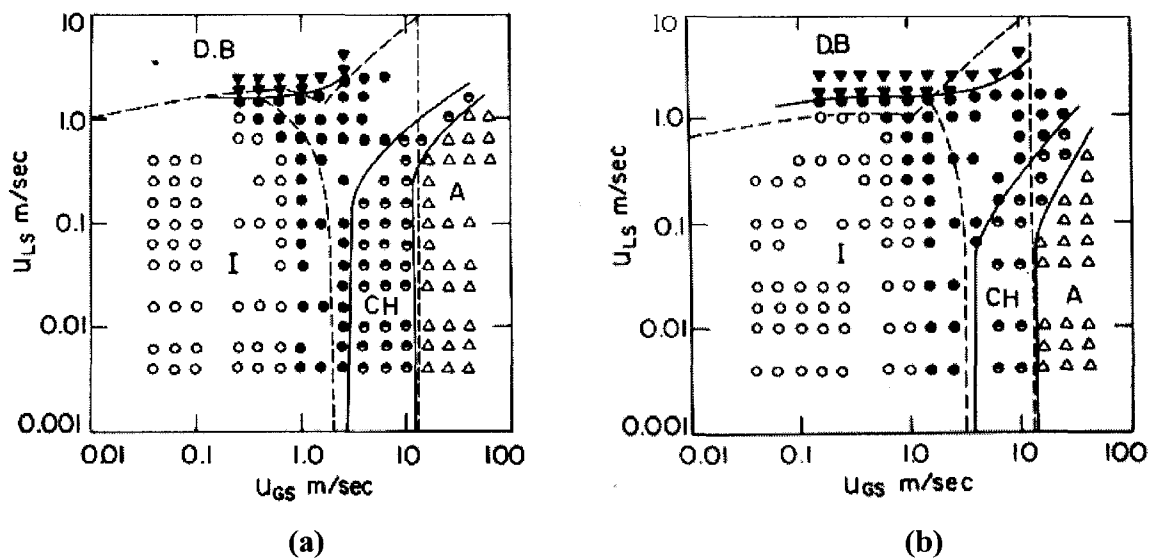


**Figure 2.7** Flow pattern map, upward vertical flow: air/water, 0.1 MPa, 25 °C. (a) For 12.3 mm pipe. (b) For 4 mm pipe [32].

For both cases of 12 and 4 mm diameter tubes, the prediction of the transition boundaries was very close with respect to the experimental data. Taitel and Barnea [19] model (solid lines) was used to compare the experimental data (dashed lines). The analytical boundaries almost overlap the transition lines drawn by using the experimental data. It was seen that the analytical model proposed by Taitel and Barnea could be accurately

used in the prediction of the transition lines. The criteria used for the flow pattern transitions in conventional pipes were valid for small diameter pipes as well.

In Figure 2.8 the axis represents the liquid and the gas superficial velocities, labeled by authors,  $J_L$  and  $J_G$  respectively [22]. The circles represent the bubble flow (B). The triangles represent the slug flow pattern (S). The squares represent the churn flow (C), and the rhombuses represent the annular flow pattern (A). The solid lines correspond to the transition limits predicted by the Mishima-Ishii model and the dashed lines those predicted by Taytel and Barnea model. In this map the transition lines predicted by Mishima-Ishii's model were also valid for capillary tubes. Mishima and Hibiki [22] observed the boundaries described for the experimental data agrees fairly good with the predictions made by those two models. They also validated predictions of the Mishima-Ishii's model by comparing data obtained from capillaries (pipe diameter of 2 mm).

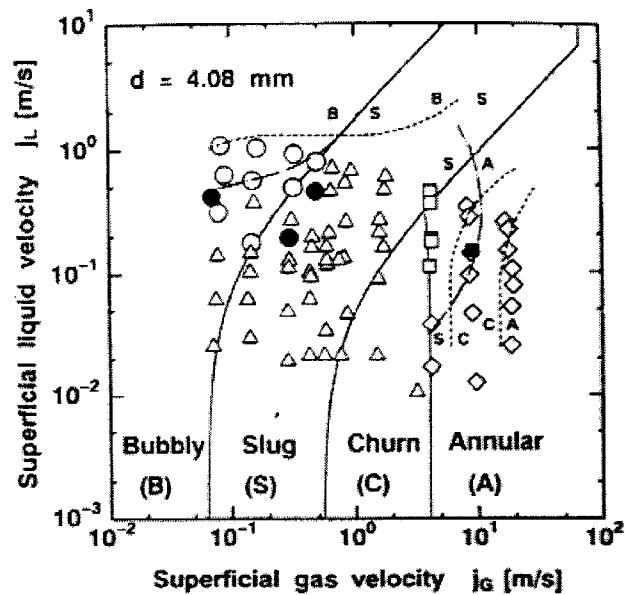


**Figure 2.8** Flow regime map for  $d=4.08$  mm [22].

#### 2.2.4 Flow patterns in capillaries

Capillaries were previously defined as the pipes with diameters less than 3.0 mm. Liquid surface tension and viscosity, and solid wettability are the main parameters that controls

the flow patterns and flow characteristics in capillaries. The patterns described for small diameter pipes are also applicable in vertical capillaries [22]. The most common flow patterns observed in vertical capillaries are: bubble, train of bubbles, slug, churn and annular flow. The nomenclature used for intermittent flow regime varied from one author to another. For instance, the “Train of Bubble” pattern defined by Stark and Manga [34] was denominated “Elongated Bubble” by Barnea-Luninski-Taitel [32] and Coleman-Garimella [35], and “Plug Flow” by other authors [36]. This discrepancy in nomenclature creates difficulties when making comparisons and cross-examinations.

#### ***2.2.4.1 Flow pattern transition maps for capillaries***

Although much work has been performed on gas-liquid two-phase flow in conventional diameter tubes, only a limited number of papers are available for capillary tubes. Among them Kariguazaki [36], Fukano et al. [37], and Barnea et al. [32] investigated flow regimes and transitions maps for multiphase flow in capillaries. Fukano et al. [37] performed extensive work on the two phase flow in capillary tubes, including the flow regimes, raise velocity of slug bubbles, void fraction, liquid film thickness and pressure loss.

Mishima-Hibiki [22] determined flow patterns and boundary transitions for a water-air mixture in capillaries from 1.0 to 4.0 mm diameter. In Figure 2.9, the solid lines correspond to the Mishima-Ishii model [33] and the dashed lines to the Kariyasaki et al. model [35]. The geometric figures used to represent a specific flow pattern are the same as described above for small diameter pipes.

The prediction made by Mishima-Ishii’s model [33] agrees well with the experimental data demonstrating this model is suitable for the prediction of flow pattern transition boundaries in capillaries.

The slug and the elongated trend of bubbles are the most common patterns in gas lifting using conventional and small diameter pipes respectively. Therefore, it is important to define critical differences between those flow patterns and understand relevant physics behind them.

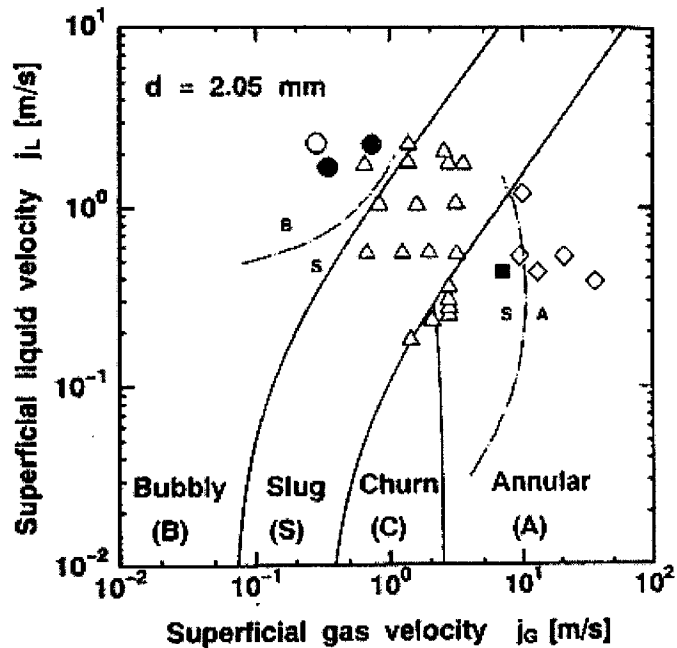


Figure 2.9 Flow regime map for  $d = 2.05$  mm [22].

### 2.3. Slug Flow and Elongated bubble flow pattern

#### 2.3.1 Slug flow pattern in vertical pipes

The slug flow is one of the most frequent patterns that appear in two-phase flow in conventional pipes. The slug flow can also be observed in inclined and horizontal pipes. In vertical pipes, the transition from bubble flow pattern to slug one occur when the gas flowrate is increased and the void fraction reaches a value of 0.25 and the liquid turbulent energy is not enough to split the long bubbles formed.

The slug flow pattern contains particular characteristics that clearly differentiate it from the rest of the patterns. The main feature of the slug flow (Figure-2.10) is the existence of a long axis-symmetric bubble called “Taylor-Dumitrescu (T-D)” bubble “ $L_{T-D}$ ”. The T-D bubble has a well-defined bullet-shape tip. A thin liquid film, which surrounds the T-D bubble and flows downward, is called liquid fallback. The liquid drains downwards

and falls into the next sub-section called Liquid Slug “ $L_{SL}$ ”. The liquid slug contains small deformable bubbles called Harmathy bubbles. The combination of the liquid slug and the T-D bubble forms a complete slug unit “ $L_U$ ” (Figure 2.10).

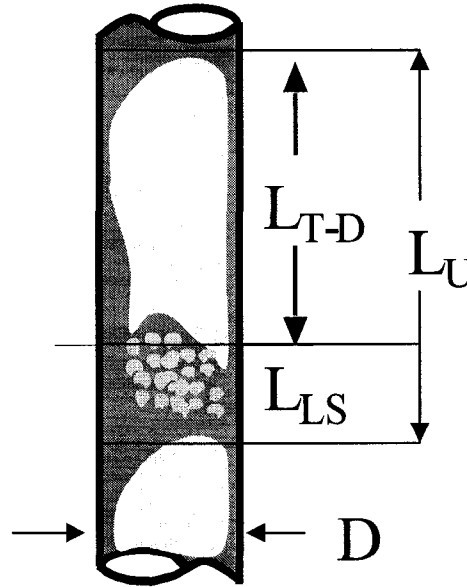


**Figure 2.10** Slug flow pattern in conventional pipes [38].

The Taylor-Dumitrescu bubble [39] is a large bubble, usually created by the coalescence of smaller bubbles. While it is forming, the T-D bubble accelerates inside the pipe until reaching a constant velocity. Taitel et al. [19] suggested that a stable slug is the one, which is long enough such that the velocity profile at the slug rear is already fully developed. The terminal velocity of a T-D bubble (Equation 2.14) was studied by Taylor and, previously, by Dumitrescu [39] in a stagnant fluid. Further experiments have been also performed by Nicklin [20]. Equation 2.14 describes the ascending, terminal velocity of a T-D bubble:

$$U_{T-D\infty} = 0.35 \left( \frac{gD\Delta\rho}{\rho_l} \right)^{1/2} \quad 2.14$$

Where,  $g$  is the acceleration of the gravity and  $D$  is the diameter of the pipe,  $\Delta\rho$  is the buoyant phase density difference and  $\rho_l$  liquid density.

Nicklin [20] observed (for conventional tube diameters) that the T-D bubble rising in a vertical pipe travels closer to the pipe's centreline. Nicklin [20] also observed that T-D bubbles move at relatively higher velocity than the liquid slug moving at its top.

The drift-flux (Equation 2.15) introduced first by Nicklin, estimates the actual gas velocity of the gas phase as function of transport velocity and terminal bubble (T-D) velocity. The coefficient  $C_o$  is generally 1.2.  $U_l$  is the liquid slug velocity just above the bubble that is usually considered very close to the mixture transport velocity  $U_m$ .

$$U_g = C_o U_l + U_{T-D\infty} \quad 2.15$$

The equation 2.15 will be used later for modeling slug flow in vertical pipes.

The liquid fall back surrounding the T-D bubble has a thickness in a range of 0.5 to a few millimetres. Therefore, the negative effect of transporting the liquid downwards is ignored in some mathematical models representing slug flow for conventional diameter tubes [41].

The gas-liquid transport-related turbulence brakes the tail of T-D bubble into small and deformable bubbles called Harmathy "H" bubbles (similar to those typical for bubble flow in conventional pipes) [20] transported in the liquid slug unit.

The relative rising velocity between the T-D bubble and the "H" bubbles in a slug unit, will define the stability of the large T-D bubble. When the T-D bubble terminal velocity is smaller than the "H" bubble terminal bubble velocity ( $U_{T-D\infty} < U_{t\infty}$ ), the large population of deformable "H" bubbles will collapse into the upper T-D bubble and enlarging it. Barnea et al. [40] described this new pattern as "Elongated Bubble Pattern".

The critical diameter pipe,  $D_{cr}$ , at which the transition to "Elongated Bubble Pattern" will occur (absence of bubble flow in the liquid slug), can be obtained by equating the

terminal T-D bubble (Equation 2.14) and “H” bubble (Equation 2.12) velocities. The equation describing the critical diameter pipe,  $D_{cr}$ , is presented in Equation 2.10.

### 2.3.2 Elongated bubble pattern in vertical pipes

Barnea et al. [40] defined the “Elongated Bubble Pattern” as the limiting case of slug, where the liquid slug is almost free of entrained gas bubbles. This pattern is common in small diameter pipes. As observed in Figure 2.11, all the gas is contained into the T-D bubbles,  $L_{T-D}$ , while the liquid slug,  $L_{SL}$ , is free of Harmathy bubbles. Sometimes this flow can allow the formation of small (spherical) bubbles in the liquid slug, but usually those bubbles do not correspond to the deformable Harmathy bubbles. Usually those bubbles are found when liquid surface tension and viscosities are low. In an air-water system the suggested critical diameter,  $D_{cr}$ , for this pattern is  $D=5.0$  cm [40].

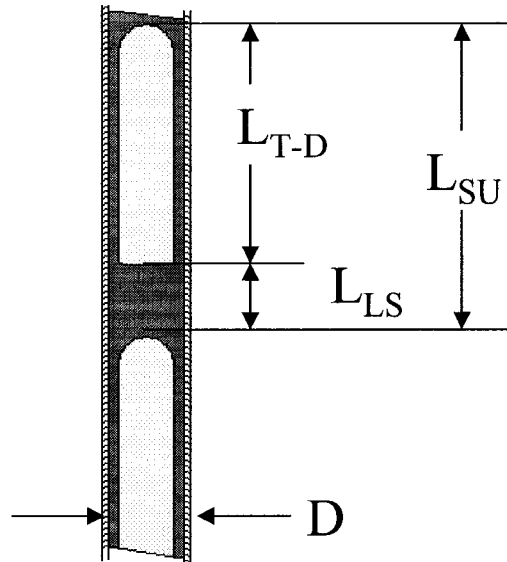


**Figure 2.11** Elongated bubble pattern in small diameter pipes [38]

For small diameter pipes, the effect of liquid surface tension has been proved to be an important parameter on the TD-bubble’s terminal velocity. Wallis [29] analyzed the general case of the flow of a T-D bubble in stagnant liquids where, besides the buoyancy force of the bubble, the liquid inertia, liquid viscosity and surface tension forces are

significant. The balance between these three forces was represented in terms of three dimensionless parameters. Wallis [29] presented the following empirical correlation for  $U_{T-D\infty}$ :

$$U_{T-D\infty} = K \left[ gD \left( \frac{\rho_l - \rho_g}{\rho_l} \right) \right] \quad 2.16$$

where the factor K is expressed in terms of the dimensionless inverse viscosity number,  $N_L$ , and Eötvös number,  $E\ddot{o}$ , defined by:

$$N_L = \frac{[D^3 g(\rho_l - \rho_g) \rho_l]}{\mu_l} \quad 2.17$$

$$E\ddot{o} = \frac{gD^2(\rho_l - \rho_g)}{\sigma} \quad 2.18$$

where  $\mu_l$  is the liquid viscosity and  $\sigma$  is the surface tension.

The empirical relationship for K is the following:

$$K = 0.345 \left( 1 - e^{\frac{-0.01N_L}{0.345}} \right) \left( 1 - e^{\frac{(3.37-E\ddot{o})}{m}} \right) \quad , \quad 2.19$$

where  $m$  is a function of  $N_L$ ,

$$m = 10 \quad \text{for} \quad N_L > 250$$

$$m = 69N_L^{-0.35} \quad \text{for} \quad 18 < N_L < 250$$

$$m = 25 \quad \text{for} \quad N_L < 18$$

According to Wallis [29] the inertia dominant regime (i.e., when liquid viscosity and surface tension forces can be neglected) is defined when [29, pp. 288]  $N_L > 300$  and  $E\ddot{o} > 100$ . If in addition to that,  $\rho_l \gg \rho_g$  then the result of Dumitrescu [39] is obtained (Equation 2.14) [50, pp. 58].

In a water/air system the limiting condition  $E\ddot{o}=100$  corresponds to a tube diameter of 27 mm.

Similar conclusions were obtained from the analytical studies made by White and Beardmore [42] who expressed the terminal velocity of gas slugs in terms of a dimensionless Froude Number,  $F_R$ .

$$F_R = U_{T-D\infty} \left( \frac{\rho_l}{(\rho_l - \rho_g)gD} \right)^{1/2}, \quad 2.20$$

which depends on the Eötvös number ( $E\ddot{o}$ ) and the Morton number ( $Mo$ )

$$M_o = \frac{g\mu_l^4 \Delta\rho}{\rho_l^2 \sigma^3}, \quad 2.21$$

where  $\Delta\rho$  is the two-phase density difference,  $\sigma$  the surface tension,  $\mu$  the dynamic viscosity, and the “l” subscript represents the liquid phase.

For low viscosity and high surface tension systems such as air/water flow systems and a sufficiently large-diameter tube, the Morton number (Equation 2.19) is rather small (on the order of  $10^{-10}$ ) compared with the Eötvös number ( $E\ddot{o} = 100$ ), and the terminal velocity of the gas slugs thus depends on the Eötvös number,  $E\ddot{o}$ , only, i.e.

$U_{T-D\infty} = 0.35 \left( \frac{gD\Delta\rho}{\rho_l} \right)^{1/2}$  which indicates that the terminal velocity of the bubble in a vertical tube with a large-diameter is proportional to  $(gD)^{1/2}$  [57].

Reinemann et al. [42] used the analysis made by White and Beardmore [44] to evaluate the effect of surface tension in small diameter pipes. When the effects of viscosity can be neglected, as in air/water systems,  $F_R$  can be expressed as a function of the surface tension parameter alone [43,44]:

$$U_{T-D\infty} = (g * D)^{1/2} * 0.352 * (1 - 3.18 * \Sigma - 14.77 * \Sigma^2) \quad 2.22$$

where  $\Sigma$  is the surface tension number (or inverse Eötvös number),

$$\Sigma = \frac{1}{Eo} = \frac{\sigma}{\Delta\rho * g * D^2} \quad 2.23$$

Reinemann et al. [42] concluded also (similarly than in Wallis' [29] study) that the effect of surface tension is significant when the diameter of the pipe is less than 20 mm (i.e. in a air/water system)

Another expression for the T-D terminal velocity,  $U_{T-D\infty}$ , was proposed by Tung and Parlange [45]. They suggested the terminal velocity for a T-D bubble in a stagnant fluid could be determined by:

$$U_{T-D\infty} = (g * D)^{1/2} * \left[ 0.272 - \frac{0.472 * \sigma}{\Delta\rho * g * D^2} \right]^{1/2} \quad 2.24$$

This equation also predicts a terminal velocity equal to zero when the tubing diameter is about 4 mm ( $E\ddot{o} = 3.37$ ) and the gas and liquid physical properties are the air and water measured at standard conditions, respectively.

For small diameter tubing,  $d < 4\text{mm}$ , the T-D bubble terminal velocity approaches zero, which means the frictional forces overcome the buoyancy forces and the bubble will not rise under the buoyant forces anymore. Mishima and Hibiki [22] used this concept in their experiments with small diameter tubes.

## 2.4 Previous experiments in small and conventional diameter pipes

### 2.4.1 Experiments with small diameter pipes

The technology of gas lifting in small diameter pipes has been used in the nuclear power industry to transport high-temperature wastewater. The necessity to determine the effectiveness of the transport promoted several researches about this topic. Kouremenos

and Staicos [46], and Reinemann et al. [42], studied the pumping efficiency of the gas lifting in small diameter pipes. Reinemann also investigated the influence of surface tension on the upward gas velocity and derived a model to predict the liquid production and pumping efficiency as a function of the gas injection rate. Cachard and Delhaye [47], observed instabilities while pumping in small diameter pipes at submergence values as low as 0.5. They proposed a combined mathematical analysis for the frictional pressure losses by interpolating results from the slug flow and the churn flow models.

#### 2.4.1.1 Experimental data Kouremenos and Staicos [46]

Kouremenos and Staicos [46] used tubes with four different internal diameters  $D$  ( $D=12.00, 14.50, 16.00, 19.23$  mm). The submergence values varied from 0.7 to 0.55. Data obtained for the 12.00 mm and 19.23 mm riser is shown in Figures 2.12, 2.13.

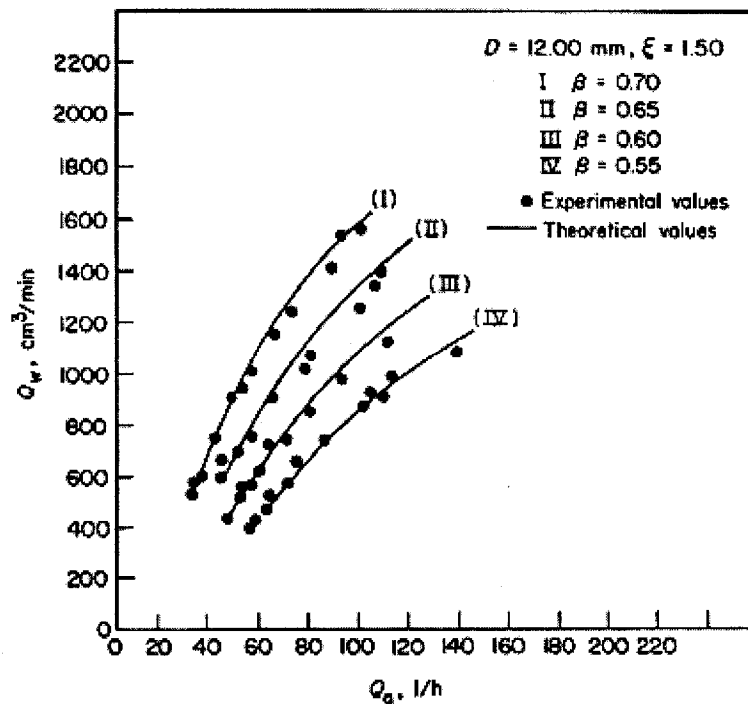


**Figure 2.12** Relationship between volumetric flow rate of water discharge and air supplied for  $D=12.00$  mm. [46]

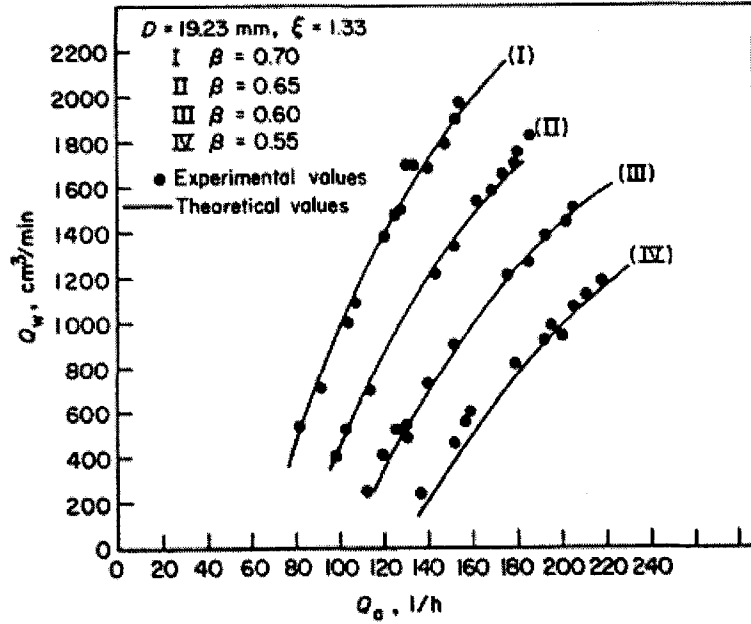


**Figure 2.13** Relationship between volumetric flow rate of water discharge and air supplied for  $D= 19.23$  mm. [46]

The periodical gas injection produced a “perfect” slug flow that generates families of curves depending of the diameter of the riser. The recorded parameters were the submergence value, (defined by the authors as  $\beta$ ), the gas flow rate,  $Q_a$ , and the liquid production,  $Q_w$ .  $\xi$  is defined as the ratio between the internal pipe diameter and the external gas injection tube diameter, and remained constant during the experiment.

The liquid production rate,  $Q_w$ , was well predicted [46] by the equation 2.25 which was derived from a momentum balance equation by taking the pressure losses at the suction pipe, injection valve and riser into consideration.

$$\frac{Q_w}{(A_o (2gl)^{0.5})} = f \left( \frac{Q_w}{Q_a} \right) \quad 2.25$$

Where  $A_o$  is the cross section area of the pipe,  $g$  is the acceleration of the gravity,  $l$  is the length of the riser measured from the gas injection point and  $f$  is the friction factor.

Even though it is shown this model matches the experimental data considerably well, the artificially ideal slug flow pattern created with the apparatus barely represents the real cases [47]. This study was the first attempt to explore air lifting with small submergence values. It also considered for the first time the entrance pressure losses effect.

#### ***2.4.1.2 Experimental data Reinemann et al. [42]***

The experiments conducted by Reinemann et al. [42] used 1800 mm long risers with diameters varying from 3.18 mm to 19.1 mm. The study investigated submergence values as low as 0.6.

The efficiency of the airlift pumping seems to be higher for smaller diameter pipes at lower gas injection rates. For example, in a 6 mm riser the efficiency is close to 0.8 at a dimensionless gas flow rate of 0.2, while for a 9 mm riser the efficiency is almost equal to zero under the same conditions.

Reinemann et al. [42] also developed a theoretical model to evaluate the air pumping efficiency as a function of the dimensionless air flow rate. They concluded that the surface tension has a significant effect on the terminal velocity of T-D bubble. They also demonstrated that the results predicted by the drift flow model proposed by Nicklin [20] could be extended to small diameter pipes. In addition, they calculated a distribution coefficient ( $C_o$ ) by measuring the rising velocity of the T-D bubble in the last meter of the tube for a single and a train of T-D bubbles. They proved experimentally that the value of  $C_o$  (that usually is assumed 1.2) increases as the liquid flow is laminar. Even though a significant lifting efficiency is obtained at low airflow rates, the eventual increment in  $C_o$ , produces higher frictional pressure losses counterbalancing the benefit obtained in efficiency with the diameter reduction.

The experimental results matched fairly well with theoretical values for higher submergence values. For submergence lower than 60%, the theory does not seem to predict well the experimental results.

### 2.4.1.3 Experimental data Cachard and Delhaye [47]

Cachard and Delhaye [47] focused their efforts to predict the frictional pressure losses in slug and churn flow pattern. They developed a model to evaluate the frictional pressure losses in gas lifting systems with tubing diameters less than 40 mm and length/diameter ratios higher than 250.

Cachard and Delhaye [47] also conducted some experiments using a 10 mm diameter riser. They compared their experimental results with the predictions from their model as well as the Reinemann's et al. model [42] (Figure 2.14).

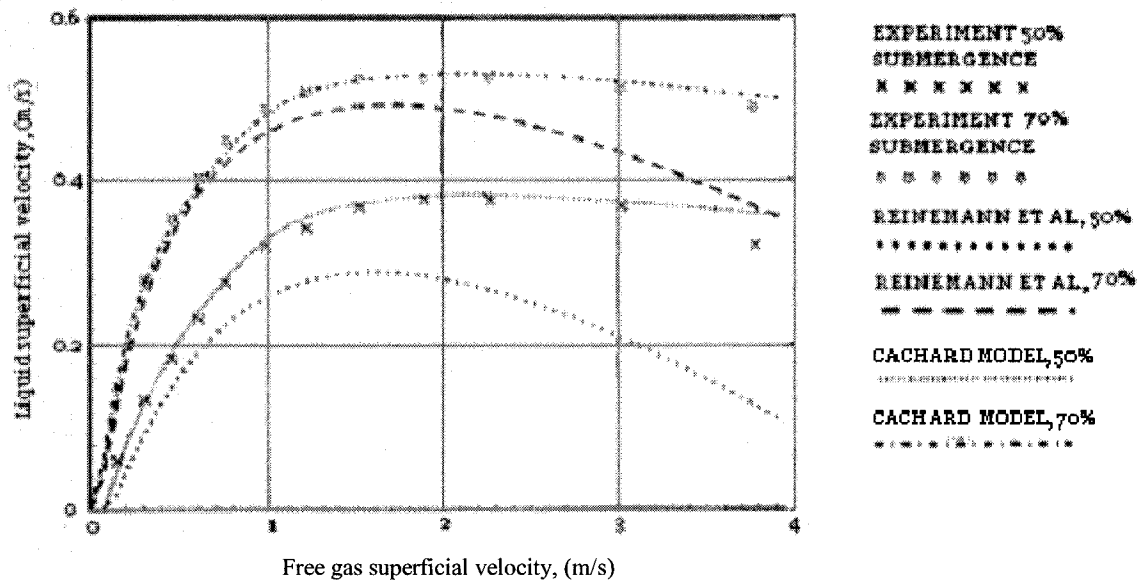


**Figure 2.14** Airlift pumping performance: experimental results vs. Cachard and Reinemann model predictions. [47]

They concluded that the differences observed between the experimental data and the Reinemann's et al. model [42] predictions are due to the fact that the model [42] did not consider changes in gas density for long risers ( $L/D > 250$ ) and neglect the liquid falling back film effect around the T-D bubble. The liquid falling back film produces a wall friction force pointing upwards, which reduces the overall frictional pressure losses of the system. Reinemann's model neglected this effect, therefore his model over estimates the frictional pressure losses and under-predicts the produced liquid flow rates, as observed

in Figure 2.14. This problem was partially solved by Cachard and Delhaye's model after calculating the frictional pressure losses as a linear interpolation between the values obtained from the slug and the churn models, which considered the liquid falling back effect.

Even though Cachard and Delhaye's model [47] gives reasonable pressure losses predictions, it presents extra difficulty in terms of practical application due to the complexity of combining two model results. Therefore, a better calculation model for small diameter gas lifting systems is still a necessity.

#### **2.4.2 Experiments with Conventional diameter pipes**

Many researchers [32,40,50,61-64], conducted experiments using conventional diameter pipes for flow pattern transitions as well as illustration of void fraction and pattern characteristics. They performed their experiments under continuous liquid and gas flow. Few of the experiments have been conducted to investigate liquid production using natural buoyancy effect in conventional diameter pipe [48].

Lawniczak et al. [48] was one of the researchers who investigated the air lifting performance in conventional pipes using natural buoyancy. They did experiments to improve the liquid production and minimize the pressure losses at the entrance by varying the design of the gas injector and the nozzle location.

Lawniczak et al. [48] evaluated the gas lift efficiency in two risers of 30 mm and 50 mm diameter and 1000 mm length. They analyzed the effect of different geometries of the gas injector under very low submergence values from 0.2 to 0.6. They observed an increasing liquid production while increasing the gas flow rate [Figure A1, Appendix A]. They found there is a critical gas injection point above which any incremental gas injection rate does not contribute to liquid production.

Guet and Ooms [49] performed experiments to investigate the effect of the nozzle position with respect to the centreline of the riser (i.e. concentric vs. eccentric) on the liquid recovery.

The experiments performed by Fernandes [50] evaluated the gas void fraction in a slug unit as well as in the T-D bubble using a magnetic tool. The liquid hold up and respective void fractions for all sections of the slug units are shown in table A.1 (Appendix A).

The experimental set up consisted of a riser of 38 mm ID and 10.084 m length riser with a gas injection inlet was located at the bottom of the tube just above the liquid injection point. The fluids were separated under atmospheric conditions at the tubing head. The liquid and the gas flow rates were set to provide all spectrums of flow patterns in vertical pipes: bubble, slug, churn, and annular flow.

A lump flow phenomenon was described by Fernandes [50] in detail and evaluated quantitatively. The lump flow was defined as a slug flow unit formed by a liquid slug rich in gas with a continuous liquid phase in the form of a foamy flow that traveled along the riser while flowing in slug, churn and annular flow pattern. The phenomenon had a remarkable periodicity and consistent characteristics, which undoubtedly interfered with the overall performance of each flow pattern.

## **2.5 Modeling slug flow in conventional and small diameter pipes**

### **2.5.1. Slug flow models in conventional and big diameter pipes**

Several literature models including Govier and Aziz [61], Begs and Brill [63], Hassan [41] and Ansari [52], were considered to determine the pressure losses in the pipe for slug flow pattern.

This research will use the models more recently developed by Hasan [41] and Ansari [52] and used by other investigators as benchmark, in order to determine their applicability in small diameter pipe gas lifting.

The main difference between the Hassan [41] and Ansari [52] models is the way that they calculated the void fraction. While Hasan's model uses semi-empirical equations to determine the void fraction in the liquid and T-D bubble zone, Ansari's model evaluated the void fraction by considering the liquid fall back in the material balance equation developed for the liquid slug unit.

The results provided in table A.1 (Appendix A) corresponds to the experimental data obtained by Fernandes et al. for a air/water system flowing under slug flow pattern under standard conditions in a 38 mm, 40 ft length ID tubing. This data are used as reference to evaluate and validate the Ansari [52] and Hassan [41] model predictions under isothermal low-pressure production conditions.

### 2.5.1.1 Hasan's Model [41]

The conventional slug flow pattern (Figure 2.10) is composed of three major sub-patterns: a) T-D rising bubble, b) a swarm of "Harmathy" ("H") type large bubbles (tailing the T-D bubble), c) fall-back liquid film.

To calculate the local averaged void fraction, Hasan combined the "H" and "TD" bubbles characteristics (Equations 2.26, 2.27).

An empirical approximation was used for estimating averaged void fraction,  $\alpha$  [53]:

$$\alpha = \frac{L_{T-D}}{L_U} \alpha_{T-D} + 0.25U_g^s \quad \text{for } U_g^s \leq 0.4 \text{ m/s} \quad 2.26$$

$$\alpha = \frac{L_{T-D}}{L_U} \alpha_{T-D} + 0.1 \quad \text{for } U_g^s > 0.4 \text{ m/s} \quad 2.27$$

A drift-flux model [20] was further used to estimate the local gas velocity  $U_g$  and the average void fraction at each specific section of the slug flow. For the T-D bubble region the void fraction is calculated using equation 2.28.

$$\alpha_{T-D} = \frac{U_g^s}{U_{gT-D}} = \frac{U_g^s}{C_o U_m + U_{T-D\infty}} \quad 2.28$$

For the liquid slug region the void fraction,  $\alpha_{LS}$ , is calculated with the equation 2.11,

$$\alpha_{LS} = \frac{U_g^s}{U_{gLS}} = \frac{U_g^s}{C_o U_m + U_{t\infty}} \quad 2.29$$

where terminal velocities for the T-D and the Harmathy bubbles, are given by equations 2.14 and 2.12, respectively.

The static and frictional pressure losses in the pipe where calculated using the equations 2.30 and 2.31, respectively:

$$\left(\frac{dP}{dL}\right)_{friction} = \frac{f_M \rho_m U_m^2}{2D} (L_{T-D}) \beta \quad , \text{ (Pa)} \quad 2.30$$

$$\left(\frac{dP}{dL}\right)_{static} = \rho_m g (L_{T-D}) \quad , \text{ (Pa)} \quad 2.31$$

$\beta$  is the ratio between the liquid slug length,  $L_{LS}$ , and the slug unit length,  $L_U$  (Equation 2.32).

$$\beta = \frac{L_{LS}}{L_U} \quad 2.32$$

Although, Hasan's model [44] (through the drift-flux model) considers the slip between the phases, it ignores the effect of liquid film fallback (considered negligible for conventional tubing slug/gas lift situations).

### 2.5.1.2 Ansari's Model [51]

Ansari's model [51] combined all the effects mentioned before, excluding interfacial tension, and uses a system of eighth linear equations describing mass balance for all three essential slug sub-patterns.

Ansari's model did consider the effect of downward falling liquid film for the analysis of the slug flow. Also, he evaluated separately the liquid hold up for both sections TD bubble and liquid slug. By combining mass balance equations and momentum equations for each section and overall slug flow, Ansari was able to determine the eight unknowns that describe a slug flow completely. The eight unknowns that define the slug flow model are:  $\beta, H_{LTD}, \alpha_{LS}, U_{gTD}, U_{LTD}, U_{GLS}, U_{LLS},$  and  $U_{TD}$ . The first attempt to obtain a complete description of a developed slug flow was given by Fernandes [50]. Ansari [51] proposed small variations to this model basically in the calculation of the gas velocity at the liquid slug section and using an analytical and numerical solution for the system of eight equations.

The equations and step-by-step procedure describing the model are given as follows:

1. Calculate T-D bubble velocity ( $U_{T-D}$ ) and liquid slug void fraction ( $\alpha_{LS}$ ) from:

$$U_{TD} = 1.2U_m + 0.35 \left[ \frac{gD(\rho_L - \rho_G)}{\rho_L} \right]^{0.5} \quad 2.33$$

$$\alpha_{LS} = \frac{U_g^s}{0.425 + 2.65U_m} \quad 2.34$$

2. Calculate the liquid hold up in the T-D bubble ( $H_{LTB}$ ) by using an iterative process. The eight equations could be combined into a single algebraic equation [54] given as follows:

$$(9.916\sqrt{gD})(1-\sqrt{1-H_{LTB}})^{0.5} H_{LTD} - U_{TD}(1-H_{LTD}) + \bar{A} = 0 \quad 2.35$$

$$\bar{A} = \alpha_{LS} U_{LTD} + (1-\alpha_{LS}) \left[ U_m - \alpha_{LS} \left\{ 1.53 \left[ \frac{\sigma_L g (\rho_L - \rho_G)}{\rho_L^2} \right]^{0.25} (1-\alpha_{LS})^{0.5} \right\} \right] \quad 2.36$$

3. Determine the liquid fall back velocity  $U_{LTD}$  using the Equation 2.36. This empirical equation was proposed by Brotz [55] based on experimental observations of liquid films falling along the surface of a vertical wall.

$$U_{LTD} = \sqrt{196.7 g \delta_L} \quad 2.37$$

Where the film thickness  $\delta_L$  is the geometrical average film thickness along the T-D bubble and given as follows:

$$\delta_L = \frac{D}{2} (1 - \sqrt{\alpha_{TD}}) \quad 2.38$$

4. Solve the following equation for the liquid velocity in the liquid slug ( $U_{LLS}$ ):

$$(U_{TDCC} - U_{LLS}) H_{LLS} = [U_{TD} - (-U_{LTD})] H_{LTD} \quad 2.39$$

5. Solve the following equation to calculate the liquid slug void fraction,  $\alpha_{LS}$ :

$$U_{gLS} = 1.2 U_m + 1.53 \left[ \frac{g \sigma_L (\rho_L - \rho_G)}{\rho_L^2} \right]^{0.25} (1-\alpha_{LS})^{0.5} \quad 2.40$$

6. Solve the following equation for the  $\alpha_{TB}$ :

$$(U_{TD} - U_{gLS})(1 - H_{LLS}) = (U_{TD} - U_{gTD})(1 - H_{LTD}) \quad 2.41$$

7. Calculate  $\beta$  from:

$$U_{LS} = (1 - \beta)U_{LLS}H_{LLS} - \beta U_{LTD}H_{LTD} \quad 2.42$$

8. Static and frictional pressure drops are calculated as a function of  $\beta = L_{TD}/L_U$

$$\left(\frac{dP}{dL}\right)_{friction} = \frac{f_{LS} \rho_{LS} \cdot U_m^2}{2D} \cdot (1 - \beta) \quad , \text{ (Pa/m)} \quad 2.43$$

$$\left(\frac{dP}{dL}\right)_{static} = ((1 - \beta) \cdot \rho_{LS} + \beta \rho_g) \cdot g \quad , \text{ (Pa/m)} \quad 2.44$$

In equations 2.28- 2.40, the nomenclature of the equations is given as follows:

$C_0$  is the distribution coefficient (usually  $C_0=1.2$ ),  $D$  is inside tube diameter, (m),  $f$  is the Moody friction factor calculated with Blasius equation (no roughness),  $g$  is the acceleration of gravity, ( $m/s^2$ ),  $H_{LTD}$  is the liquid holdup for the T-D bubble section,  $H_{LLS}$  is the liquid holdup for the liquid slug section,  $L_T = L_{T-D}$  is the Taylor-Dumitrescu bubble length, (m),  $L_U$  is the slug unit length, (m),  $U_{gLS}$  is the gas velocity in the liquid slug, (m/s),  $U_{LTD} = U_{film}$  is the falling-back liquid film velocity, (m/s),  $U_{LLS}$  is the velocity of the liquid in the liquid slug section, (m/s) and  $U_{TD}$  is the velocity of the T-D bubble, (m/s).

The average void fraction was represented by  $\alpha$ .  $\alpha_{LS}$  is the void fraction at the Liquid slug section,  $\alpha_{TD}$  is the void fraction at the Taylor-Dumitrescu bubble section,  $\beta$  is the ratio between  $L_{TD}$  and  $L_U$ ,  $\delta_L$  is the film thickness, (m), and  $\sigma$  is the surface tension, (N/m).

### 2.5.2 Slug flow model in Small Diameter Pipe- (Reinemann's Model [42])

Relatively few attempts have been made to model the slug flow in small diameter pipes. Barnea and Taitel [32] studied the transition boundaries between the flow patterns but they did not propose a model for the elongated bubble pattern they observed in small diameter pipes. Later on, Kouremenos and Staicos [46] proposed a model for the elongated bubble pattern under controlled conditions of gas injection for a “perfect” slug flow. They also considered the pressure losses that appeared at the injector section.

Reinemann et al. [42] proposed a model taking into consideration the effect of the surface tension on the rising velocity of the T-D bubble. The elongated bubble flow pattern was utilized for his calculations. The experiments were performed under standard conditions.

De Cachard and Delahye [47] developed a model for similar set of experiments and included a more accurate calculation of the frictional pressure losses, which has been overestimated before by interpolating between the pressure losses calculated for slug flow and the pressure losses calculated for churn flow.

For all practical purposes Reinemann's model [42] provides a quick estimation of the applicability of certain diameter pipe for unloading liquid under specific submergence value and gas flow rate, and can be used to evaluate the performance of the proposed gas lifting system.

The Reinemann's model [42] described the T-D bubble velocity using the Nicklin's theory [20] for drift flux (Equation 2.11).

Following the analysis used by Nicklin [20], the average void fraction  $\alpha$  can be represented by the ratio between the superficial gas velocity into the actual gas velocity, (equation 2.41).  $U_g$  is the same Taylor – Dumitrescu bubble velocity  $U_{T-D}$ .

$$U_{T-D} = U_g = \frac{U_g^s}{\alpha} \quad ; \quad \alpha = \frac{U_g^s}{U_g} \quad 2.45$$

Now, the flow rates and velocities could be expressed in terms of dimensionless Froud numbers as follow:

$$Q_l' = \frac{Q_l}{A(gD)^{0.5}} \quad 2.46$$

$$Q_g' = \frac{Q_g}{A(gD)^{0.5}} \quad 2.47$$

$$U_{T-D\infty}' = \frac{U_{T-D}}{(gD)^{0.5}} \quad 2.48$$

Where  $Q_l'$  is the dimensionless volumetric liquid flow,  $Q_g'$  is the dimensionless volumetric gas flow, and  $U_{T-D\infty}'$  is the dimensionless bubble rise velocity in static column.

By combining Equations 2.8, 2.11, 2.41 - 2.44, the gas void fraction in the riser can be expressed as follows:

$$\alpha = \frac{Q_g'}{C_o(Q_l' + Q_g') + U_{T-D\infty}'} \quad 2.49$$

The submergence,  $s$ , is defined as:

$$s = \frac{Z_s}{Z_l + Z_s} \quad 2.50$$

Where  $Z_s$  is the length of the tube measured from the gas injection point to the liquid column under shut-in conditions,  $Z_l$  is the lifting length measured from the top of the liquid column to the well head under shut-in conditions (2.14).

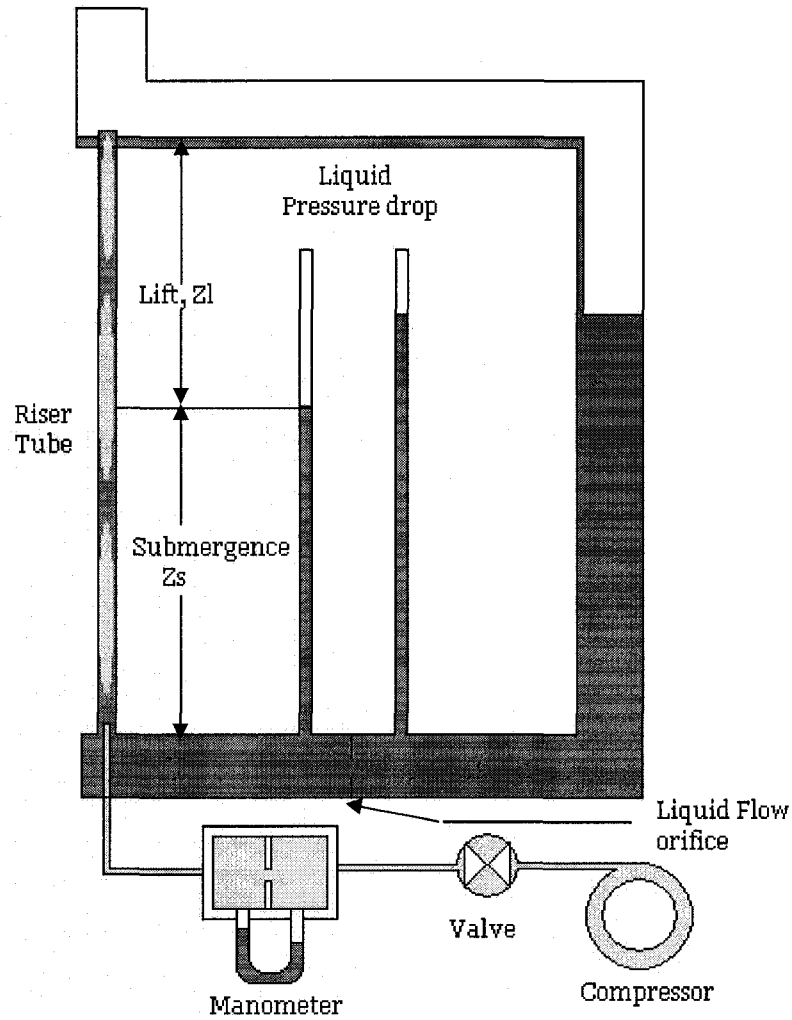


**Figure 2.15** Experimental apparatus - Reinemann et al. [42]

The Equation 2.51 represents the balance between the reservoir pressure and the static and frictional pressure losses caused by the fluid mixture in the tubing.

$$\rho g Z_s = \rho g (1 - \alpha) (Z_s + Z_l) + f \frac{(Z_s + Z_l) \rho U_m^2}{2D} (1 - \alpha) \quad 2.51$$

Where  $\rho$  is the liquid density. In definition of Equation 2.51, the density of the gas is assumed to be negligible in comparison to the liquid density. This means that the solution is given only for short pipe lengths where the compression of the gas does not have considerable effect. The frictional effects of the liquid fall back were shown to be small compared to those in the liquid slug and are therefore neglected [51].

Dividing both sides by  $[\rho g (Z_s + Z_l)]$  and rearranging gives:

$$s = (1 - \alpha) \left[ 1 + \frac{f}{2} (Q_l' + Q_g')^2 \right] \quad 2.52$$

The friction factor,  $f$ , can be calculated from the equation 2.49.

$$f = \frac{0.316}{\text{Re}^{0.25}} \quad 2.53$$

$$\text{Re} = \frac{DU_m}{\nu} \quad 2.54$$

Where  $\nu$  is the kinematic viscosity of the liquid ( $\text{m}^2/\text{s}$ ).

The terminal velocity of the T-D bubble included the surface tension effect, which was evaluated by White and Beardmore [44].

The terminal velocity of T-D bubble equation proposed for systems with low viscosity and high surface tension, as the air-water systems, was written as a function of the inverse Eötvös Number. The expression for this equation was described in Equation 2.18.

The efficiency of the system,  $\eta$ , was defined as the net work done in lifting the liquid, divided by the work done by the isothermal expansion of the air [20].

$$\eta = \frac{Q_l Z_l \rho g}{Q_g P_a \ln \left( \frac{P_o}{P_a} \right)} \quad 2.55$$

Where,  $P_a$  is the atmospheric pressure ( $N/m^2$ ), and  $P_o$  is the pressure at the base of the riser tube ( $N/m^2$ ).

Neglecting frictional effects, and combining the Equations 2.45, 2.48 and 2.50 the efficiency of the airlift can be written as follows:

$$\eta = \frac{Q'_l}{C_o (Q'_l + Q'_g) + U_{T-D\infty} - Q'_g} \quad 2.53$$

By using the Equations 2.45 to 2.57, Reinemann et al. [42] modeled the slug flow in small diameter pipes under low-pressure condition and short riser lengths. Reinemann et al.'s [42] model determined gas lift efficiencies and provided a new understanding of a real effect of surface tension on small diameter pipes. They also used the model to evaluate the efficiency of airlifting systems by comparing the positive effect of reducing the diameter under low air flow rates versus the negative effect provided by increasing  $C_o$  values when the liquid flow rates does not reach turbulent flow due to the reduced pumping velocities.

Reinemann et al.'s model was compared with experimental results in this study to determine its applicability at very low submergence values.

## 2.6 Instabilities in small diameter pipes

Unstable airlift operation involves low frequency oscillations of the liquid flow and pressure at the pump outlet [58]. In the worst cases, the flow takes the form of violent, periodic expulsion of liquid jets.

The instabilities result from density oscillations in the riser, coupled with oscillations of the single-phase liquid flow upstream of the air injection [58].

De Cachard and Delhaye's performed experiments by using a 9.2 mm riser at three different submergence values (i.e. 0.3, 0.5, and 0.7).

De Cachard and Delhaye observations concluded that for low submergence values, (less than 0.5), the instability behaviour exists no matter what the gas velocity was.

Instabilities respond to an oscillatory or wavy behaviour that was modeled using a linear stability analysis [58]. De Cachard and Delhaye proposed an empirical stability criterion based on the first oscillatory frequency obtained by the linear stability analysis.

In the present work, the submergence values are always below 0.2 that is considered a range of complete instability. The influence of instabilities in liquid production will be analyzed and evaluated for practical applications.

## CHAPTER 3

### EXPERIMENTAL PROGRAM

---

#### 3.1 Experimental Set Up

The experimental set up (Figure 2.15) was designed by adapting the concept of similar experimental rigs (Reineman et al. [42], and Toma et al. [15]). A schematic view of the experimental set up is shown in Figure 3.1. Details of the experimental set up design are presented in Appendix B.

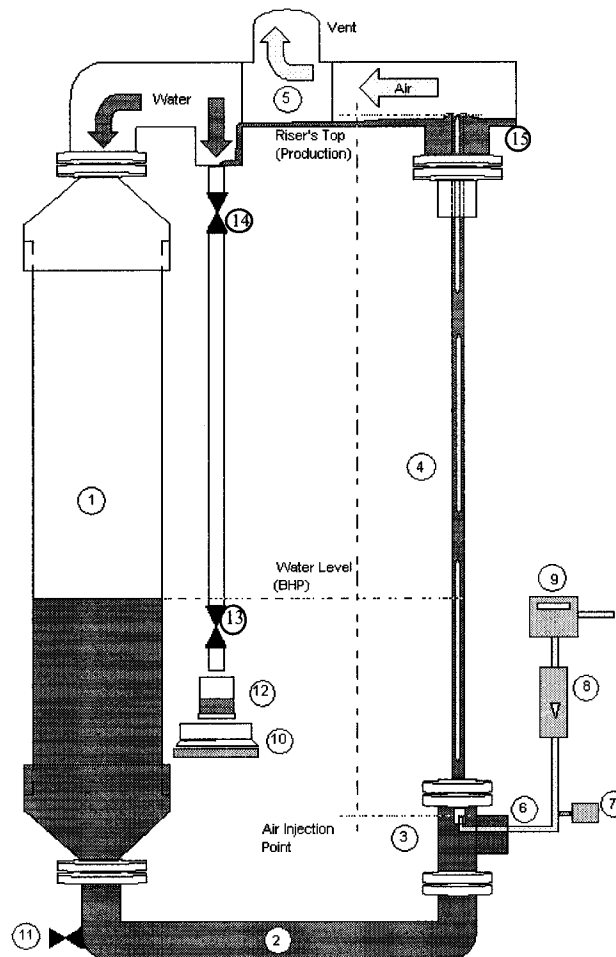


**Figure 3.1** Experimental set up.

A closed flow-loop was built in clear PVC and used to observe and measure the upward flow of water, methanol+water and air.

The apparatus is composed of five main sections. Section #1 is a vertical storage tank. This section was formed by a 6 inches (15.24 cm) OD x 10 feet long (304.8 cm) clear PVC pipe filled with water. A certain level was selected for each experiment to provide the desired “reservoir pressure” or submergence. Section #2 is a 2 inches (50.8 cm) OD clear PVC pipe, which connects the Storage tank to the air injection section, Section #3. According to design calculations, 2 inches pipe diameter was sufficient to avoid large frictional pressure losses along the pipe with a liquid flow rates smaller than 1 liter/min ( $1.67\text{E-}4 \text{ m}^3/\text{s}$ ). A general view of the apparatus (sections one and two) is shown in Figures 3.2.a,b.

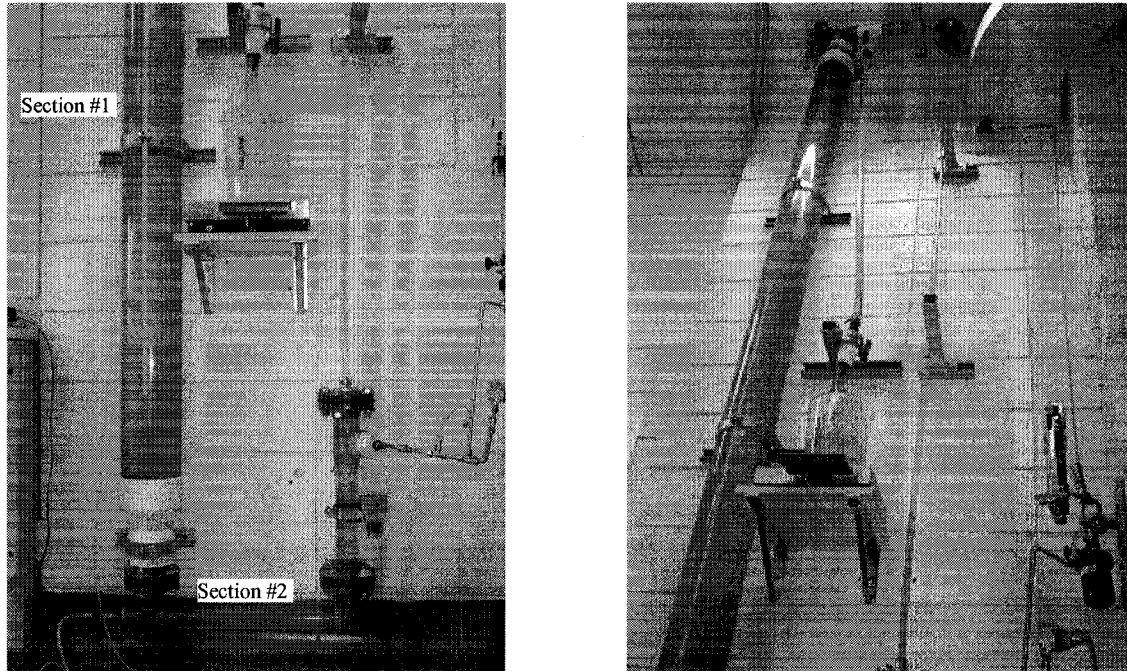
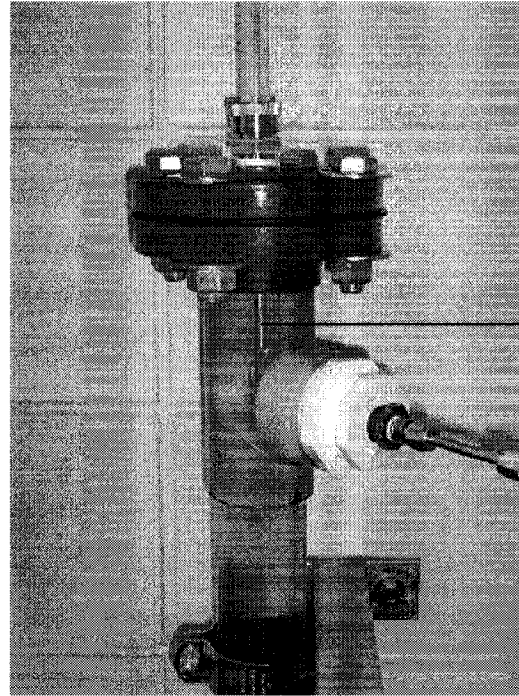


**Figure 3.2** Views of experimental apparatus

In Section #3, (Figure 3.3) the air was injected through a nozzle, #6, coaxially located inside the riser (1 cm from the bottom). The nozzle was changed according to the riser’s diameter. For 12 mm and 7.8 mm ID riser, a 6.3 mm OD nozzle was used, and a 1.6 mm OD nozzle was used for 4.0 mm ID riser.

This design allows the air to flow freely inside the riser and avoid air blockage at the entrance. Figure 3.3 shows a detailed of the gas injection point.



Nozzle 6.3 mm  
in a 12 mm riser

**Figure 3.3** Detail of the gas injection (section #3)

The riser, section #4, was designed to be exchangeable. Clear PVC pipes of 12 mm, 8.0 mm and 4 mm ID were used for the present work.

Located at the top of the apparatus, Section #5, is the gas-liquid separator. It was built from 2" ID clear PVC. The separation occurs at the top where the air and liquid are released from the riser. The air is immediately separated from the liquid and conveyed to a vent. The water is collected in the annulus section formed by the riser and the receiving tube in the separator, #15. Once the water overflows the chamber it has two possible paths, to return the storage tank #1, or to be collected in the liquid collector #12. The test could be run in a closed or open loop depending on whether the liquid production is required for the experiment or not.

The liquid collector #12 receives the water from the production line. The receiving cup rested on an electronic scale, #10, which weighs the liquid recovered during the experiment and was

programmed to display the flow rate in Kg/min. The scale had a precision of  $\pm 0.2$  g. The atmospheric pressure and temperature were continuously recorded to determine the reference conditions.

For air flow rates less than 1.0 L/min, the gas flow rate was measured using an F& P® rotameter, (Figure 3.1 #8). A thermal Matheson® flowmeter, (Figure 3.1 #9), was used for air flowrates up to 20 L/min. The two flowmeters were connected in series. The pressure of injected air was measured (Figure 3.1, #7,) using a “Validyne”® pressure transducer. For the 1.25 psi diaphragm  $\pm 0.01$  psi precision was achieved. When the 8-psi diaphragm was used in combination with the 1.6 mm diameter nozzle the accuracy decreased.

The reservoir static pressure was measured using the same pressure transducer. The two-phase column pressure was measured at the bottom of the tubing under flowing conditions.

Seven parameters were monitored by using the equipment described above: (1) Air flow rate, (2) liquid flow rate, (3) atmospheric pressure, (4) temperature, (5) injected air pressure, (6) reservoir pressure and (7) two-phase column pressure at the bottom of the riser. In addition, the air-liquid interfacial tension (IFT) was separately measured using a Du-Nouy ring tensiometer and a precision scale.

## **3.2 Calibrations**

The pressure transducer, the gas flow meters and the IFT tensiometer were calibrated prior to the experiments for reliable data.

### **3.2.1 Pressure Transducer Calibration**

The Validyne® pressure transducer (Figure 3.4) used for bottom hole pressure measurements was equipped with high sensitive stainless steel membranes graded in accordance to the range of pressure to be measured. When the pressure losses through the nozzle were almost negligible ( $\ll 1.0$  psi), (when a 6.3 mm nozzle was used), the

selected membrane was 1.0 psi; whereas for 1.6 mm nozzle, the membrane was rated to 8 psi (since the pressure loss through the nozzle was about 5 psi).

The apparatus used for pressure transducer calibration was an Omega® DPI 610 (Figure 3.5) with a precision of  $\pm 0.025$  psi. The pressure transducer transmitted a signal to the control box where the slight deflection of the diaphragm is converted to 0-10 volts. The calibration process consists of a consecutive adjustment of “zero” and “span” calibration screws in such a way that the maximum and minimum pressure values will be equivalent to 0 and 10 volts, respectively. For intermediate pressure readings, a calibration curve should be built in order to further improve the measurement accuracy. In most of the cases this calibration curve is linear. In some cases, however, the points may fit a second order curve. The calibration curves for the 8 psi and 1.0 psi diaphragms are shown in figures 3.6 and 3.7 respectively.

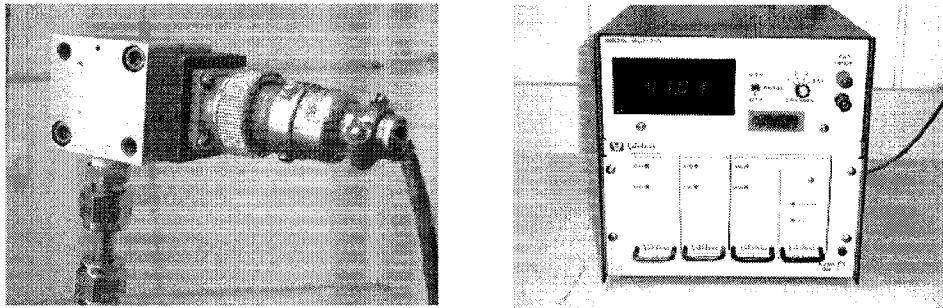


**Figure 3.4** Picture of the Validyne’s pressure transducer and the control box

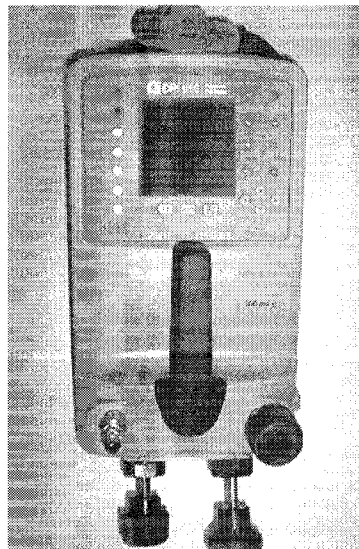


**Figure 3.5** Picture of the Omega® DPI 610 pressure calibrator

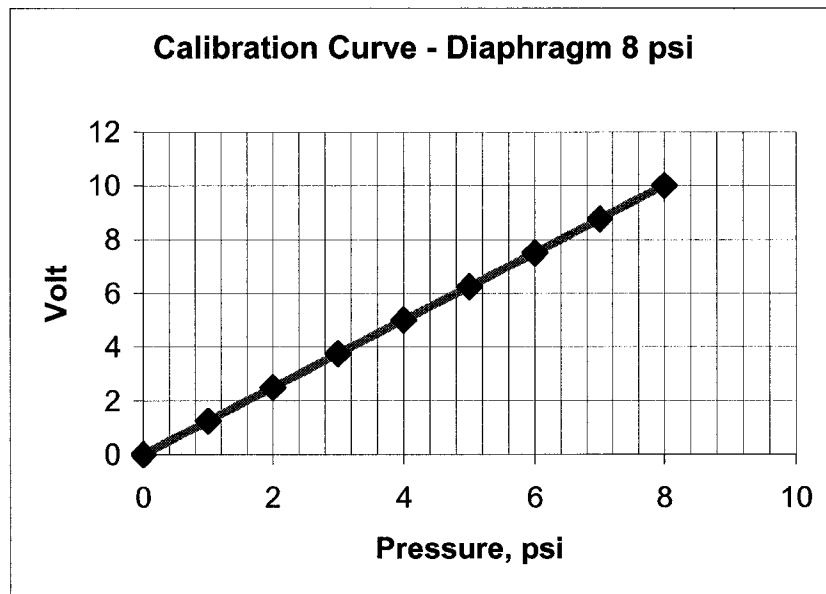


**Figure 3.6** Calibration curve for the 8.0 psi diaphragm.

In the case of 8.0 psi diaphragm the increment used for calibration was 1.25 volts for every 1.0 psi; while for 1.0 psi diaphragm, the increment was 1.0 volts every 0.1 psi. In both cases, the calibration curve was a straight line.

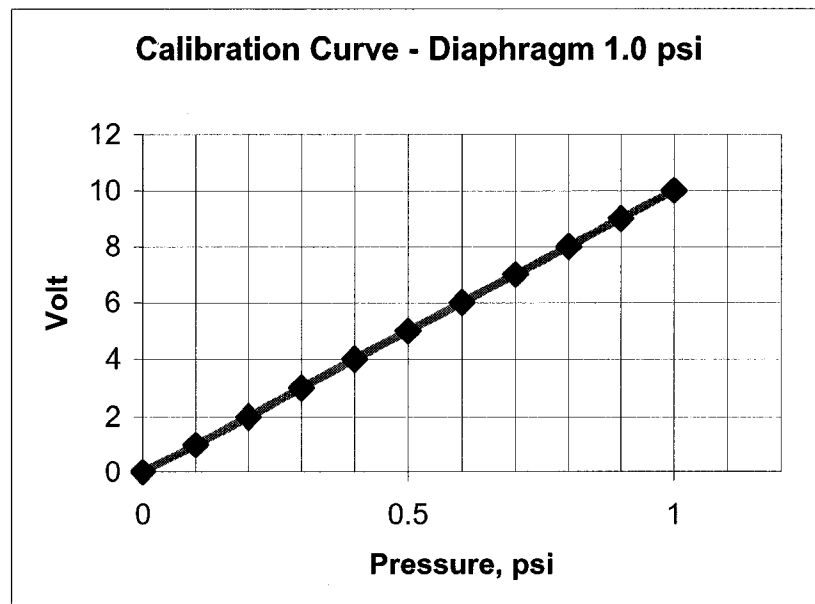


**Figure 3.7** Calibration curve for the 8.0 psi diaphragm.

### 3.2.2 Flowmeter Calibration

Two type of flow meters were used to measure the gas flow rate: (1) F& P Co.® Precision bore variable area gas flow meter, and, (2) Matheson® Model 8112-0424 thermal air-flowmeter. .

Figure 3.8 show a picture of each one of the equipments.

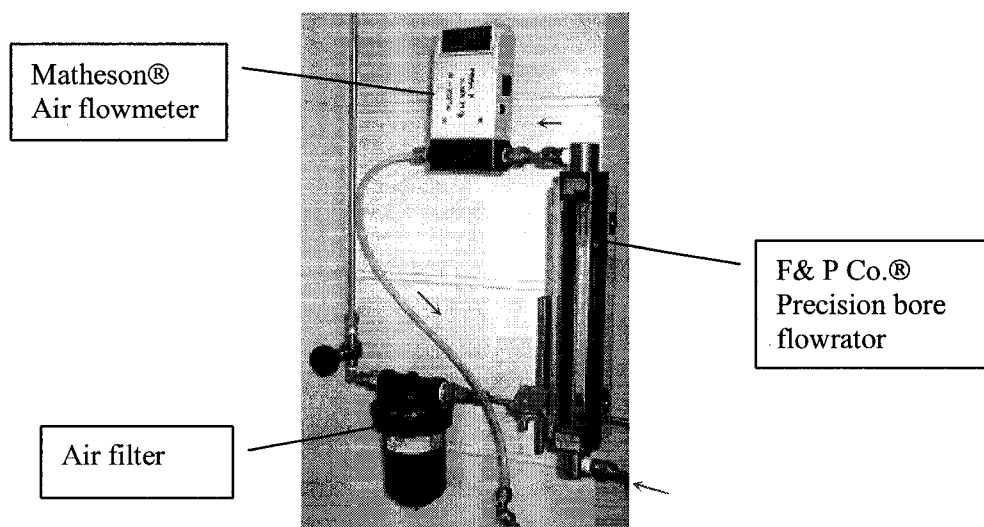


**Figure 3.8** F& P® and Matheson® flowmeters

The calibration of the flowmeters was performed with a positive displacement pre-calibrated gas flowmeter SINGER DTM 115. The range of precision was  $\pm 10$  mL/min.

For improved accuracy, the gas calibrator and the flowmeter were connected in series. The calibration for the F& P® rotameter (figure 3.9) was conducted at constant pressure and temperature conditions (100.74 Kpa and 19°C).

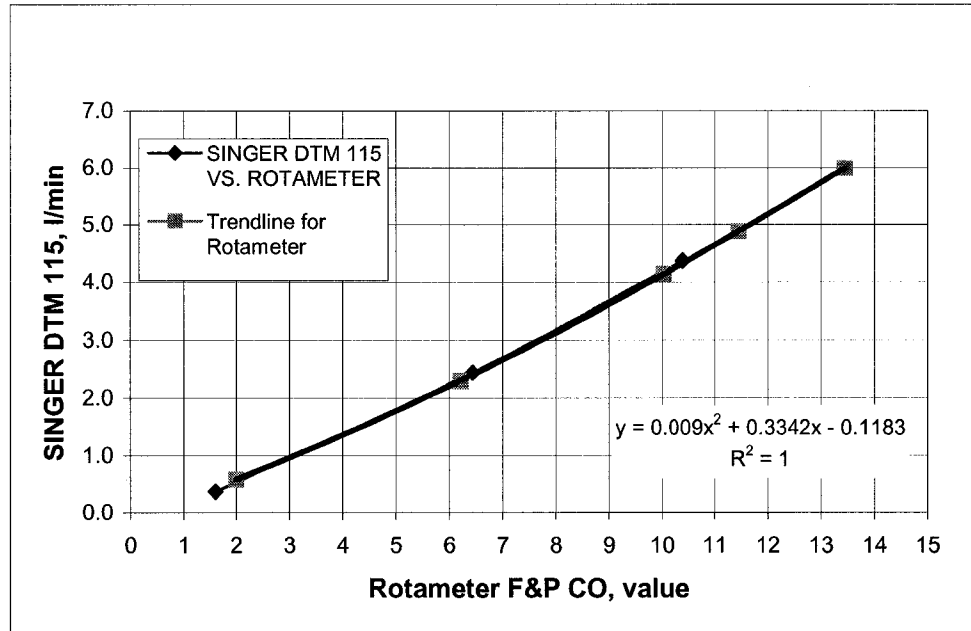


**Figure 3.9** Calibration curve for F& P® rotameter

The trend line (curve fitting procedure in EXCEL) was calculated from the experimental values and used to determine the calibration curve in L/min for the rotameter raw scale. As it is seen in Table 3.1, the F& P® rotameter measured the gas flow rates under 1.0 L/min with a precision of ±0.1 L/min. Between 0.2 and 1.0 l/min, the F& P® readings falls within the indicated, acceptable range of errors; for gas flow rates under 0.2 L/min the reading is not reliable.

F&P® value	L/min Equivalent	F&P® value	L/min Equivalent
1	0.22	6	2.21
1.5	0.40	6.5	2.43
2	0.59	7	2.66
2.5	0.77	7.5	2.89
3	0.97	8	3.13
3.5	1.16	8.5	3.37
4	1.36	9	3.62
4.5	1.57	9.5	3.87
5	1.78	10	4.12
5.5	1.99	14	6.32

**Table 3.1** Equivalent L/min flow rates for the F&P® read values.

The same calibration procedure was used with the thermal Matheson® flowmeter. In this case the calibration was repeated several times in order to adjust the calibration screws of the Matheson® flowmeter until similar values were obtained with the SINGER DTM 115 flowmeter. The results and the fitting calibration curve are presented in Figure 3.10.

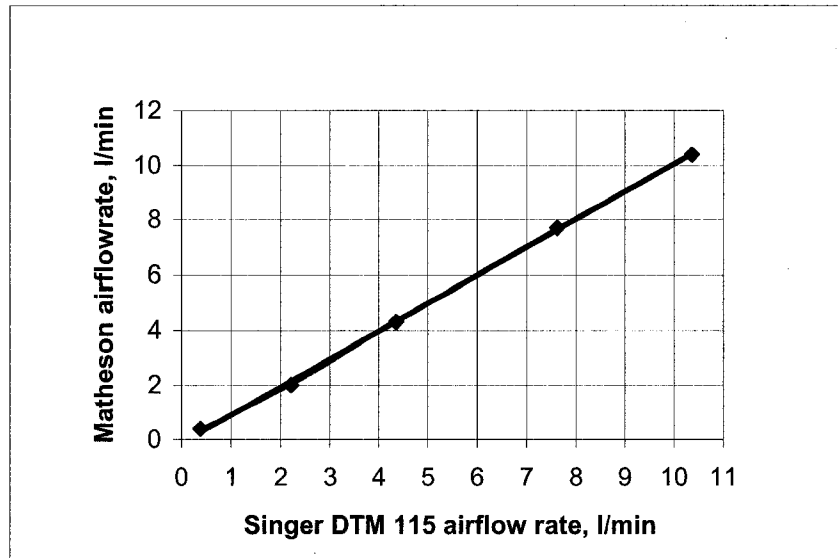


**Figure 3.10** Calibration data for the Matheson® air flowmeter

The precision of the Matheson® air flowmeter is  $\pm 0.1$  L/min. The minimum acceptable flow reading is 1.0 L/min. This air flowmeter was used only for the 1.0 to 20.0 L/min range.

### 3.2.3 Surface tension measurement (Fisher Surface Tensiomat Model 21)

The tensiometer was calibrated in accordance with the Fisher Surface Tensiomat manual. Figure 3.11 shows the equipment and the ring utilized for this purpose.

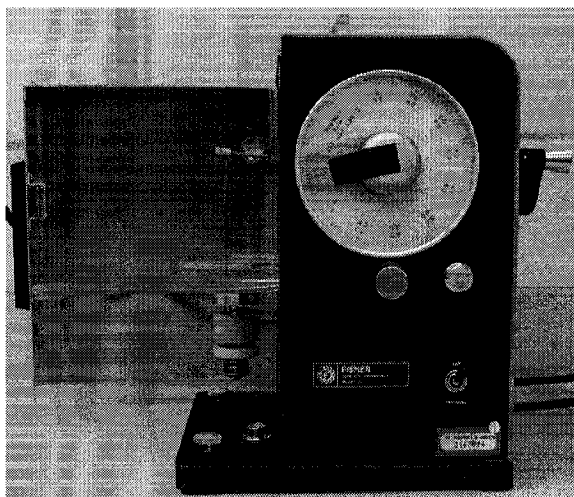


**Figure 3.11** Picture of the Fisher Surface Tensiomat ® Model 21

According to the calibration manual, the first calibration procedure should be done to determine the correct position of the arm. A weight should be placed just on the platinum-iridium ring that is hanged from the outer extreme of the arm. The reading in Dynes/cm should be in agreement with the mathematical result obtained from Equation 3.1.

$$S = \frac{M \cdot g}{2 \cdot L} \quad 3.1$$

S= Tension, [Dyne/cm].

M= mass, [gr].

L= Perimeter of the ring, [cm].

g= Acceleration of the gravity, [cm/s<sup>2</sup>].

The following data were used for calibration: M= 0.67 gr, L=8.06 cm, g=980 cm/s<sup>2</sup>. Entering data into Equation 3.1, gives the value of theoretical surface tension as S = 40.73 Dyne/cm, which should be equal to the value read from the dial. In this case the average surface tension reading was 41.8 Dyne/cm. The difference was 1.03 Dyne/cm with 2.54% error with respect to the theoretical value. Finally, the arm was properly

located no readjustment of its length was necessary. With this procedure, the surface tension could be measured within an acceptable range of error.

Since the diameter of the ring and the wire thickness actually interfere with the reading; an additional correction was introduced to further improve the reading accuracy. The measured surface tension values was corrected using the by multiplying with a correction factor F.

$$F = 0.4250 + \sqrt{\frac{0.01452 * P}{c^2 * (D - d)} + 0.04534} - \frac{1.679 * r}{R} \quad 3.2$$

Where, P is the reading from the dial in Dyne/cm, c is the circumference of the ring in cm, D is the density of the lower fluid (i.e. water, water-methanol mixture), d is the density of the upper fluid (i.e. air) in g/cm<sup>3</sup>, R is the radius of the ring in mm, and r is the radius of the wire in mm.

For this specific case the ring circumference was 8.06 cm, the wire diameter was 0.5 mm, and the ring diameter was 25.5 mm. The fluid densities were 1.0 g/cm<sup>3</sup> for water and 0.0012 g/cm<sup>3</sup> for air measured at standard conditions 15°C and 1 atm.

The correction factor F was simplified to the following expression in the case of water:

$$F = 0.7250 + \sqrt{2.271 * 10^{-4} * P + 0.01241} \quad 3.3$$

In the case of water and methanol mixtures, correct values for the density of mixture (adjusted for room temperature) where applied.

For all cases the value of surface tension is obtained from the following equation:

$$S = P * F \quad 3.4$$

Where  $S$  is the true value of surface tension in Dyne/cm,  $P$  is the read value (apparent surface tension) Dyne/cm, and  $F$  is the correction factor.

### **3.2.4 Viscometer (Brookfield Viscosimeter Model DV-II)**

The calibration of the Brookfield Viscometer Model DV-II was made under controlled temperature conditions. A water bath controlled the liquid temperature at  $25 \pm 0.1^\circ\text{C}$ .

The viscometer utilizes a spindle specially designed for a specific range of viscosity. For water and water-methanol mixture, the expected viscosity was less than 10 cP. Therefore, a cone-plate spindle type (CP 40) was selected. The equipment calibration is performed using a silicone based Newtonian fluid with a known viscosity. In this case, a Brookfield Engineering Lab calibration fluid 10 was used. The viscosity of the calibration fluid at  $25^\circ\text{C}$  was 9.4. The read viscosity at  $25^\circ\text{C}$  was 9.24. The range of error of the equipment was about  $\pm 0.1$  cP.

## **3.3 Experimental Procedure**

The first sets of experiments were conducted to determine the liquid production under defined submergence and air flowrate conditions. Flow patterns, bubble rising velocities and general flow behavior were observed. The procedure used to achieve the experimental goals is described below.

### **3.3.1 Liquid preparation and physical properties**

Two liquids, tap water and water-methanol mixture were used for the tests. A 60/40% volume water-methanol mixture was prepared, mainly, to modify the surface tension. The IFT value decreased from 72 dyne/cm (water) to 38 dyne/cm for the selected water-methanol mixture.

The liquid density was calculated by measuring the volume of liquid in a 250 ml calibrated cup and the weight of the cup with fluid. The density of the fluid was recorded as the ratio between weight and volume at the measured liquid temperature.

The liquid viscosity was determined using the Brookfield Viscometer Model DV-II. As discussed, the equipment was calibrated using a silicone-based fluid at 25 °C. The measured viscosity for water was 1.003 cP, for pure methanol 0.540 cP, and for the 60/40% water-methanol mixture 1.710 cP.

The liquid properties were measured three times and an average value was used for calculations.

### 3.3.2 Experimental program

The experimental procedure included seven steps:

1. **Calibrations:** pressure transducer, flowmeters.
2. **Adjustment of submergence:** The storage tank was filled with the liquid up to a desired liquid level or submergence value. Table 3.2 shows the submergence values used for the three risers.

Liquid level from the gas injection point, cm					
4.0 mm Riser		7.8 mm Riser		12.0 mm Riser	
Liquid level, cm	Submergence %	Liquid level, cm	Submergence %	Liquid level, cm	Submergence %
63.5	20.1	63.5	20.1	63.5	20.1
50.8	16.7	50.8	16.7	50.8	16.7
38.1	12.5	38.1	12.5	38.1	12.5
25.4	8.3	25.4	8.3	25.4	8.3
12.7	4.2	17.8	5.8	---	---

**Table 3.2** Liquid level and submergences used for the 4.0, 7.8 and 12 mm risers

3. **Pressure transducers verification:** The bottom hole pressure was measured under static conditions and compared with the theoretical static pressure value

(i.e.  $\rho_1 g h$ ). This data was used as quick criteria to determine the proper operation of pressure transducer.

4. **Recording of atmospheric pressure and operating (fluid) temperature:** Due to negligible range of temperature variations during a run, this experiment is considered to be conducted under isothermal conditions.
5. **Air flowrate:** During a single run the airflow was kept constant and the maximum length reached in the riser by the two-phase column was registered. The gas flow rate varied according to the installed riser. Table 3.3 shows the airflow rated used for the experiments.
6. **Recording the liquid production:** The mass flow rate was calculated by dividing the mass of collected liquid by the collecting (run) time. The value was recorded in Kg/min.
7. The procedure was repeated from steps 3 to 7 until all the gas flow rates were completed.

After finalizing all the experiments for one submergence value, steps 2 to 7 were repeated for the other submergence values. In order to observe repeatability, the complete sets of experiments were repeated three times for a single riser.

Air flow rate injected, L/min		
4.0 mm Riser	7.8 mm Riser	12.0 mm Riser
0.2	0.2	0.2
0.6	0.6	0.5
1	1	1
1.4	1.4	1.4
1.8	1.8	1.8
---	2.2	2.2
---	2.7	2.7
---	4.1	3.7
---	6.3	4.8
---	---	6.3
---	---	8
---	---	10
---	---	11

**Table 3.3** Air flow rate used for 4.0, 7.8 and 12 mm riser.

### 3.3.3 Rising bubble velocity

A movie digital picture technique was developed and used to evaluate the rising velocity of bubble (T-D). Experiments using water and water/methanol mixture in 12 and 7.8 mm risers (60 cm of visual field was considered only) have been repeated in order to achieve this information.

In these series of tests, the T-D bubble rising movement was recorded using a Panasonic digital camera with 32 frames per second.

The measurement was started 109 cm above the gas injection point to avoid any disturbance related to entrance effect and bubble acceleration. According to Taitel and Barnea [19] the unsteady slug flow could be present until the T-D bubble developed a complete tail velocity profile; this requires an entry length of approximately 80D. For the 12 mm tube, this length corresponds to 96 cm. 109 cm in length was considered a safe distance.

The T-D bubble rising velocity was recorded 10 different times for a single gas flowrate and submergence value. The bubble traveling time (across 60 cm observation of vertical zone) was obtained from processing the digital image (by using the movie editor “Windows Movie Maker – version 1.1.2427.1” with a time precision of 0.03 second).

This experiment was designed to determine the influence of different liquid surface tension on the rising T-D bubble velocity.

## CHAPTER 4

### EXPERIMENTAL RESULTS AND OBSERVATIONS

---

The experimental results were presented under two categories: 1) Data from tests with water, and 2) Data from tests with water/methanol mixture.

Systematic recording of gas-liquid upward flow parameters (mainly static and total pressures as well as pressure oscillations) and of visual/photographic observations (mainly the shapes of bubbles and liquid film, and specific of each flow regime) are presented.

#### **4.1 Experimental results. Part 1:**

##### **Water/Air System**

Water-air up flow experiments have been performed for all three risers: 4, 8 and 12 mm. Use of clear PVC pipe allowed visual observations on flow patterns while air was injected at different flow rates.

##### **4.1.1 Observations on flow patterns specifics**

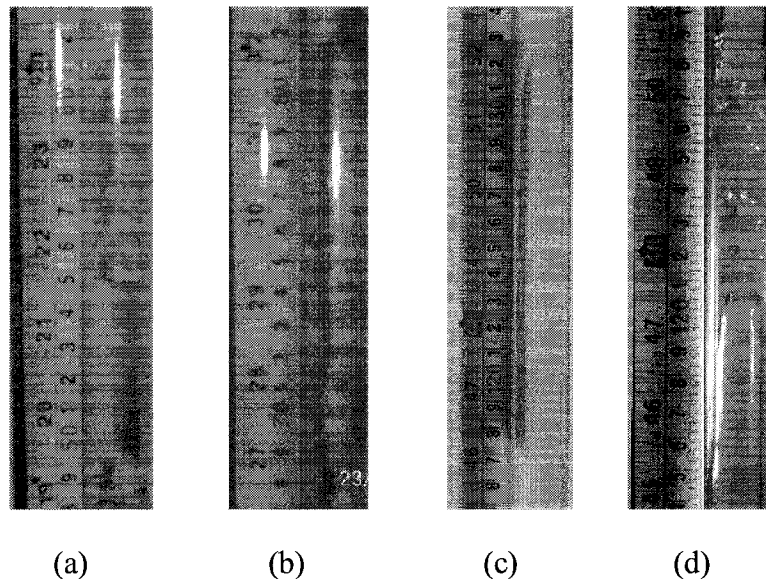
As previously reported by Barnea et al. [32], Mishima and Hibiki [22], the flow patterns changed depending on the gas injection rate.

Figure 4.1 is a sequence of pictures taken during experiments with water-air in a 12 mm riser at 20.1% submergence. Figures 4.1 (a) and corresponds to a bubble flow pattern [22], and (b-c and d) were defined as Elongated Bubble flow pattern. At very low air injection rates, 0.2 L/min ( $U_g^s = 0.092$  m/s), small trains of small cap shaped bubbles of about 1 cm length are observed. The bubbles separated from each other by a small liquid section similar to a liquid slug (Figure 4.1 (a)) traveled together without coalescing.

As the air injection rate was increased from 0.2 L/min up to about 1.0 L/min some of the bubbles coalesced forming elongated bubbles as shown in Figure 4.1 (b). After the air

flow rate was further increased, all the bubbles coalesced and formed a bullet shaped T-D bubble. The liquid slug units that separate two consecutive T-D bubbles were free of gas (Figure 4.1 (c)).

As the gas flow rate was increased further, due to the turbulence caused by the injected air, some entrained bubbles are formed in the tail of the T-D bubble similarly to the conventional slug flow pattern. A pseudo-slug flow pattern is therefore observed, but, without exhibiting the dynamics proper to slug flow with conventional diameter pipes, this regime, falls into the “elongated bubble flow pattern” mainly, because of the reduced bubble population and tailing edge limited activity. The observed bubbles are totally different to the deformable “Harmathy” bubbles typical to conventional slug flow patterns. Most of the formed bubbles were elliptical or spherical and the equivalent spherical diameter was between 1 and 2 mm (Figure 4.1 (d)).



**Figure 4.1** (a) Bubble flow (0.2 L/min air injection rate) and (b-c-d) Elongated bubble flow pattern (1.0, 1.36 and 2.66 L/min air injection rate, respectively), 12 mm riser.

Since the maximum injected airflow rate in the 12 mm riser was limited to 11 L/min ( $U_g^s=1.62$  m/s), the transition to annular flow was not detected at any submergence.

Similar flow patterns were also observed for 7.8 mm riser. The only difference was the absence of small bubbles in the liquid slug even under high turbulence conditions. The elongated bubble flow pattern was the most common flow pattern observed for most of the gas injection flow rates used in this test (Figure 4.2).

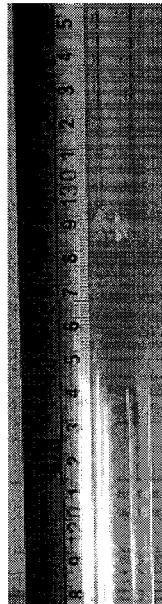


**Figure 4.2** Picture of the elongated bubble flow pattern for a water/air flow in a 7.8 mm diameter riser; gas flow rate 1.36 L/min ( $U_g^s = 0.47$  m/s)

#### **4.1.2 Lump flow in small diameter pipes – description of visual observations**

A special flow pattern previously defined by Fernandes [50] as “Lump Flow” was observed in all risers. A singular slug unit traveling upward the riser with a high content of gas characterizes this flow pattern. The occurrence of this flow pattern varied from one tube diameter to another. For instance, for the 12 and 7.8 mm risers the lump flow appeared only at gas injection velocities greater than 2.0 m/s, whereas, for the 4.0 mm riser, the “lump flow” pattern appeared at low gas velocities between 0.3 and 0.8 m/s.

For the 4.0 mm riser, the liquid slug unit engulfed several small gas bubbles that bridged the tube and divided the liquid slug into mini-gas-liquid sub-sections. It appears that this “foamy liquid slug unit” is transported to the separator with the help of a long T-D bubble

pushing behind. The liquid falling back was limited indicating that most of the liquid was transported under a plug flow like conditions [37]. Once the liquid contained between two elongated bubbles was produced, the T-D bubble filled the riser with air reducing the bottom hole pressure to a minimum value. The pressure difference between the liquid column in the storage tank and the riser's air column forced the water to fill the riser again creating a new "foamy" liquid slug that started the process over again. A high frequency of "lump pattern" occurrence was observed under this low gas flow rate conditions.

The lump flow was also formed at high air flow rates in the 12 and 7.8 mm risers. The liquid slug had a high void fraction and was pushed by a long bullet-shaped T-D bubble. Similarly to what happened in the 4 mm riser, after the liquid slug was produced, for a very short period of time, the tube was totally filled with air. However, in this case the next liquid slug unit was formed from the falling back of the liquid film surrounding the T-D bubble and the inflow of water coming from the storage tank. The lump flow was not observed as frequent as in the case of the 4.0 mm riser.

#### **4.1.3 The effect of tube diameter - liquid production and calculated efficiency**

Experiments were conducted to demonstrate and to assess the effectiveness of upward liquid transport under very low submergence with small diameter pipes. Experimental results were summarized in tables C.1 – C.26 (Appendix C).

The following parameters were recorded: Atmospheric pressure, temperature, maximum, minimum and average voltage from the pressure transducer (essential to assess and quantify instabilities), air flow rate, mass liquid production and production time.

Repeatability was calculated by using Equation 4.1:

$$\% \text{ repeatability} = 100 - |\% \text{Variation}| \quad 4.1$$

Where variation is obtained from Equation 4.2:

$$\%Variation = \frac{Q_{liquid\ 1} - Q_{liquid\ 2}}{Q_{liquid\ 1}} 100 \quad , \quad 4.2$$

The repeatability of experimental measurements for all submergences and tube diameter are shown in table 4.1.

Average % Repeatability						
D, mm	% Submergence					
	20.1 %	16.6%	12.5%	8.3%	6.25%	4.25%
12	99.4	99.2	96.9	90.0	----	---
7.8	82.5	87.5	66.7	82.6	66.7	---
4.0	93.2	93.7	96.5	82.6	---	92.7

**Table 4.1** Average Repeatability (in percentage) of experimental measurements

The repeatability was usually higher than 80% and, in some cases, closer to 90%. Some experiments performed with 7.8 mm riser where the repeatability was lower than 80% were cancelled and a fourth set of data was obtained where repeatability was greater than 90%.

Figure 4.3 shows the water flowrate versus injected gas rates in 12, 7.8 and 4 mm diameter risers with submergence values of 20.1%, 16.6%, 12.5% and 8.3%. Experimental data are summarized in Figure 4.3 in three groups in accordance with the pipe diameter used (4, 7.8 and 12 mm). Generally, higher liquid production rates were obtained using larger diameter pipes. However, small diameter pipes allowed liquid to be produced at the lower gas injection rate. It was also observed that with increasing the submergence (reservoir pressure) the production rate was higher for the same diameter and the same gas injection rate.

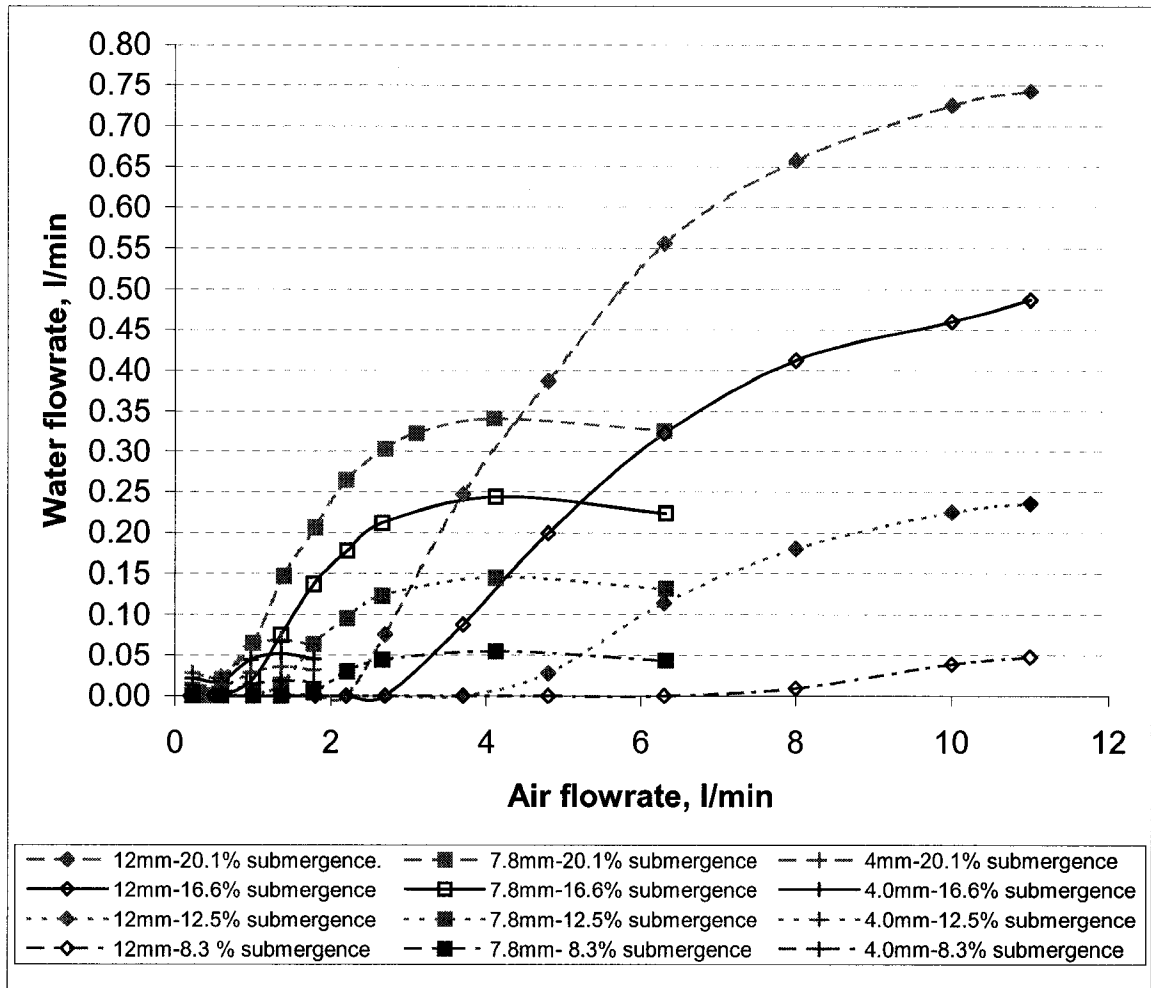


**Figure 4.3** The effect of injected gas (air) on produced liquid (water) for three groups of experiments (12, 7.8 and 12 mm ID risers) and various.

Experimental data measured at the same submergence values and different riser diameters were grouped for comparison.

Figure 4.4 compares the airlift efficiency with 4.0, 7.8 and 12 mm diameter risers from experiments performed at 16.6% submergence. It is generally observed that a higher liquid production rate is achieved when a larger pipe diameter is used. For example, the maximum liquid production rates were obtained at 0.48 L/min, 0.34 L/min and 0.075 L/min when pipes with diameters of 12 mm, 7.8 mm and 4 mm were used, respectively with 16.6% submergence. However, the onset of the liquid production (defined as the critical, minimum gas rate injection required to initiate production of liquid) occurred al

lower gas injection rates as the pipe diameter is decreased. For example, the liquid production in 12 mm diameter pipe started when the air injection rate was 2.7 L/min as compared with 7.8 mm riser requiring only 0.59 L/min. The required air injection rate was even lower than 0.59 L/min to initiate liquid production rate from 4.0 mm diameter pipe.

Therefore, for the selection of a tube diameter, two critical parameters have to be considered: 1) Maximum allowable liquid production rate, 2) Critical production condition (minimum gas rate injection required to initiate production of liquid).

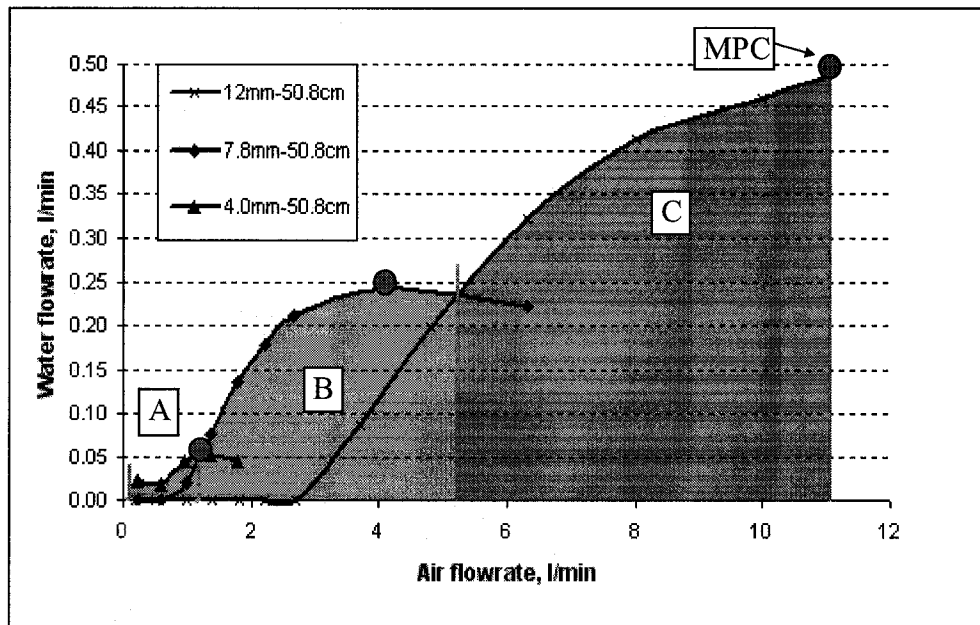


**Figure 4.4** Liquid production with 4, 7.8 and 12 mm risers at a simulated reservoir pressure of 50.8 cm water column (16.6% submergence); – recommended zones of use (laboratory data performed with 3 m risers)

As shown in Figure 4.4, each tube diameter displays an optimal range of gas injection rate where the highest rate of liquid production is obtained. Therefore, for the range of 0 to 1.0 L/min air injection rate, zone A, the best water production is obtained with the 4.0 mm riser; for the range of 1.0 to 5.5 L/min, zone B, the optimum pipe diameter is 7.8 mm; for air injection rates between 5.5 and 11.0 L/min, zone C, 12 mm riser is the best.

The curve formed by the points indicating the maximum liquid production obtainable with a certain pipe diameter for a certain depth and reservoir pressure is named maximum production condition (MPC), Figure 4.4.

In order to better quantify the optimal gas lift transport efficiency, the water/air ratio is further used as a comparison criterion (Table 4.2). This value will indicate the volume of water produced per unit volume of gas (air) injected.

<b>D</b> <b>mm</b>	<b>Area</b> <b>m<sup>2</sup></b>	<b>Water</b> <b>L/min</b>	<b>Air</b> <b>L/min</b>	<b>Water/Air</b>
<b>12</b>	3.60E-05	0.486	11	0.0442
<b>7.8</b>	1.52E-05	0.244	4.12	0.0592
<b>4</b>	4.00E-06	0.051	1.36	0.0375

**Table 4.2** Water/air ratios at maximum production conditions for 12mm, 7.8 mm, and 4.0 mm diameter pipes, 16.6% submergence.

The table 4.2 compares the performances measured at the maximum liquid transport rate (circular dots in Figure 4.4) with three different diameters at the same (16.6%) submergence. The water/air ratio obtained from the 7.8 mm riser (0.06) is significantly higher, compared to the other two risers, where water/air ratios were 0.044 and 0.0375 for the 12 and 4.0 mm risers, respectively.

From this analysis it could be concluded that although the onset of production appears earlier for smaller diameter pipes and the maximum liquid production is increasing with the diameter, the most efficient gas lift system (greatly depending on submergence, tube diameter and the air injection rate) may be obtained for a smaller, intermediary diameter size.

A detail illustrating the liquid production versus gas injected for 4 mm diameter (Figure 4.5) shows an additional feature. The S-shape of the production curve appears to be specific for 4 mm pipe.

At very low air flow rates of approximately 0.2 L/min, the liquid production rate is unexpectedly high. A possible explanation of this phenomenon is the effect of the pipe diameter on the two-phase flow column. The liquid slug that contains several small bubbles separated by small liquid sections is gently pushed up to the wellhead by a long rounded tip T-D bubble, and the liquid is produced from the top. The absence of turbulence allows the liquid to be transported in a convenient plug-flow pattern [37] that carries the most of the liquid contained in the liquid column. At this low air injection levels the water production is enhanced due, probably to a reduced fall back effect specific to this flow pattern.

As the air injection is further increased, the liquid production rate starts to decrease. This is possibly related to increasing of the T-D bubble velocity and tip shape change leading to increasing of the liquid (film) fall back. The fall back liquid feeds into the oncoming slug unit. As the size of the liquid slug unit increases, the hydrostatic pressure exerted at the bottom of the well also increases which cause hindering or water production.

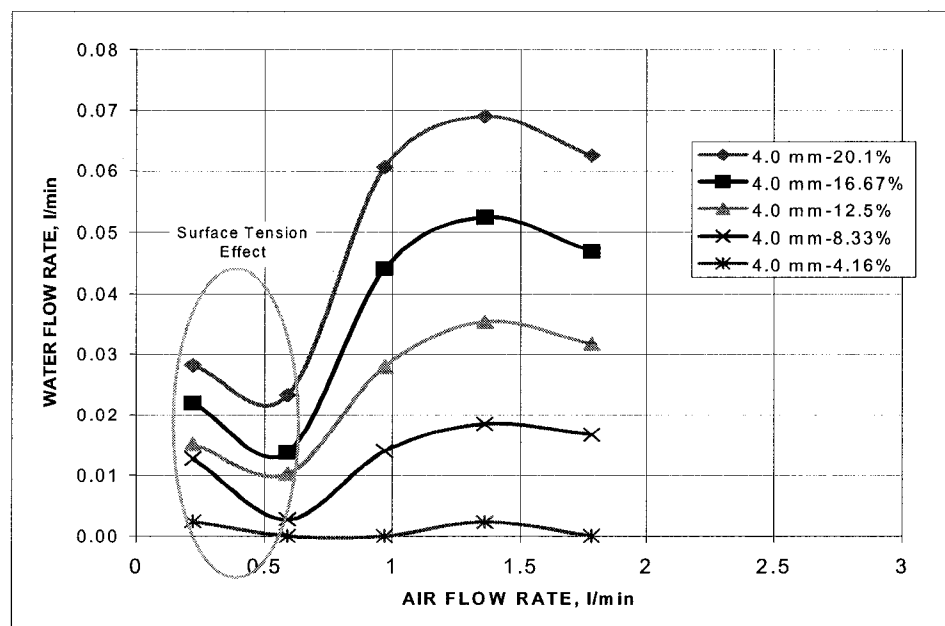


**Figure 4.5** Water production vs. Air injection flow rate in a 4 mm riser for 20.1, 16.6,12.5,8.3, and 4.16% submergence

If the air flow rate is increased further, the reduction in the two-phase column density created by longer and more frequent T-D bubbles overcomes the negative effect of the liquid falling back and the water production starts increasing again. Beyond a maximum production level, however, injection of more air results in a reduction of the liquid production as consequence of the frictional pressure losses effect (related to the square of gas velocity).

#### **4.1.4 The effect of submergence**

All experimental results have shown the salient effect of submergence on the liquid production.

Generally, the onset water production did not appear until certain gas injection rate was reached. In all cases, the onset of water production occurred at higher air injection rates for lower submergence values (Figure 4.6). Additionally, the reduction in submergence caused a visible decline of airlifting efficiency since more gas was required to produce the same amount of liquid. This effect has to be particularly considered for production operations with marginal bottom hole pressure.

The hydrostatic pressure reduction appears to be more significant with smaller diameter pipes at marginally low submergence values. The small diameter gas-liquid flow condition helps to sustain a stable elongated bubble flow pattern even at very small liquid levels and to minimize the liquid fall back effect. By reducing the T-D bubble upward velocity, an overall increase of void fraction is obtained with positive effects on reducing the static pressure [42,44].

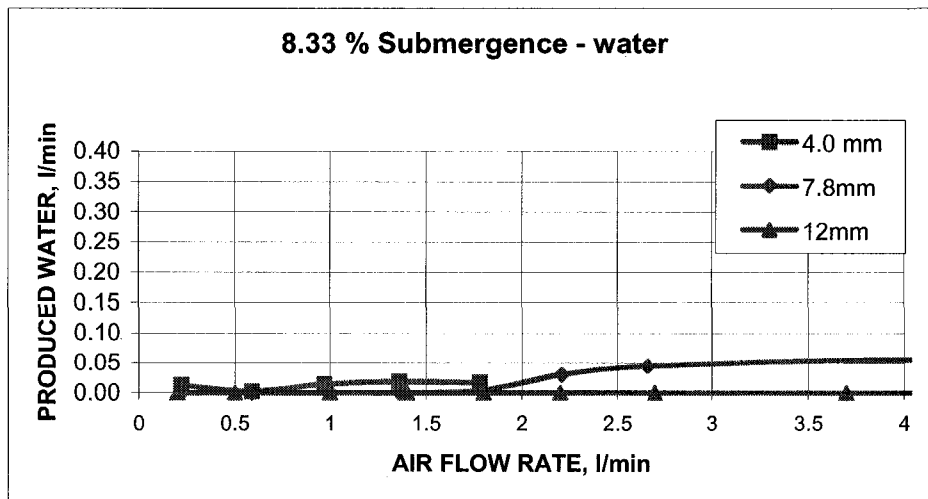
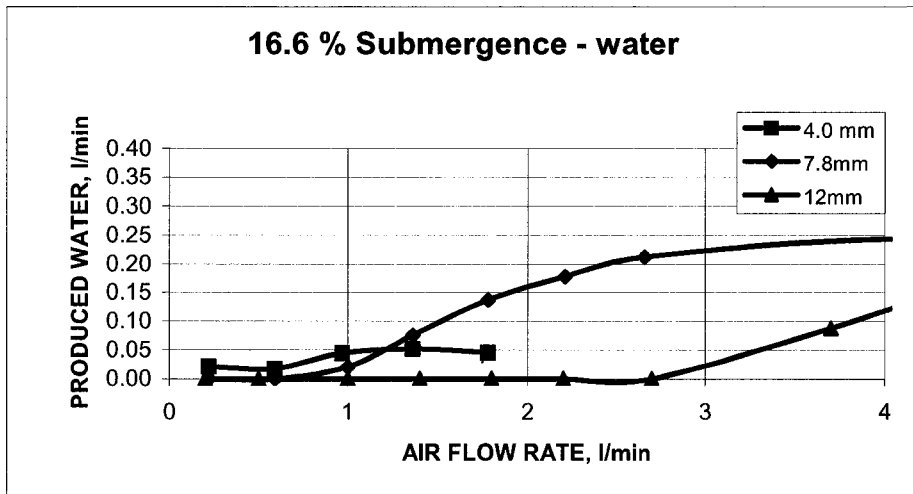
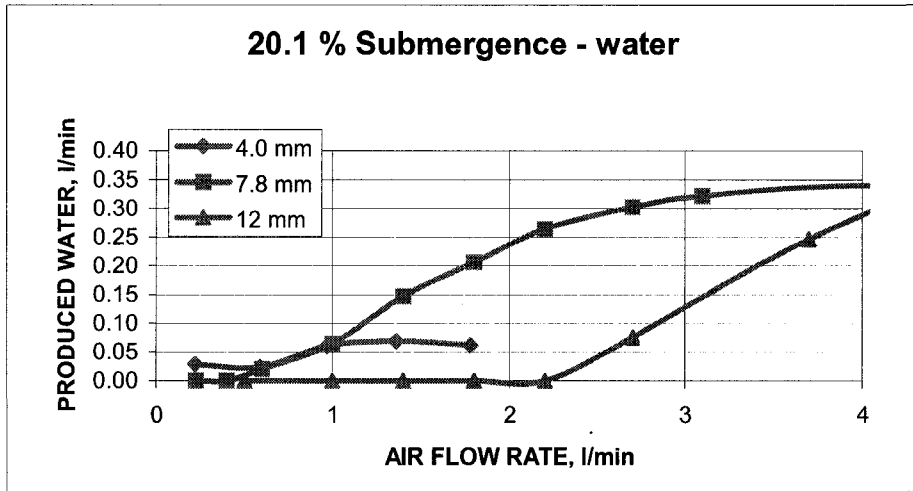


**Figure 4.6** Water production with 4, 7.8 and 12 mm risers at a) 20.1%, b) 16.6 %, c) 8.33% submergence.

As shown in Table 4.3, comparing the effect of submergence on water/air (W/A) ratio, calculated at maximum liquid production rate, the best W/A ratio is observed for 7.8 mm riser at 20% submergence. However, when submergence is reduced to 8.33%, the 4 mm riser displays the highest W/A for this submergence condition.

D mm	63.5 cm -20.1% Water/Air	50.8 cm -16.6% Water/Air	38.1 cm -12.5% Water/Air	25.1 cm -8.33% Water/Air
12	0.0675	0.0442	0.0214	0.0043
7.8	0.0828	0.0592	0.0352	0.0133
4	0.0507	0.0375	0.0260	0.0136

**Table 4.3** Submergence effect on the water/air ratio measured at the maximum production conditions for the 12, 7.8 and 4.0 mm riser.

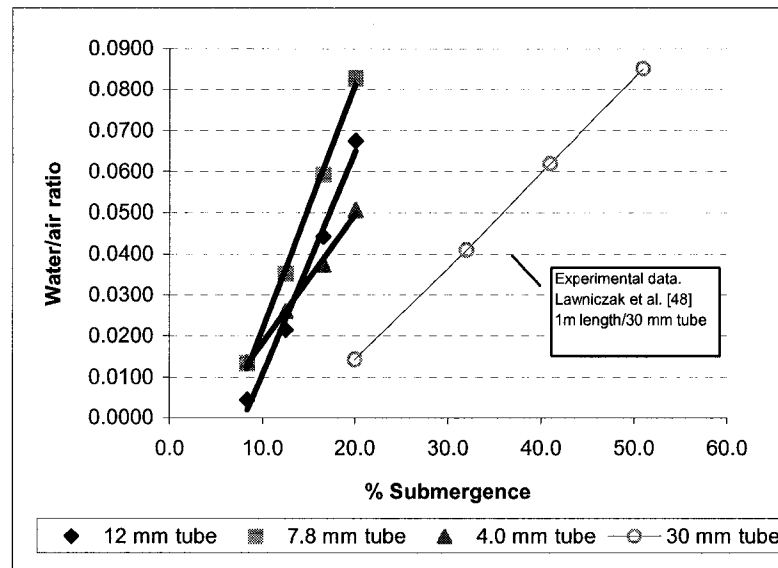


**Figure 4.7** Comparison of present experiments and similar data from literature – indicating the effect of length of tube -Water/air ratio versus submergence for 4, 7.8 and 12 mm and 3.05 m length risers; and 30 mm ID, 1.0m length riser (Lawniczak et al. [48])

Figure 4.7 illustrates data tabled in 4.3. The W/A ratio at the maximum production rate (MPC) varies linearly as a function of submergence value. The maximum liquid production is achieved when the pressure losses in the pipe are minimum. Similar trends reported by Lawniczak et al. [48] (for 30 mm tubes and only 1 m in length) are added in the graph for comparison purpose.

The minimum required submergence for initiating liquid production is obtained from Figure 4.7 by cross-sectioning the W/A versus submergence characteristics with the abscissa at zero W/A value. Table 4.4 summarizes the results data.

4 mm Riser	7.8 mm riser	12.0 mm riser	30 mm riser [48]
4.09 % submergence	6.27 % submergence	7.92 % submergence	13.78% submergence

**Table 4.4** Minimum submergence required for initiating the liquid production for 4, 7.8, and 12mm diameter (L=3m) and for ref. [48] (D=30 mm L=1.0 m)

It is important to note that this linear behavior and procedure is valid for small-length airlift systems only. Numerical integration to include non-linear effects of fallback and local pressure variations are required for higher elevation transport condition.

#### 4.1.5 Superficial velocities and pattern transitions

##### 4.1.5.1 Transition conditions

Barnea et al. [32] suggested that the differences in the transition boundaries for the two-phase flow pattern in vertical conventional and small diameter pipes are negligible; therefore, the same flow pattern transition criteria may be applied in both cases. This, however, should be cautiously applied to bubble-slug transition as the typical “H” bubble are not possible with small-diameter conditions.

The transition boundary between intermittent (I) and annular (A) flow patterns was at a superficial gas velocity of 12.3 m/s (Equation 2.13). The liquid and gas densities used into the equation were 999 Kg/m<sup>3</sup> and 1 Kg/m<sup>3</sup>, respectively. The surface tension of water was measured as 0.072 N/m.

The transition between bubble and intermittent flow was defined by the diameter of the pipe. The experiments were conducted using 4, 7.8, and 12 mm diameter risers. The critical diameter of the pipe,  $D_{cr}$ , that defines the minimum pipe diameter below which the Harmathy “H” bubble disappear to coalesce in a T-D bubble, is given by the Equation

2.10. Using the same air and water physical properties given above, the critical pipe diameter for an air-water system was 51.47 mm; in consequence, it was determined that the elongated bubble flow pattern was the only one present in this set of experiments.

#### 4.1.5.2 Superficial velocities for evaluating the system efficiency

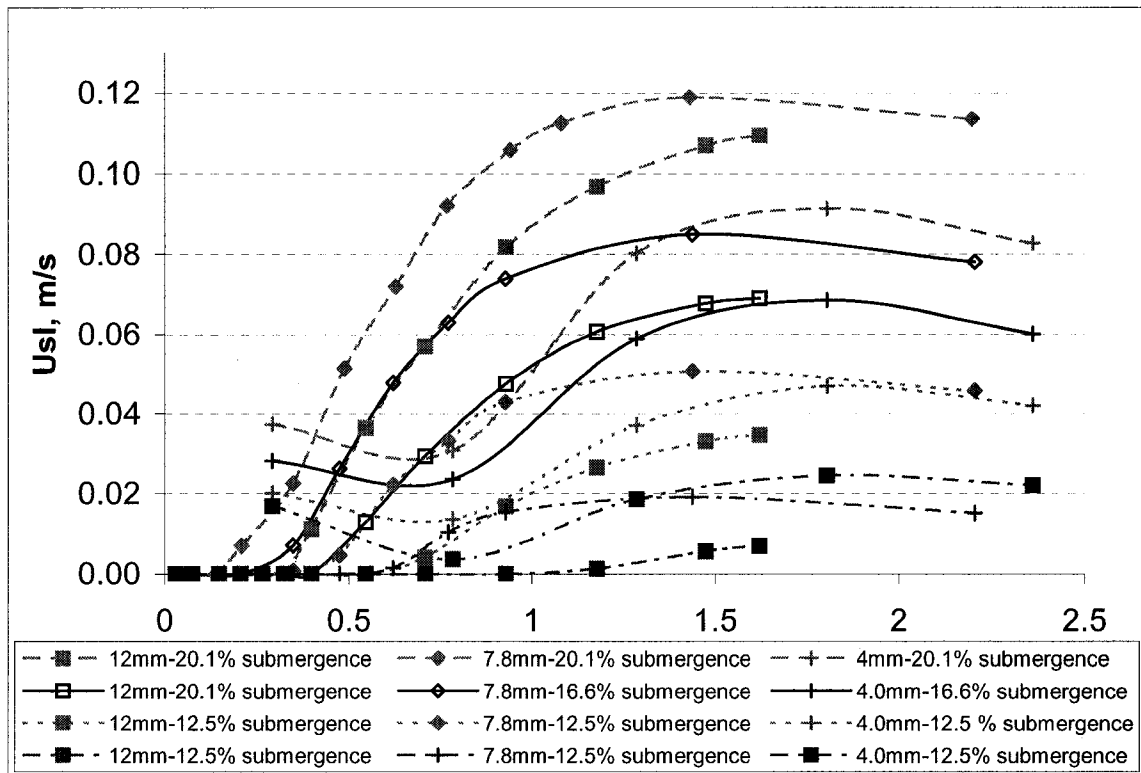


**Figure 4.8** Liquid superficial velocities versus gas superficial velocity for 4, 7.8 and 12 mm risers

The superficial velocity (Equation 2.8) is a measure of the fluid flow ratio passing through per unit of tubing cross sectional area. Therefore, the superficial velocity graph can be used as a practical visual tool for selecting the best (optimum) pipe diameter for the specific air injection rate and submergence conditions.

Data shown in Figure 4.8 where superficial velocity of liquid versus superficial velocity of gas injected is used (instead of flowrates) indicate that as the submergence decreases,

efficiency (measured as the liquid superficial velocity) is superior with 4 mm tubes (than 7.8 or 12 mm).

Figure 4.9 using laboratory measurements performed at 16% submergence, illustrates the gas lifting performance expressed through superficial gas-liquid velocities. For (superficial) gas velocities exceeding 0.4 m/s, the performance obtained with 7.8 mm diameter pipe is superior to 4 and 12 mm pipes.

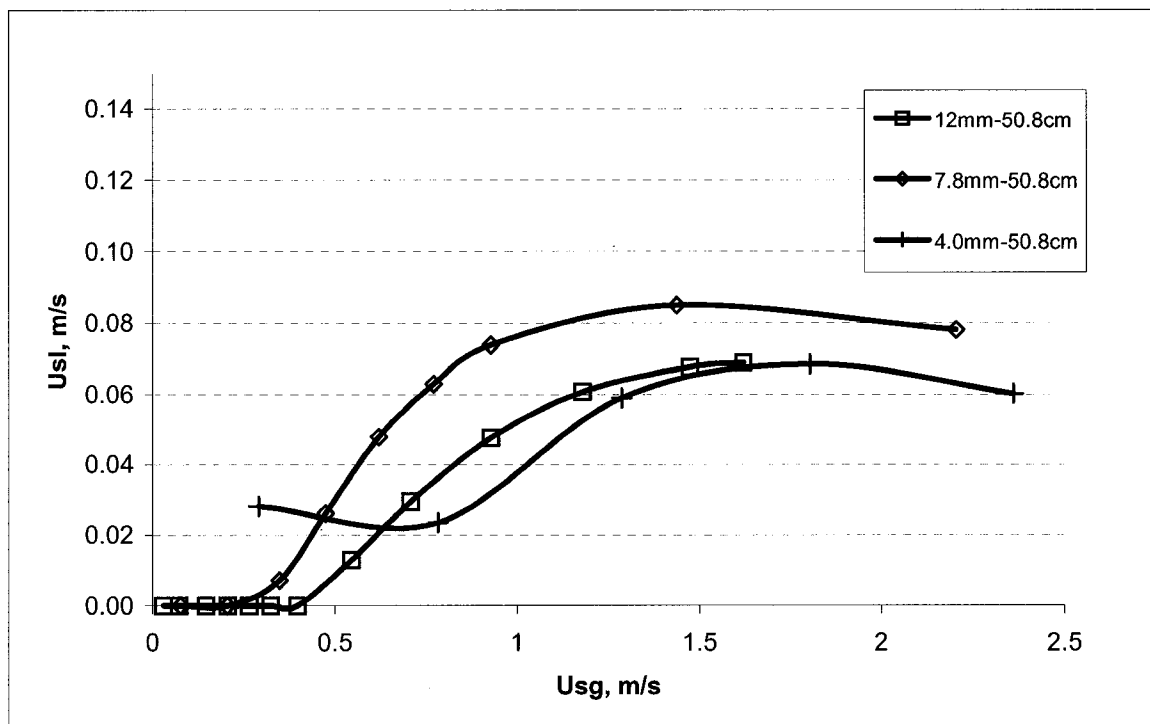


**Figure 4.9** Liquid superficial velocity versus gas superficial velocity for 4, 7.8 and 12 mm risers (at 16.6% submergence)

At very low air velocities (lower than 0.4 m/s), however, the 4.0 mm diameter riser showed to be more efficient. A similar conclusion was mentioned in section 4.1.4 where the submergence effect on liquid production was discussed and efficiency was considered for gas and liquid recorded flowrates.

## 4.2 Experimental results Part 2:

### Water-Methanol/Air system

The water-methanol/air system was used to determine qualitatively and quantitatively the effect of surface tension on the liquid production.

7.8 and 12 mm diameter risers at 20.1% and 12.5% submergence values were used in the same laboratory rig as previous reported experiments.

#### 4.2.1 Water-methanol mixture physical properties

Following the procedure described in the Chapter 3, the physical properties for water and pure methanol and for 60-40 % Vol. mixture are:

<b>Temperature</b>	20 °C
<b>Pressure</b>	101.3 Kpa

<b>PURE COMPOUNDS</b>	<b>Molecular weight [g/mol]</b>	<b>Density @ SC, [g/cm<sup>3</sup>]</b>	<b>Viscosity cP</b>	<b>Surface Tension @ SC (25°C)</b>
<b>Metanol</b>	32	0.791	0.58	22.5
<b>Water</b>	18	0.998	0.99	72

<b>METANOL-WATER MIXTURE</b>				
<b>MIX</b>	<b>Molar</b>	<b>Visc. Mix @ 21°C</b>	<b>Surface tension @ 21°C</b>	<b>Density @ 21°C</b>
<b>Methanol-Water %</b>	<b>Fraction</b>	<b>cP</b>	<b>Dyne/cm</b>	<b>g/cm<sup>3</sup></b>
40 - 60	0.27	1.71	38	0.947

**Table 4.5** Physical properties of water, methanol and water-methanol 60:40 mixture

#### 4.2.2 Flow Patterns – visual observations

Similar to the water/air flow in small diameter pipes, the water-methanol/air system was also dominated by the elongated bubble pattern.

Most of the visual observations are related to the shape, number and interaction of TD and small bubbles. However, less visible, but more important for determining the transport of gas-liquid is the thickness of the fall-back film, essentially related to the liquid surface tension modifications. The main observed difference was between the water-methanol/air and water/air flow systems was in the increased population of small (spherical) bubbles that appeared in the liquid slug section. These bubbles were generated at the tail of the long T-D bubbles due to of the local turbulence initiated by the liquid falling back in the liquid slug unit. A photographic comparison of the elongated bubble pattern observed in water and water/methanol systems is shown in Figure 4.10.

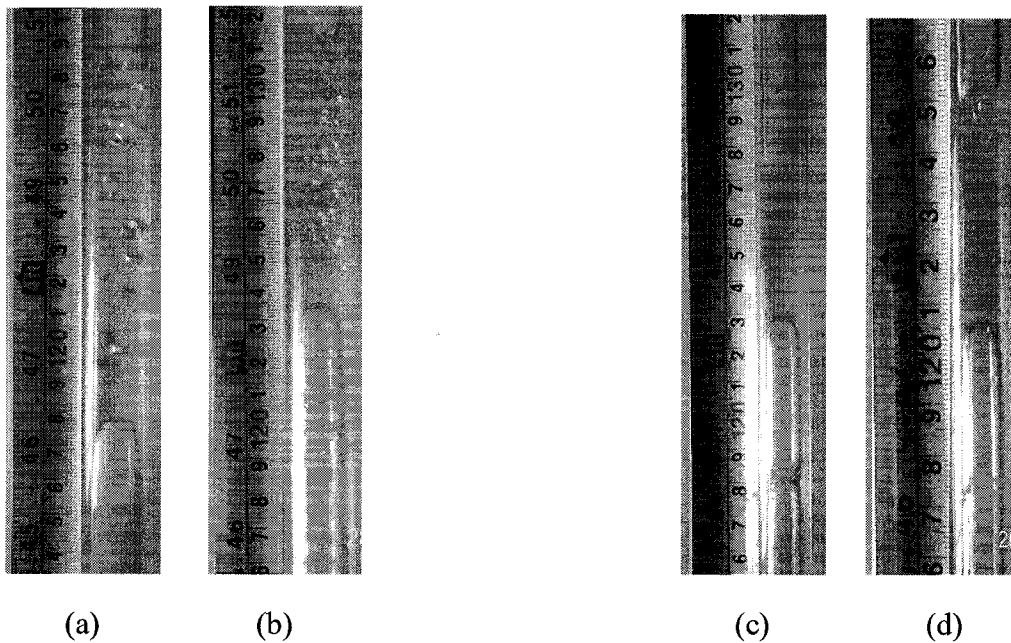


**Figure 4.10** (a) Elongated bubble flow pattern in 12 mm riser water/air system. 20.1% submergence, 3.7L/min air flow rate. (b) Elongated bubble flow pattern in 12 mm riser water-methanol/air system. 20.1% submergence, 3.7 L/min air flow rate. (c) Elongated bubble flow pattern in a 7.8 mm riser water/air system. 20.1% submergence, 1.4 L/min air flow rate. (d) Elongated bubble flow pattern in 8.0 mm riser water-methanol/air system, 20.1% submergence, 0.6 L/min air flow rate.

Figures 4.10 (a) and (b) show the results of water/air (Figure 4.10 (a)) and water-methanol/air (Figure 4.10 (b)) with 12 mm riser performed at 20% submergence condition. The production of liquid was compensated by continuous feed of water from

the storage tank so the liquid level and the reservoir pressure were kept constant during the test.

Measured surface tension of water and water-methanol mixture is 72.4 Dyne/cm and 38.0 Dyne/cm, respectively. The reduction in surface tension visible affected the flow pattern behavior in 12 mm riser.

Figure 4.10 (a), shows an elongated bubble flow pattern formed by a liquid slug unit with a relatively small quantity of small bubbles followed by a well-defined TD bubble. Figure 4.10 (b) shows a uniform elongated bubble flow pattern observed with the water-methanol mixture. The lower surface tension favored the formation of small bubbles in the liquid slug. The local turbulence induced due to the immersion of falling back liquid onto the liquid slug was sufficient to engulf small quantities of gas dragged from the TD bubble. This action is considered to be responsible for creating a significant population of small spherical bubbles, relatively smaller than observed in the pure water.

According to Equation 2.10, the bubble flow pattern should disappear if the tubing diameter is smaller than a critical value. In this case the critical diameter,  $D_{crit}$ , calculated for water and water-methanol mixture are 51.4 and 38.4 mm, respectively. Since the tubing diameter was 12 mm only, it was expected that “H” (Harmathy) bubbles are not possible to form. Since the “H” bubbles are considered deformable bubbles with equivalent spherical diameter much larger than 5 mm, it was proved that bubble flow pattern was never reached even at very small air flow rates.

An interesting behavior of the small bubbles contained in the liquid slug is also mentioned: During the water tests, these bubbles traveled upward with a velocity closer to or even faster than the TD bubble ahead of them, therefore, they joined into the TD bubble above them and eventually disappear through coalescence into the TD bubble. In the water-methanol mixture, however, because of the increased small bubble population, these bubbles were constantly absorbed/coalesced into the TD bubble following them.

Although most of the bubbles moved upwards ahead of the liquid slug unit, small portion of the small bubbles were captured by the falling back liquid stream, and carried downwards, as observed in Figure 4.10 (c) and (d). Similar phenomenon was also reported by Iguchi [59] who suggested that the tube wettability could cause some of the bubbles in the liquid slug to attach the wall of the tube and be easily captured by the liquid falling back.

Figures 4.10 (c) and (d) shows the elongated bubble flow pattern in a 7.8 mm tubing. For water and water-methanol mixture, the differences in the flow pattern were negligible. The number of tiny bubbles in water-methanol/air flow in 7.8mm tubing seems to be less than the ones in 12 mm diameter pipe.

Similar to the water/air system, deformable bubbles in water-methanol/air flow also traveled nested in a simple elongated flow pattern as shown in Figure 4.11.

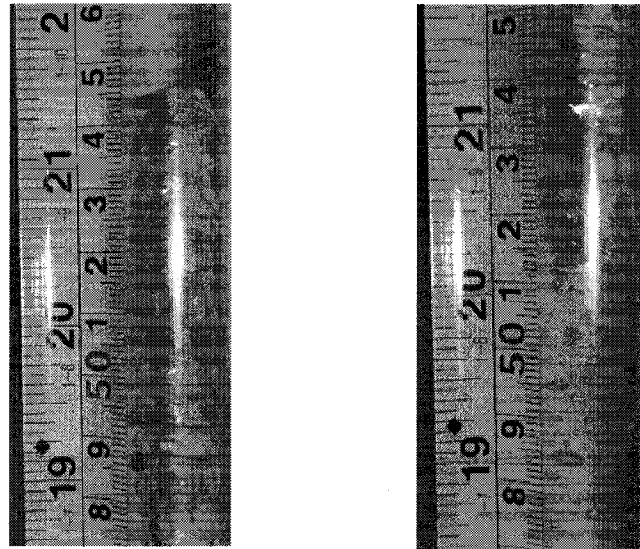


**Figure 4.11** Elongated bubble pattern with grouped but un-coalesced bubbles forming a T-D bubble structure, water methanol mixture, 0.2 L/min air flow rate, 12 mm riser.

### 4.2.3 Flow instabilities

The elongated bubble flow pattern that dominated the experiments in water and water-methanol mixture, created frequent fluctuation of the local and averaged two-phase flow densities which in turn caused oscillating variations of the BHP. These variations were identified as instabilities and observed for the whole range of air injection rates and submergences.

Reinemann et al. [42] suggested that instabilities are improving the liquid production rate as compared to his model predictions. In this study, instabilities are observed and quantified.

Two sources of instabilities were detected both in water and water/methanol mixture:

- a) Instabilities induced by bubble coalescence, and
- b) Instabilities by bubble breaking/dissipation (Figure 4.13).

Instabilities, as described by De Cachard and Delhaye [58], result from variations of mixture density in the riser, coupled with oscillations of the single-phase liquid flow rate upstream of the air injection. The changing density causes the bottom-hole pressure to fluctuate between a maximum and a minimum value.

Instabilities observed during the slug flow pattern, are related to both bubble dissipation (no liquid production) and production conditions. In the bubble dissipation stage, which precedes production stage, the T-D bubble that belongs to the previous slug unit approaching the top of the riser, brakes down in the pipe causing the liquid to fall back to the previous slug unit. It changes the local distribution of the phases and causes alterations of the bottom-hole pressure (Figure 4.12 (a)).

Instabilities related to local production conditions are associated to local dynamic of pattern flow transition [15] occurring as a result of pressure-density changes.

Flow instabilities can be detected by monitoring oscillations of the bottom-hole pressure. The bubble coalescing effect is shown in Figure 4.12 (a) where a T-D bubble captures a small bubble located above it. The presence of a numerous population of small bubbles, some of them attached to the wall, is specific to the elongated bubble pattern for the water-methanol mixture. The Figure 4.12 (b) shows two consecutive T-D bubbles just after coalesce. The thickness of the film becomes considerably thicker in the section corresponding to the previous liquid slug unit.

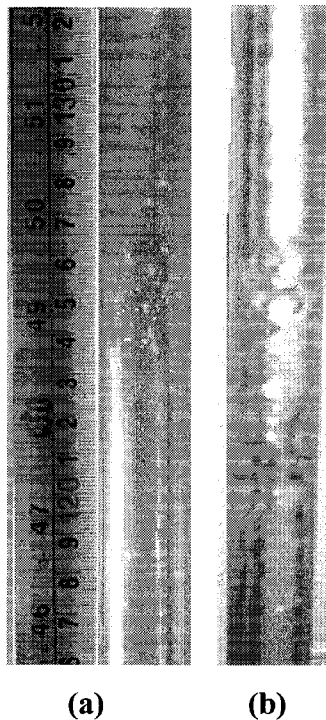


**Figure 4.12** (a) Picture of a T-D bubble capturing a small bubble just above it. (b) Picture of two consecutive T-D bubbles just after coalescing.

A summary of experimental pressure data (for water and water-methanol mixture) is presented in Appendix D. Using these data a set of figures showing the maximum, minimum and average bottom hole pressure were collected to quantify the occurrence and the magnitude of instabilities (Figure 4.13).

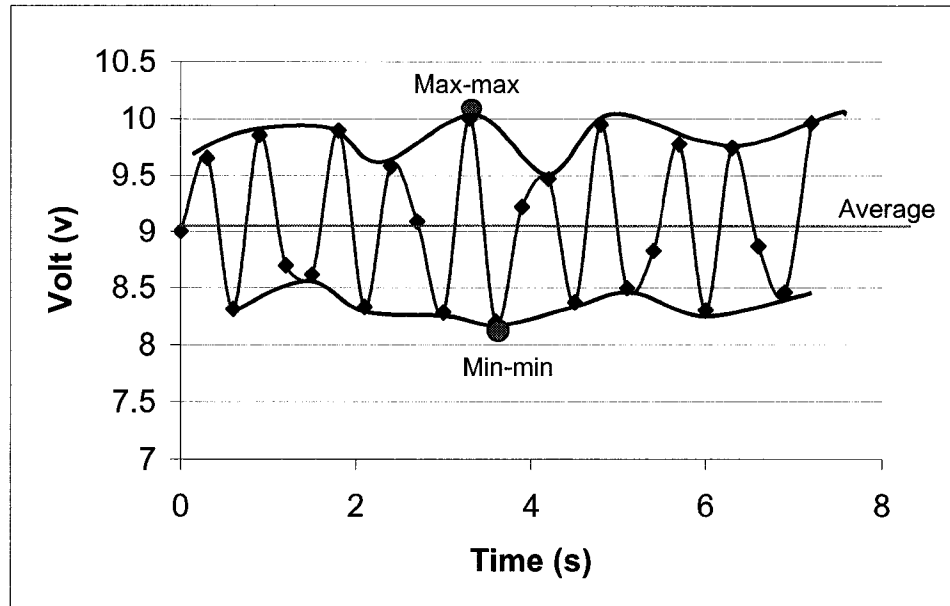


**Figure 4.13** Example of a RMS graph showing the maximum-maximorum (max-max), minimum-minimorum (min-min), and average value (i.e. Water 12 mm riser and 6.3 L/min air injection rate).

The Figure 4.13 shows an example of a continuous data acquisition (RMS figure). The volts signal from the pressure transducer are plot in a graph volts versus time. The maximum of the highest volts (maximum-maximorum) and the minimum of the lowest volts (minimum-minimorum) are represented by the full dots. The max-max and min-min voltages are selected after 5 minutes of continuous recording for each submergence and gas injection rate. The voltage is converted into pressure (psi) using the calibration curve for the installed pressure diaphragm (i.e. 1 psi diaphragm: 1 volt = 0.1 psi).

Figures 4.14 and 4.15 show the maximum-maximorum and minimum-minimorum envelopes and illustrate the variation of bottom hole pressure BHP (differences between the two envelopes) during increments of gas injection flowrate (water-methanol and water systems in a 12 mm riser at 20.1% submergence). The difference between maxi-max and min-min of the BHP oscillations was in the range of 0.2 psi for the water-methanol system, and 0.3 psi for the water system. The average variation of BHP corresponds to 23.5% and 33% of the static liquid column pressure for water-methanol mixture and water systems, respectively.

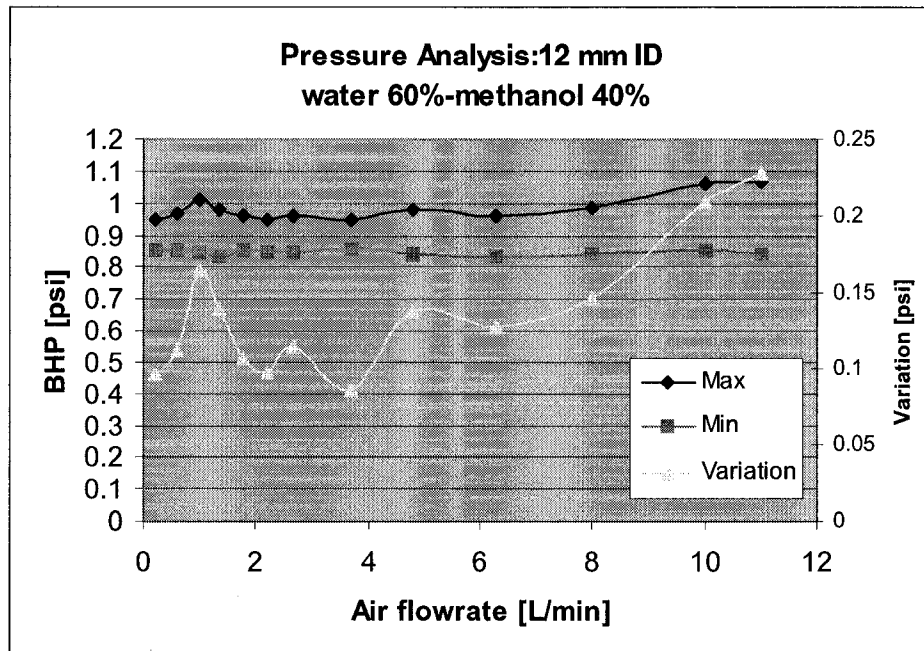


**Figure 4.14** Extreme of BHP oscillations (envelopes) observed with a 12 mm riser in a water-methanol system – 20.1% submergence.

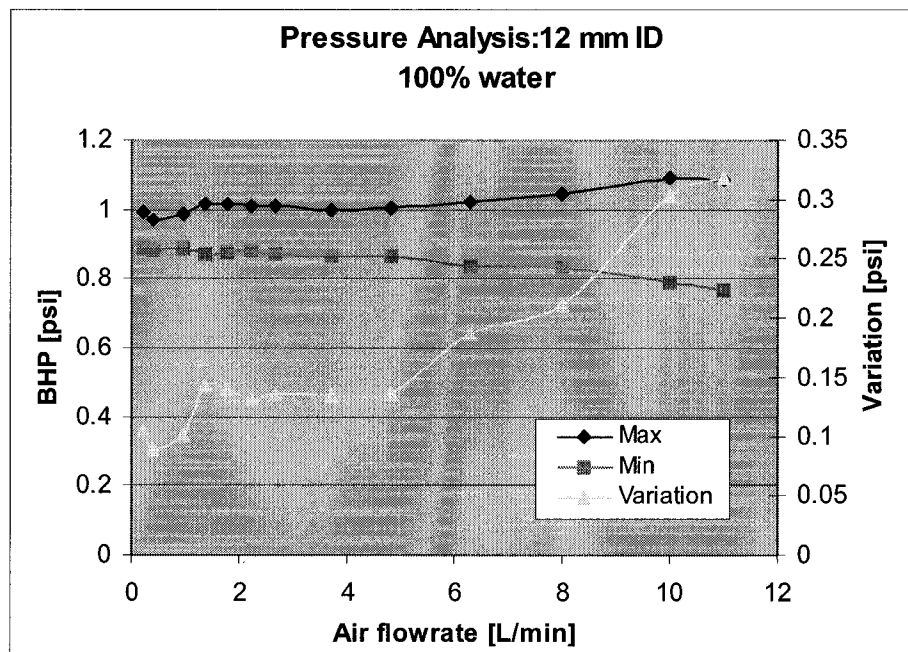


**Figure 4.15** Extreme of BHP oscillations (envelopes) observed with 12 mm riser in a water system – 20.1% submergence.

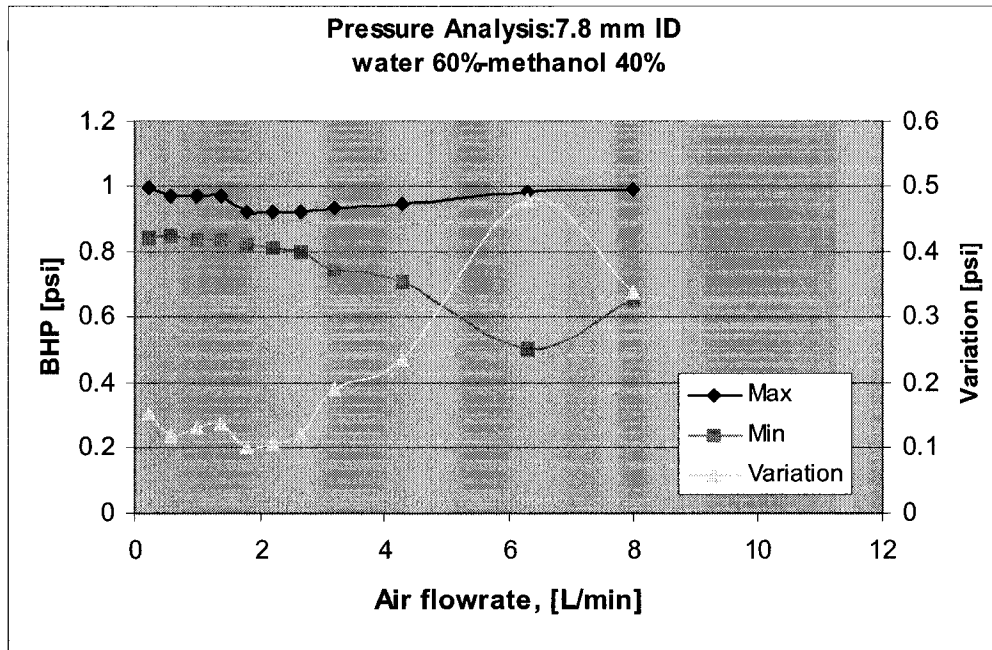


**Figure 4.16** Extreme of BHP oscillations (envelopes) observed with 7.8 mm riser in a water-methanol system – 20.1 % submergence

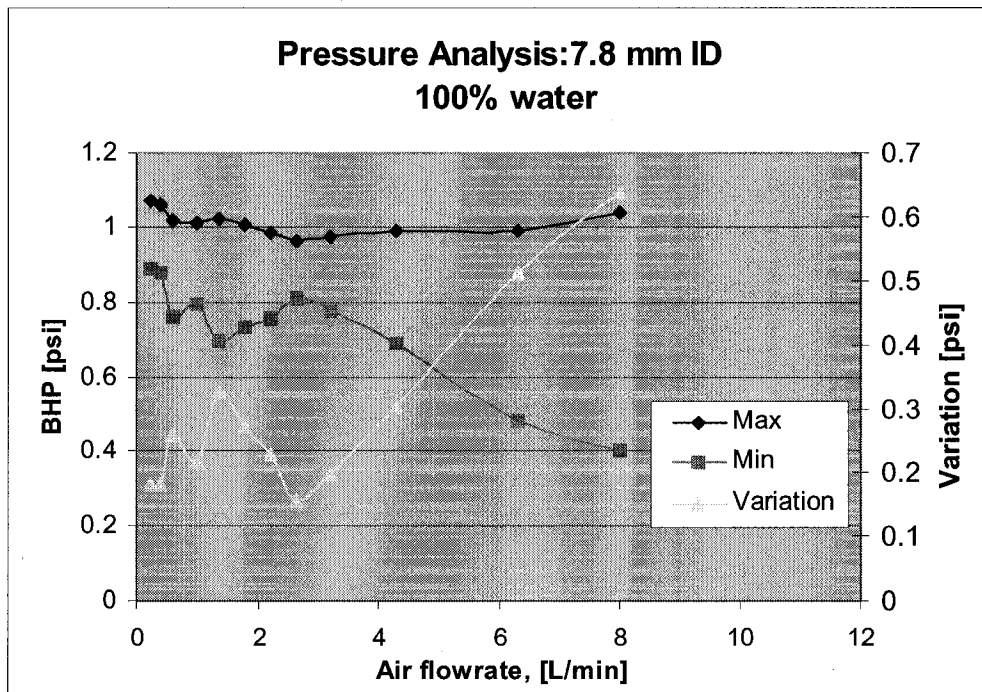


**Figure 4.17** Extreme of BHP oscillations (envelopes) observed with 7.8 mm riser in a water system – 20.1% submergence

The difference between “max-max” and “min-min” envelopes extracted from the continuous measurement of bottom hole pressure (representing the maximum possible amplitude of the instability-related pressure oscillations) for water-methanol/air flow in 7.8 mm diameter raiser varied between 0.1 and 0.5 psi (Figure 4.16).

The maximum amplitude (variation) of the BHP oscillations was between 0.2 and 0.6 psi for water/air flow in 7.8 mm diameter pipe. It was observed that the maximum amplitude of BHP oscillations increased with gas velocities (Figure 4.17). The magnitude of the amplitude of BHP oscillations (0.6 psi) was very high compared with the RMS value (averaging the static liquid column pressure (0.90 psi)). The relative value of amplitude versus the RMS (averaged) pressure was 20% at low gas injection rates and approximately 65% calculated for high gas injection rates.

Instabilities were also recorded for low submergence conditions. For example, the maximum amplitude of BHP was equivalent to 65% of the RMS (averaged) BHP value for 12.5% submergence.

#### **4.2.4 Surface tension effect**

Experimental results for water-methanol mixture are summarized in Appendix D. The recorded data included: Temperature, tube diameter, submergence, bottom hole pressure, mass rate of liquid, time, and T-D bubble upward velocity.

Figure 4.18 shows the results obtained from the experiments conducted by using 60:40 water methanol mixture (dashed lines) and 100% water (solid lines) with 7.8 and 12 mm risers under 20.1% (63.5 cm) and 12.5% (38.1 cm) submergence.

Measured interfacial tension (IFT) for water and 60:40 water-methanol mixture was 72.4 and 38.0 Dyne/cm, respectively.

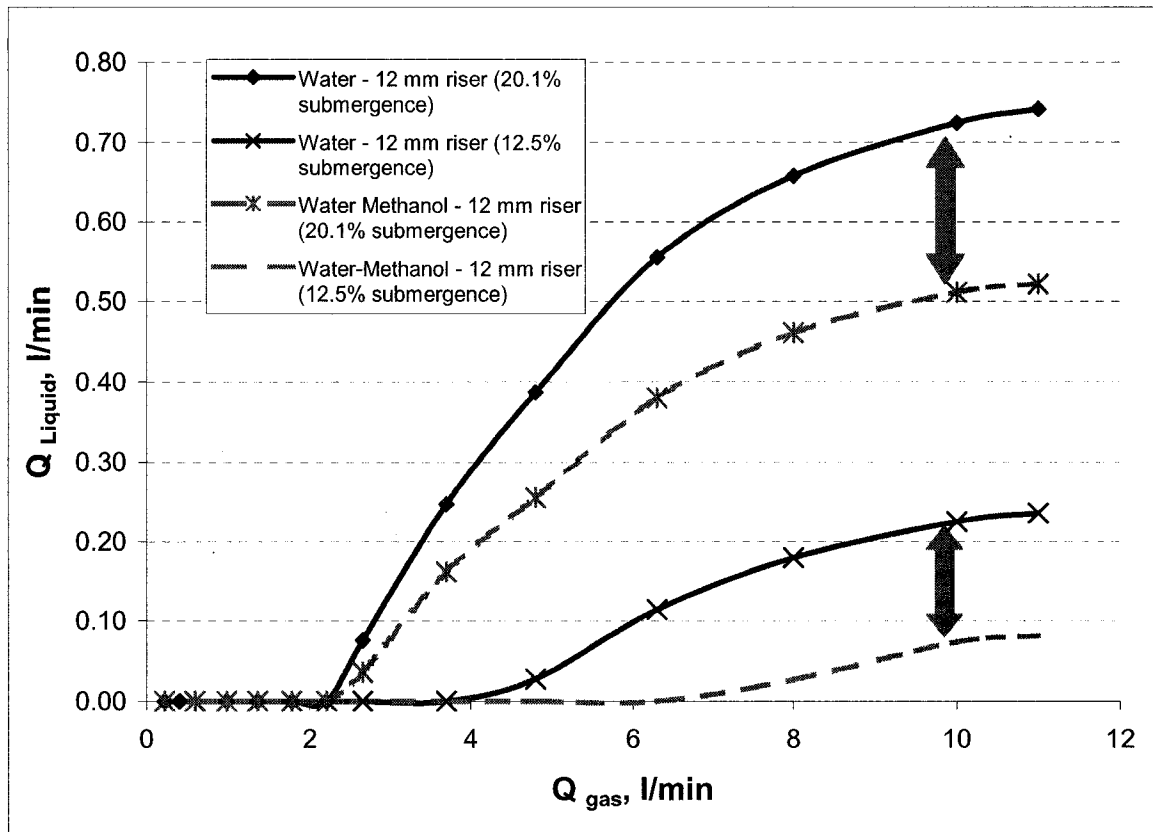


**Figure 4.18** IFT Effect on Liquid production at 12.5 and 20% submergence with 12 mm riser

As the difference in density between water and water-methanol is of approximately 5% ( $998 \text{ Kg/m}^3$  for water and  $947 \text{ Kg/m}^3$  for water-methanol mixture) and test conditions were very similar for both fluids, the surface tension relative difference of approximately 45% is considered to be the cause of observed performance differences.

For the 12 mm riser (Figure 4.18), the relative reduction in liquid production was about 30% at 20.1% submergence and reached 65.6% at 12.5% submergence. Therefore, the effect of IFT reduction was more visible for experiments conducted at lower submergence.

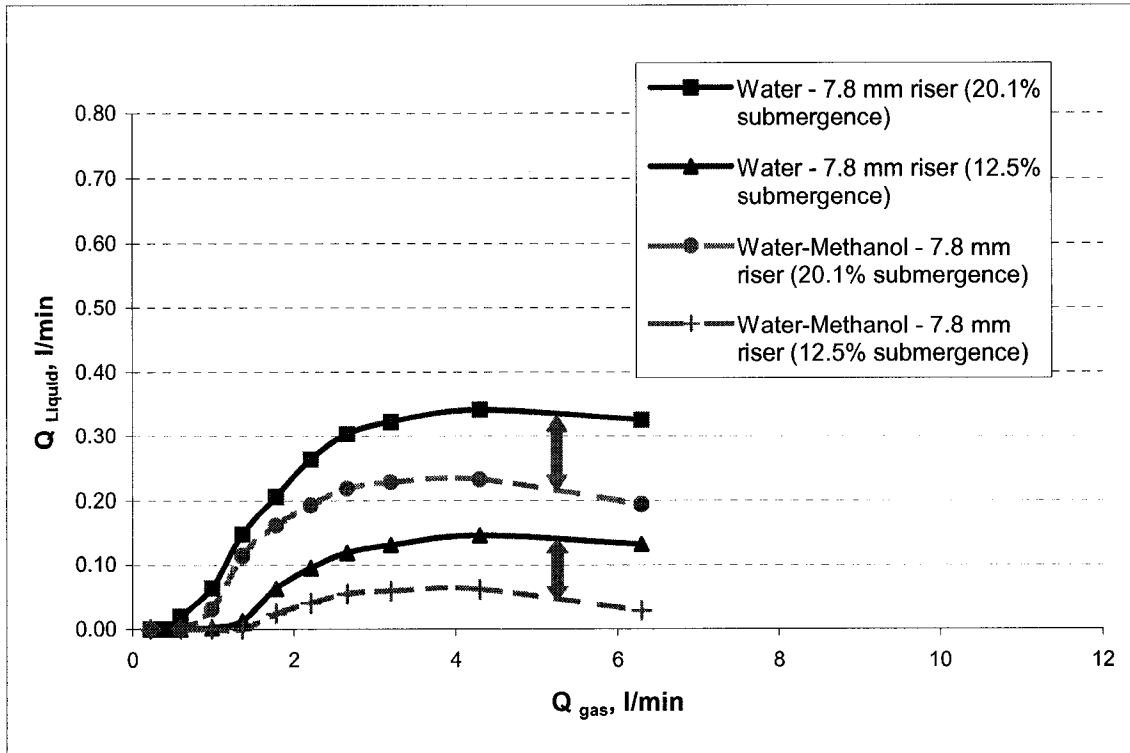


**Figure 4.19** IFT Effect on Liquid production at 12.5 and 20% submergence with 7.8 mm riser

For the 7.8 mm pipe diameter (Figure 4.19), the reduction in liquid production was 40% and 78% for the 20.1% and 12.5% submergence, respectively. Therefore the effect of IFT reduction increased with reduction of diameter.

The possible reason for these differences may be due to the fact that at lower liquid surface tension the liquid film surrounding the T-D bubble becomes thicker, which produces an increment of liquid falling back. In small diameter pipes, the liquid production is very sensitive to changes in the liquid film thickness since the liquid slug (transporting the liquid from the bottom to the well head) will be drain faster when thicker liquid film. The variation in film thickness with respect to the liquid surface tension (IFT) will be explained in section 4.2.6.

On the other hand, the onset of liquid production, (observed as minimum of gas injected required to initialize the production - critical production condition – CPC-), was not

visible modified with the reduction of IFT. For instance, for 12 mm riser the CPC increased from zero to 23% when submergence decreased from 20.1% to 12.5%.

#### 4.2.5 Submergence and tubing diameter effects

The liquid/air ratio and the  $U_l^s$  vs.  $U_g^s$  graph were used to determine the optimum tube diameter at 20.1% and 12.5% submergence values.

Figure 4.20 shows the superficial liquid velocity versus the superficial air velocity. The 7.8 mm riser exceeded the liquid productivity performance compared to the other riser, since more liquid was produced per unit of gas injected.

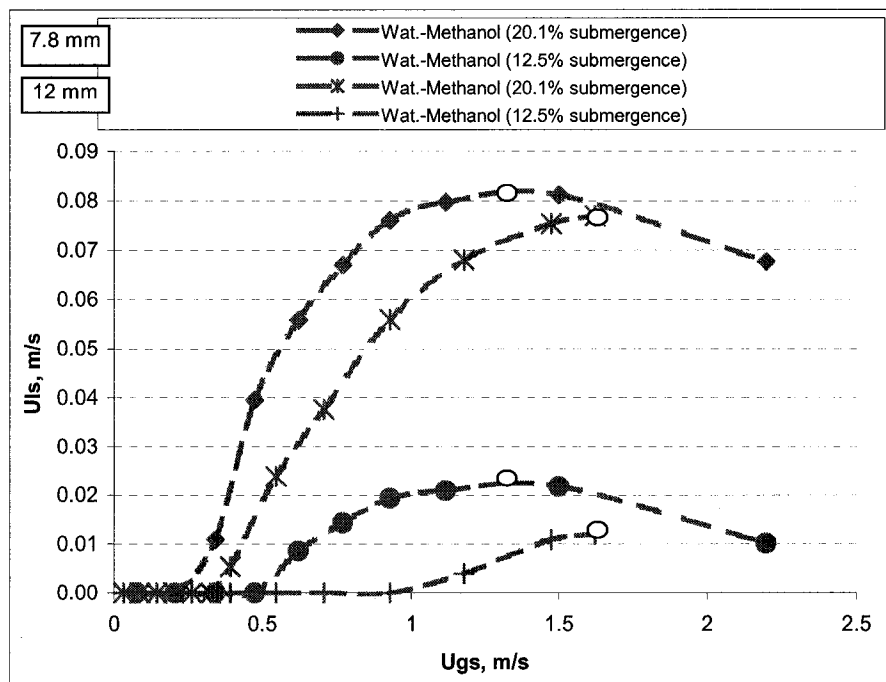


**Figure 4.20** Superficial liquid velocity versus superficial gas velocity for water-methanol experiments conducted in 7.8 and 12 mm at 12.5 and 20% submergence

The liquid/air volumetric ratio calculated at the maximum liquid production rate (Maximum Production Condition, MPC see open circles in Figure 4.20) was used to summarize and compare the liquid production efficiency with 7.8 mm and 12 mm diameter tubing. The results are shown in table 4.6.

% Submergence	Tubing Diameter (mm)	
	12	7.8
20.1	0.04747	0.05857
12.5	0.007345	0.01571

**Table 4.6** Liquid (water-methanol)/air ratio at maximum production conditions (MPC) with 7.8 and 12 mm risers at 12.5 and 20.1% submergence

The summary in table 4.6 suggests that the MPC expressed for Liquid/air ratio, is superior for 7.8 mm riser than for 12 mm for both submergences. Similar results were also observed with water [Table 4.3] showing a consistent behavior even at reduced surface tension values.

#### 4.2.6 The upward T-D Bubble velocity

A digital video camera was used to capture the upward movement of T-D bubbles for various injection and diameters. Detailed data and procedure is summarized in the Appendix D.

Figures 4.19 – 4.22 show the results. The T-D bubble rising velocity was first theoretically calculated using the drift flux (Equation 2.15) proposed by Nicklin [20]. Equation 2.15 was rewritten as Equation 4.2:

$$U_g = U_{T-D\text{Nicklin}} = C_o U_l + U_{T-D\infty} \quad 4.2$$

$$\text{where } U_{T-D\infty} = 0.35\sqrt{gD} .$$

The velocity distribution coefficient  $C_o$  in equation 4.2 was taken equal to 1.2.

In case of small diameter pipes it is assumed that all the gas is contained inside the T-D bubble. Therefore, the gas velocity  $U_g$  could be interpreted as the theoretical T-D bubble velocity ( $U_{T-D\text{Nicklin}}$ ).

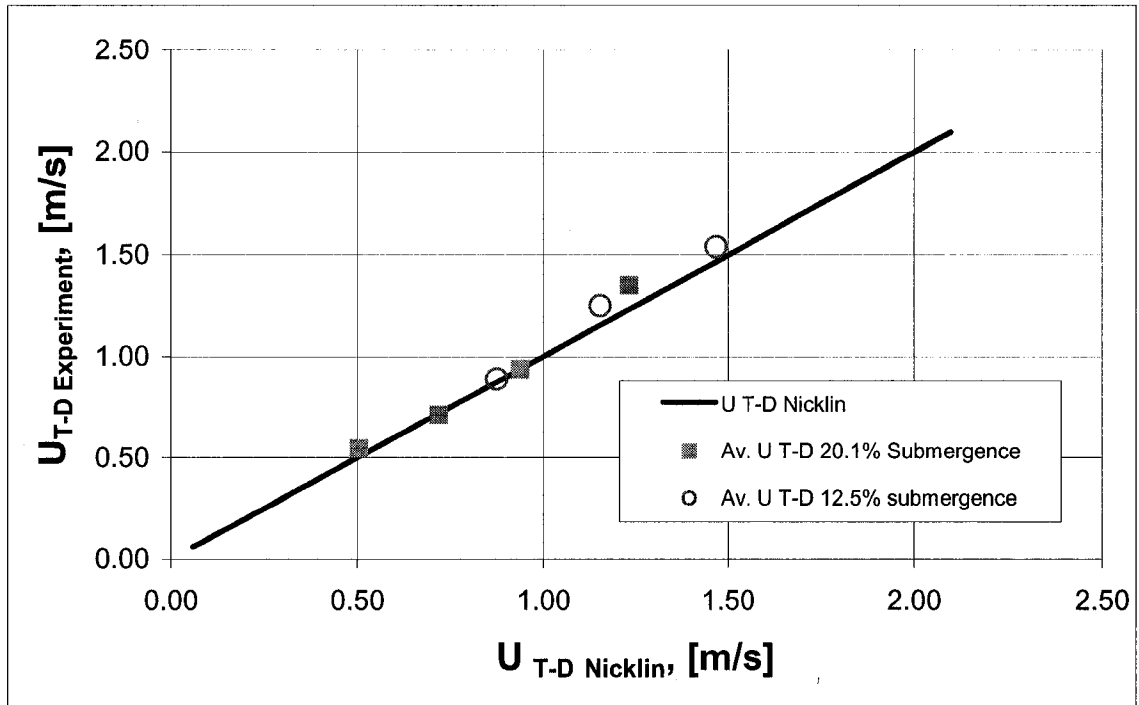


**Figure 4.21** Measured and calculated rising velocity of T-D bubble (12 mm diameter riser, 20.1% and 12.5% submergence, 100% water)

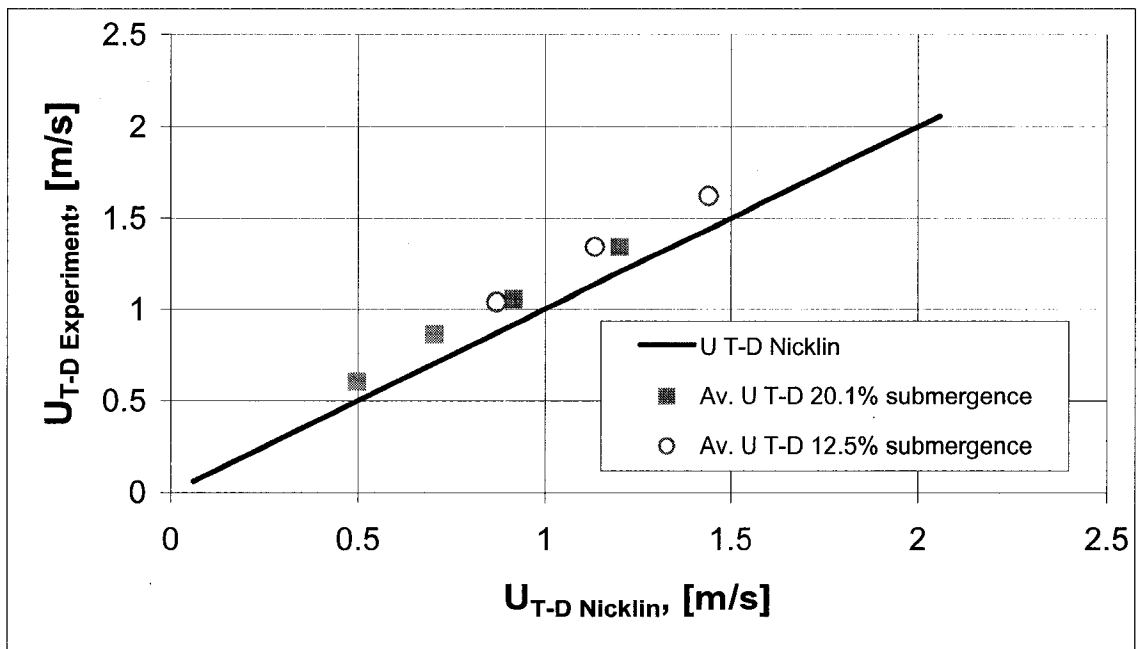


**Figure 4.22** Measured and calculated rising velocity of T-D bubble (12 mm diameter riser 20.1% and 12.5% submergence, 60:40 water/methanol)

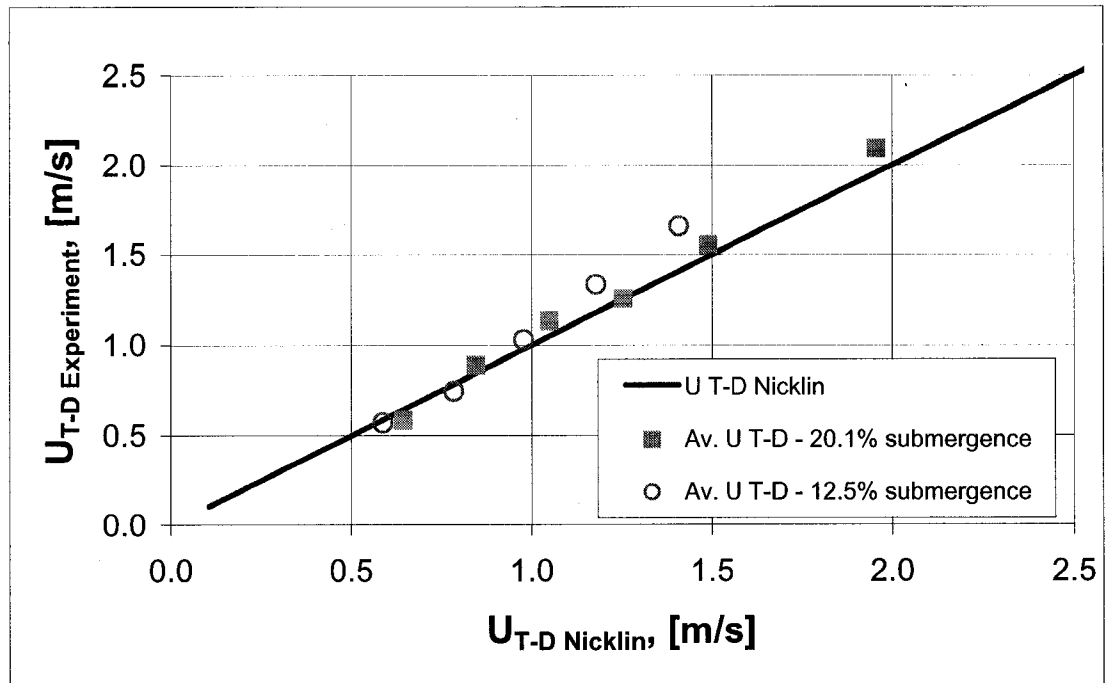


**Figure 4.23** Measured and calculated rising velocity of T-D bubble velocity (7.8 mm diameter riser, 20.1% and 12.5% submergence, 100% water)

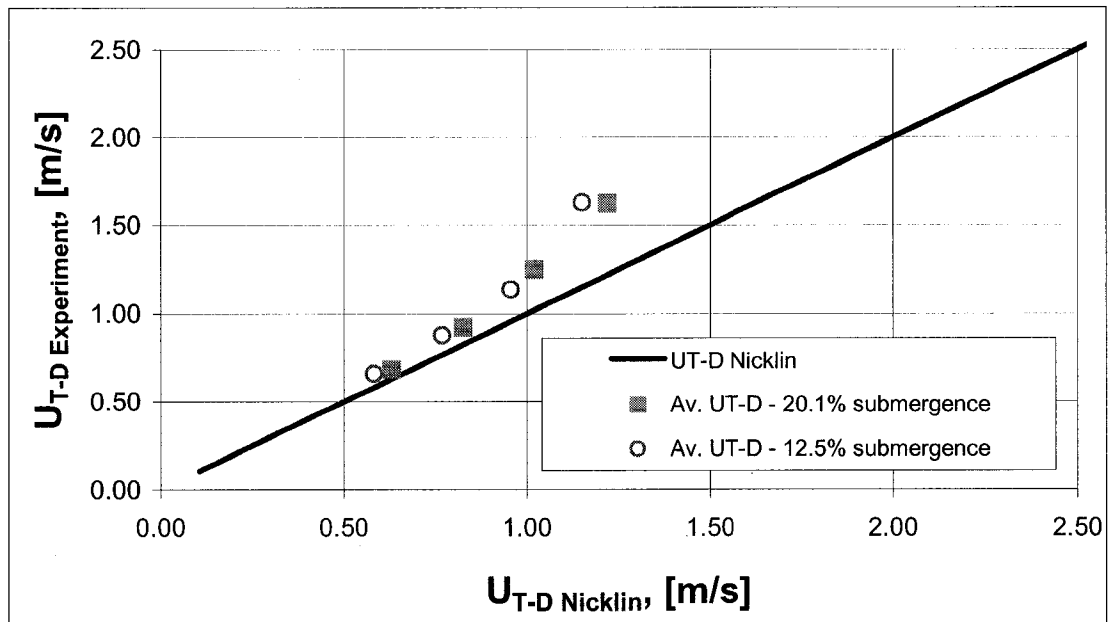


**Figure 4.24** Measured and calculated rising velocity of T-D bubble (7.8 mm diameter riser, 20.1% and 12.5% submergence, 60:40 water-methanol)

In all figures the solid line corresponds to calculated gas velocity  $U_{T-D \text{ Nicklin}}$  and is used as a comparative reference for the experimental values. The experimental values for the

T-D bubble rising velocity at 20.1% and 12.5% submergences were represented with full squares and open circles, respectively.

The calculated gas velocity ( $U_{T-D \text{ Nicklin}}$ ) compared satisfactorily with the experimental measured rising T-D bubble velocities ( $U_{T-D \text{ Experiment}}$ ) when measured using water with the 12 mm riser (Figure 4.21).

For the cases when only water was used (Figures 4.21 and 4.23), the experimental T-D bubble velocity was within the 10% error range of calculated theoretical value. For the 60:40 water-methanol mixture the bubble velocity exceeded 10% of the calculated series of values (Figures 4.22 and 4.24). This suggests another effect related to IFT. Similar observations were obtained with 7.8 and 12 mm diameter tubing.

By assuming that the  $U_{T-D\infty}$  (terminal velocity) is negligible as compared to the  $U_g$  (e.g.  $U_g=0.707$  m/s,  $U_{T-D\infty}=0.02$  m/s) the increased gas velocity at lower surface tension could be explained by the reduction in the gas flowing area. This reduction is a consequence of a thicker liquid film that surrounds the T-D bubble.

This effect is calculated and results are presented in table 4.7. The average film thickness,  $\delta$ , and the average void fraction,  $\alpha$ , were calculated by using Equations 2.38 and 2.28, respectively. Theoretical, calculated values are usually disregarding the IFT effect and are labeled “NO” in Table 4.7. The experimental values were labeled as “EXP”.

For experiments performed in the 12 mm tube at 4.8 L/min gas, the liquid film thickness (evaluated on the basis of measured velocity of bubble) was 74.37% higher for the methanol-water mixture (38 dyne/cm) than for water only. The same effect was also observed when other air injection rates and submergence levels were considered.

Therefore, modifications of IFT affected both the T-D bubble velocity and the liquid film thickness. The two values being correlated and strongly influencing the fall back liquid velocity and finally, the gas lifting performance.

<b>WATER</b>							
<b>Surface Tension Effect</b>	<b>D (m)</b>	<b>A (m<sup>2</sup>)</b>	<b>Q<sub>g</sub> (L/min)</b>	<b>U<sub>g</sub><sup>s</sup> (m/s)</b>	<b>Void fraction α</b>	<b>Film thickness δ (mm)</b>	<b>Film δ % Difference</b>
NO	0.012	0.0001131	4.8	0.707	0.809	0.603	7.93
EXP	0.012	0.0001131	4.8	0.707	0.795	0.651	
<b>60:40 WATER-METHANOL</b>							
NO	0.012	0.0001131	4.8	0.707	0.809	0.603	74.37
EXP	0.012	0.0001131	4.8	0.707	0.680	1.052	

**Table 4.7** Liquid film thickness and local void fractions evaluated using theoretical calculations for the rising velocity of T-D bubble and measured values

The current models for small diameter pipes did include a suitable calculation of liquid film thickness as function of the liquid surface tension. An improved mechanistic theoretical model applicable for the small diameter pipes is further proposed and described in Chapter 5.

**CHAPTER 5**  
**COMPARISON OF EXISTING NUMERICAL MODELS**  
**AND**  
**IN-HOUSE MODEL DEVELOPMENT**

---

Before proposing a new model, three models frequently used by the industry were investigated and compared. The Ansari [51] and Hassan's [41] models are well known in the industry and are widely used for conventional pipes. The third model was proposed by Reinemann [42] to be used, particularly, for small diameter air lifting systems operating under submergences higher than 60%.

An EXCEL program and suitable macros have been used to create a unitary tool capable to validate third-party and this work experimental data.

The first addressed question investigated the possible applicability of Ansari [51] and Hassan's [41] (conventional-diameter pipes) models for low-reservoir pressure conditions. Fernandes [50] experimental data was used to validate the predictions of Hasan and Ansary models.

### **5.1 Conventional pipe models – Validation at low-pressure systems**

Spreadsheet (EXCEL) programs using the Ansari and Hasan's models were developed and tested first (Appendix E). The input data was obtained from literature (Fernandes [50]). The experimental void fractions were validated against different model predictions. Percent error deviations (Equation.5.1) are shown in Table 5.1. The percent error was defined as follows:

$$\%Error = \frac{\alpha_{calc} - \alpha_{exp}}{\alpha_{exp}} * 100 \tag{5.1}$$

where  $\alpha_{calc}$  is the void fraction of the slug unit calculated by the model and  $\alpha_{exp}$  is the void fraction measured during the experiment.

The symbol  $\alpha_{SU}$  represents the calculated slug unit void fraction and  $\alpha_{SU exp}$  is the experimental slug unit void fraction obtained from the Fernandes [50] experiments.

$U_g^s$ (m/s)	$U_l^s$ (m/s)	Fernandes			Hasan		Ansari	
		$\alpha_{SU}$ Fernandes (%)	$\alpha_{SU exp.}$ (%)	$\alpha_{SU}/\alpha_{SU exp.} * 100$ (%)	$\alpha_{SU}$ Hasan (%)	$\alpha_{SU}/\alpha_{SU exp.} * 100$ (%)	$\alpha_{SU}$ Ansari (%)	$\alpha_{SU}/\alpha_{SU exp.} * 100$ (%)
64	63	1.6	61.0	-3.2	62.0	-1.6	64.0	63.0
72	69	4.3	70.0	1.5	71.0	2.9	72.0	69.0
73	73	0.0	72.0	-1.4	72.0	-1.4	73.0	73.0
59	58	1.7	53.0	-8.6	55.0	-5.2	59.0	58.0
71	69	2.9	69.0	0.0	70.0	1.5	71.0	69.0
62	61	1.6	55.0	-9.8	59.0	-3.3	62.0	61.0
70	69	1.4	66.0	-4.4	69.0	0.0	70.0	69.0
72	70	2.9	70.0	0.0	72.0	2.9	72.0	70.0
54	49	10.2	43.0	-12.2	50.0	2.0	54.0	49.0
61	61	0.0	53.0	-13.1	59.0	-3.3	61.0	61.0
66	68	-2.9	60.0	-11.8	65.0	-4.4	66.0	68.0
56	56	0.0	45.0	-19.6	53.0	-5.4	56.0	56.0
60	60	0.0	45.0	-25.0	58.0	-3.3	60.0	60.0
63	60	5.0	55.0	-8.3	62.0	3.3	63.0	60.0
69	69	0.0	63.0	-8.7	68.0	-1.5	69.0	69.0
55	55	0.0	43.0	-21.8	53.0	-3.6	55.0	55.0
60	64	-6.3	49.0	-23.4	58.0	-9.4	60.0	64.0
66	66	0.0	57.0	-13.6	65.0	-1.5	66.0	66.0
53	53	0.0	40.0	-24.5	50.0	-5.7	53.0	53.0
58	58	0.0	47.0	-19.0	57.0	-1.7	58.0	58.0
62	64	-3.1	52.0	-18.8	62.0	-3.1	62.0	64.0
55	56	-1.8	41.0	-26.8	53.0	-5.4	55.0	56.0
59	63	-6.3	47.0	-25.4	58.0	-7.9	59.0	63.0
51	54	-5.6	37.0	-31.5	50.0	-7.4	51.0	54.0

**Table 5.1** Void fraction comparisons using Fernandes' [50] experimental data against Hasan and Ansari's model predictions

Hasan's model predicted the void fraction within a range of +6.0 and -16% error for low liquid and medium gas flow rates. With increasing the flow rates, the percent error

increased up to  $-31\%$ , indicating that the void fraction was significantly under-predicted. This is less than acceptable for predicting production with small diameter pipes. Ansari's model predicted the experimental results within an acceptable  $\pm 8.0\%$  range.

Figure 5.1 shows the percent error of Fernandes, Hasan and Ansari's models versus the experimental slug unit void fraction from Fernandes [50] experiments. Hasan's model predictions show a trend of increasing error while decreasing the void fraction from 70 to 54%. The maximum under-prediction percent error was  $-31\%$  for the 54% void fraction. For void fractions below 54%, the accuracy in Hasan's model prediction increases, but still remains above  $-10\%$ . Ansari's model shows a variable percent of error while increasing the void fractions. The percent error curve keeps between  $-8\%$  and  $3\%$  range, and describes similar path than the Fernandes' model percent error curve. A common characteristic for the three models is the low percent error (less than  $\pm 3\%$ ) for void fractions greater than 70%.

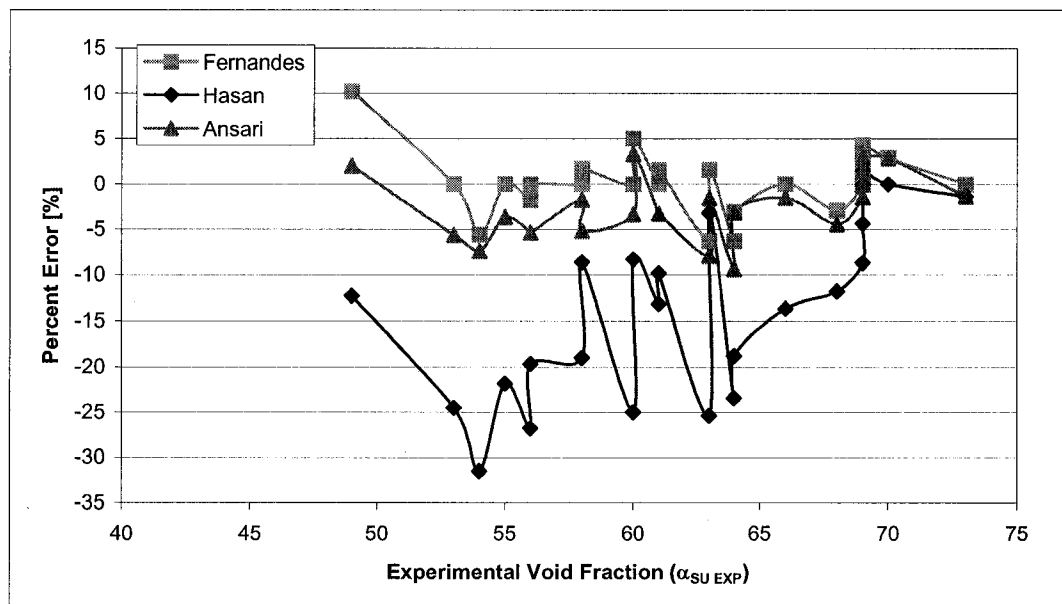


**Figure 5.1** Comparison between experimental data (Fernandes [50]) and modeled void fraction (Hasan and Ansari) – conventional-diameters

Based on this initial screening, the Ansari's model was chosen to be used as benchmark for future comparisons.

## 5.2 Experimental results versus existing model predictions – small diameters

The experimental results obtained from the water and water-methanol / air systems were compared to the predictions made by the Ansari's model and Reinemann's model. Experimental data obtained with 7.8 and 12mm risers at a submergence of 20.1% (63.5 cm) were compared with modeled performances (Ansari). Superficial liquid versus superficial gas velocities (calculated versus measured – present work) is illustrated in figure 5.2.

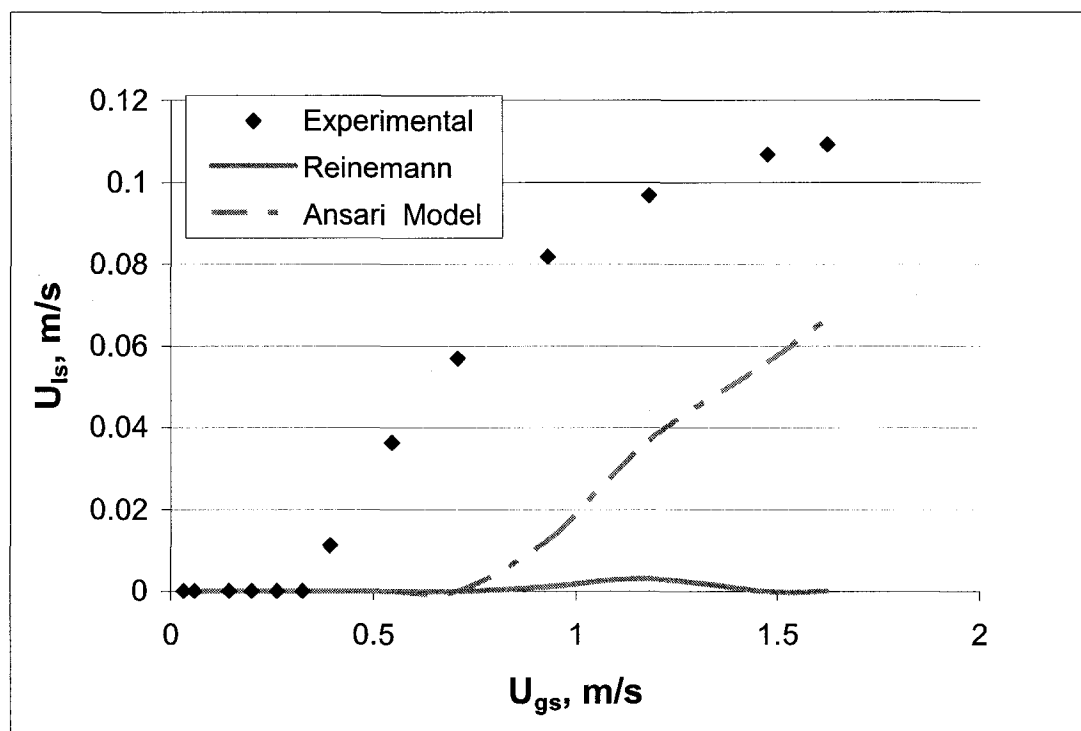


**Figure 5.2** Water versus air superficial velocities; experimental results from this work compared with calculations using the Ansari and the Reinemann models (12 mm ID-riser, 20.1% submergence)

The prediction made by Ansari's model indicated a trend similar to the experimental data, however, it significantly under predicted measured liquid superficial velocity. It is also observed from figure 5.2 that the onset of liquid production (critical production condition - CPC) is calculated for higher gas injection than the experimental CPC value. While the CPC appeared at  $U_g^s = 0.32$  m/s in the experimental curve, the model predicted the initial

production at  $U_g^s = 0.707$  m/s (121% difference). The percentage of error measured at the maximum production condition is about 40%.

It is observed in figure 5.2 that the Reinemann's model did not follow the trend of the curve using present experimental data. The Reinemann's model under predicted present laboratory data. This model showed good agreement at submergence values higher than 60%, but did not predict the air lift behaviour at lower submergences [42].

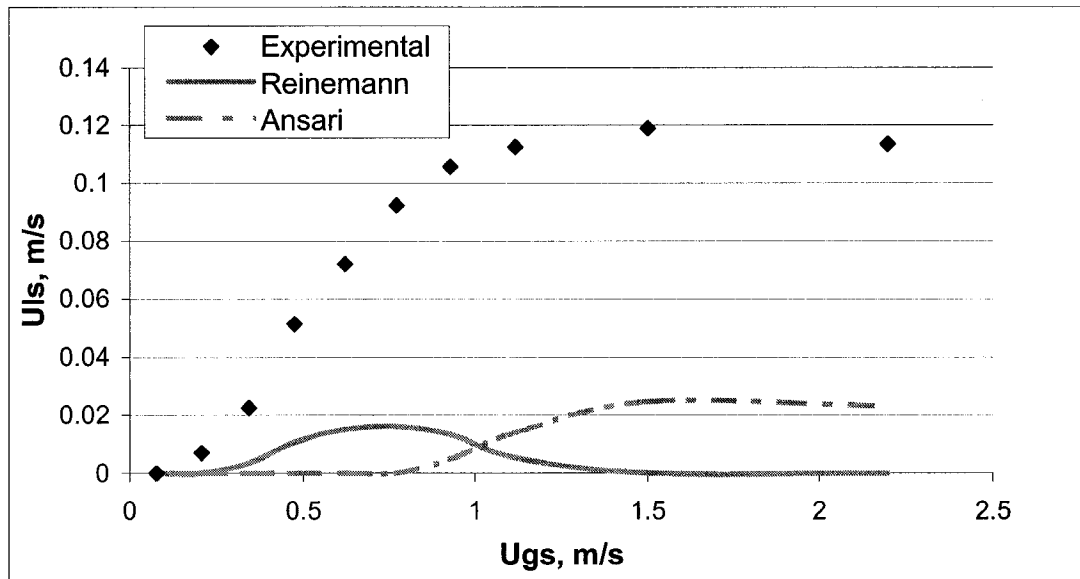


**Figure 5.3** Water vs. air superficial velocities – this work experimental result and Ansari and Reinemann liquid flow predictions (7.8 mm ID riser, 20.1% submergence - 63.5 cm)

A similar comparison to that presented in figure 5.3 (between modeled flow characteristics using liquid versus gas superficial velocities) is repeated in Figure 5.3 for 7.8 mm ID riser. The shape of the curve described by the experimental data was well followed by the Ansari's model predictions. Again, the CPC was shifted to the right, and the discrepancy was more drastic than for the 12 mm riser. The experimental maximum production condition at  $U_g^s = 1.5$  m/s was 4.8 times higher than the predicted by Ansari's model.

Experimental results with 4 mm riser were also compared to the model predictions. Both, Ansari and Reinemann's models, predicted no liquid production for 3.0 m (laboratory) tube length, while the experimental results showed liquid production for the whole range of injected gas.

Based on this preliminary analysis, it was concluded that a suitable model is required in order to transfer laboratory data (limited at 3 m depth) to a field situation (depth in excess of 100 m). Two models are proposed and discussed.

### **5.3 Critical production condition model (CPC)**

The critical production condition (CPC) is defined (first time in this work) as the minimum injected gas required to initiate the liquid production for certain submergence and a certain tube length. Figure 5.2, for example, indicate that CPC will occur at a gas injected rate corresponding to the superficial gas velocity  $U_g^s = 0.32$  m/s.

For a given pipe diameter and gas injection rate, CPC can be expressed as the critical (vertical) tube length beyond which no liquid production is recorded.

In this study, the CPC model was suggested to better capture the limiting liquid transport situation, particularly for small-diameters pipe and extreme low submergence situations.

The following simplifications have been adopted for developing a mechanistic predictive CPC model:

- a) The liquid will be transported from the bottom to top as a single liquid slug unit followed by a large T-D bubble (similar to a lump flow).
- b) The void fraction will linearly change from the calculated entrance value (using the entrance liquid and air flow rates) to the top (wellhead level). The outlet void fraction will be 1.0, since at CPC the pipe cross-section is occupied by gas only.

- c) For short airlift systems such as the experimental set up, the gas expansion effect is considered negligible
- d) The model considers the void fraction changes while traveling up to the top of the riser as related to the action of falling back liquid film (a counter-current, counter-action with the upward transport of liquid found between two consecutive T-D bubbles)

### 5.3.1 CPC model formulation

INLET conditions:

Superficial Velocities:

$$U_g^s = \frac{Q_g}{A}, \text{ m/s} \quad 5.2$$

$$U_l^s = \frac{Q_l}{A}, \text{ m/s} \quad 5.3$$

Mixture (transport) velocity:

$$U_m = U_l^s + U_g^s \quad 5.4$$

Gas Velocity-Drift flux according to Nicklin [20] velocity:

$$U_g = 1.2U_m + U_{T-D\infty} \quad 5.5$$

Terminal T-D bubble velocity

$$U_{T-D\infty} = 0.35\sqrt{gD} \quad 5.6$$

Void fraction:

$$\alpha_{in} = \frac{U_g^s}{U_g} \quad 5.7$$

Where  $Q_l$ ,  $Q_g$ , ( $m^3/s$ ) are the liquid and gas flow rates,  $A$  ( $m^2$ ) is the tubing cross section area, and  $\alpha_{in}$  is the void fraction calculated at the inlet.

OUTLET condition:

The void fraction at outlet of the tubing is assumed to be equal to one,

$$\alpha_{out} = 1.0 \quad 5.8$$

The inlet and outlet void fractions will give us the range at which the void fraction will vary from the bottom to the top of the riser. Assuming the void fraction varies linearly along the riser the average void fraction in the riser can be found as follows:

$$\bar{\alpha} = \frac{\alpha_{in} + \alpha_{out}}{2} \quad 5.9$$

The assumption of a linear variation of void fraction from the entrance (known) value to the limiting exit (1) offers a simple way to estimate the variation of static and dynamic pressure. By integrating this pressure (from entrance to wellhead) (Equation 5.10) a measure of bottom hole pressure (at CPC conditions) is numerically obtained. This allow for the rapid estimation of maximum possible length (given a certain gas injected and tube diameter).

$$P_{Res} = \rho g h = \sum_{L=0}^L \left[ \left( \frac{dP}{dL} \right)_{st} + \left( \frac{dP}{dL} \right)_{fr} \right] \quad 5.10$$

The pressure balance equation suggests that the reservoir pressure,  $P_{Res}$ , (the hydrostatic pressure of the liquid column ( $h$ ) measured for no-flow static conditions from the gas injection point) is equal to the sum of the locally calculated static and dynamic flow pressures.

The frictional and static pressure drop components of the Equation 5.10 are estimated by using Equations 5.11 and 5.12, respectively.

$$\left(\frac{dP}{dL}\right)_{fr} = f_M \frac{\rho_m \cdot U_m^2}{2D} \cdot (L) \quad 5.11$$

$$\left(\frac{dP}{dL}\right)_{st} = \rho_m g (L) \quad 5.12$$

where the local two-phase density  $\rho_m$  is calculated by using an average void fraction  $\bar{\alpha}_{calc}$  as follows:

$$\rho_m = \bar{\alpha}_{calc} \rho_G + (1 - \bar{\alpha}_{calc}) \rho_L \quad 5.13$$

By combining the Equations 5.11, 5.12 and 5.13, the expression for the void fraction that satisfies the pressure balance (Equation 5.10) can be developed as shown in the Equation 5.14.

$$\bar{\alpha}_{calc} = \frac{\rho_l}{\rho_l - \rho_g} \left[ 1 - \frac{gh}{L \left( g + f_M \frac{U_m^2}{2D} \right)} \right] \quad 5.14$$

where L is the length of the riser measured from the gas injection point to the wellhead at static conditions, h is the liquid column measured under static conditions from the gas injection point,  $f_M$  is the Moody friction factor which was calculated assuming a smooth pipe using the Blasius friction factor Equation (Equation 5.16) and  $\bar{\alpha}_{calc}$  is the average void fraction calculated from the pressure balance equation.

$$f_M \text{ Laminar flow : } f_M = \frac{64}{Re} \quad 5.15$$

$$f_M \text{ Turbulent: } f_M = \frac{0.184}{Re^{0.2}} \quad 5.16$$

The critical depth,  $L_{CPC}$ , can be calculated when the condition  $\bar{\alpha} = \bar{\alpha}_{calc}$  is fulfilled. By introducing the average void fraction,  $\bar{\alpha}$  from Equation 5.9, into Equation 5.14 and solving for L, the maximum tubing length ( $L_{CPC}$ ) representing the maximum length required to obtain a transport of an infinitesimal amount of liquid is calculated as follows:

$$L_{CPC} = \left[ \frac{gh}{\left[ 1 - \bar{\alpha} \frac{(\rho_l - \rho_g)}{\rho_l} \right] \left[ g + f_M \frac{U_m^2}{2.D} \right]} \right] \quad 5.17$$

The EXCEL program used for estimation of the  $L_{CPC}$  is presented in Appendix E.

### 5.3.2 CPC model validation

Laboratory data obtained from water/air gas lifting experiments with 7.8 mm and 12 mm diameter tubes were used to validate the CPC model.

The first set of experiments was conducted in 7.8 mm diameter tube and a gas injection rate corresponding to a superficial velocity of 0.206 m/s. Three experimental data points shown in Figure 5.4 were obtained at static water levels of 38.1, 50.8 and 63.5 cm (corresponding to reservoir pressures of 4, 5, and 6.2 KPa, respectively). The predicted critical depth  $L_{CPC}$  agrees reasonably well with the measured values (Figure 5.3).

The second group of experiments was conducted by using the 12 mm diameter tube at a specific gas injection rate of 0.316 m/s (Figure 5.4). The CPC model predictions of critical depth also agreed well with the experimental data in this case.

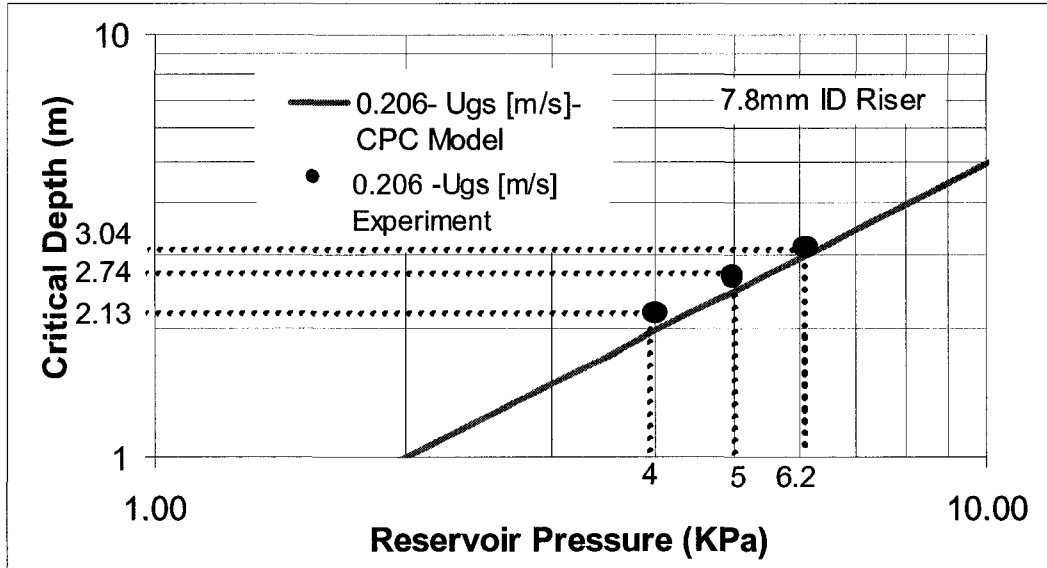


**Figure 5.4** Calculated (CPC Model) critical depth ( $L_{CPC}$ ) versus critical depth measured at three variable reservoir pressures (7.8 mm diameter tubing – air injection rate corresponding to 0.234 m/s).

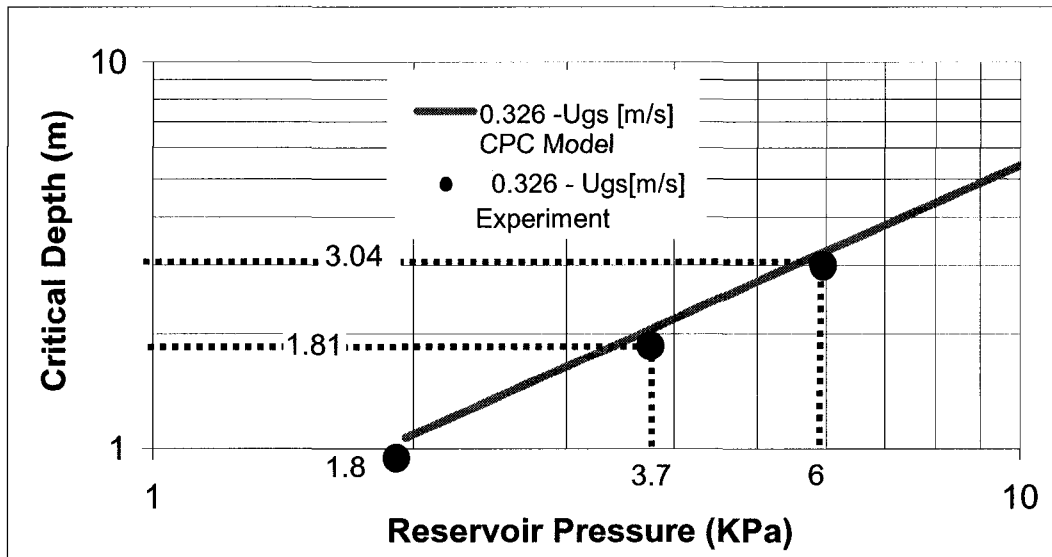


**Figure 5.5** Calculated (CPC Model) critical depth ( $L_{CPC}$ ) versus critical depth measured at three variable reservoir pressures (12 mm diameter tubing - air injection rate corresponding to 0.326 m/s)

For a reservoir pressure of 3.7 Kpa and  $U_g^s=0.326$  m/s (Figure 5.5), the model predicted critical depth  $L_{CPC}=2.1$  m while the measured critical depth for this case was 1.81 m (14% difference). For all investigated situations, the maximum difference between measured and calculated critical depth was less than 18%.

For the water/methanol air lift system, the model also accurately predicted the  $L_{CPC}$  length. Figures 5.6 and 5.7 shows the results obtained from the experiments.

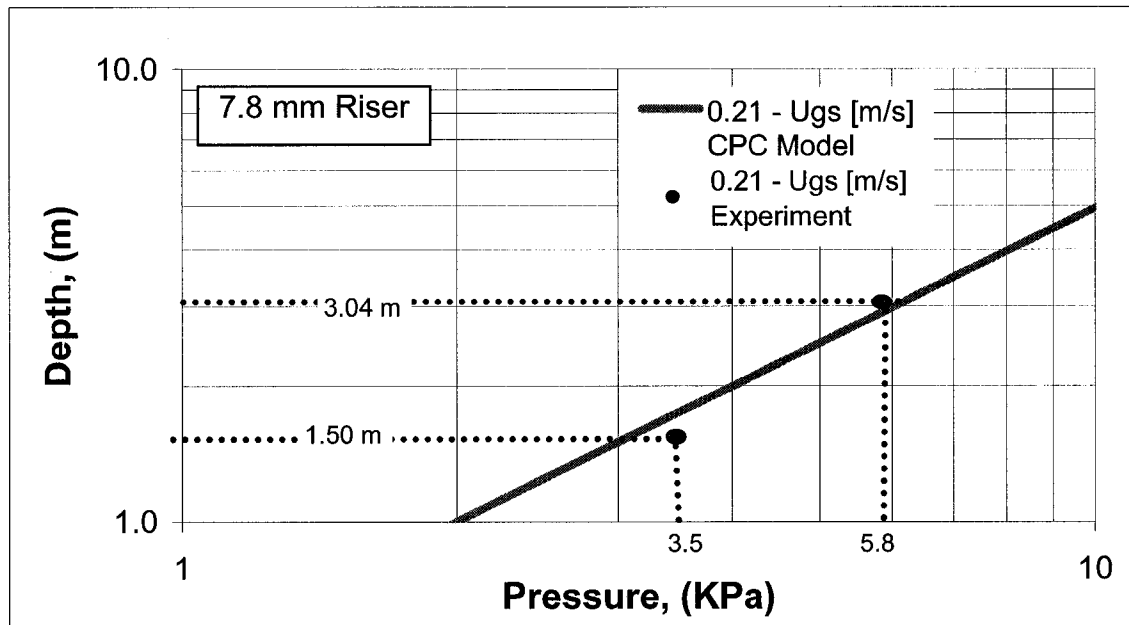


**Figure 5.6** Calculated (CPC Model) critical depth ( $L_{CPC}$ ) versus critical depth measured at three variable reservoir pressures (7.8mm diameter tubing-air injection rate corresponding to 0.21 m/s - water-methanol/air system).

In Figure 5.6, (7.8 mm riser, 0.21 m/s air superficial velocity) the model prediction is represented by the solid line and indicates a deviation from experimental measurements of approximately 13.0%. For higher gas superficial velocities the error increased up to 25% (i.e.  $U_g^s=0.47$  m/s). The increasing error at higher superficial velocities was possibly caused by the increased instabilities.

For the 12 mm diameter riser, the results were similar to the ones from 7.8 mm diameter tubing (Figure 5.6). Two different gas injection rates corresponding to superficial gas velocities of 0.35 and 0.93 m/s were tested. For the lower air velocity, the percent error was about 3% and for the higher one the error was 8%.

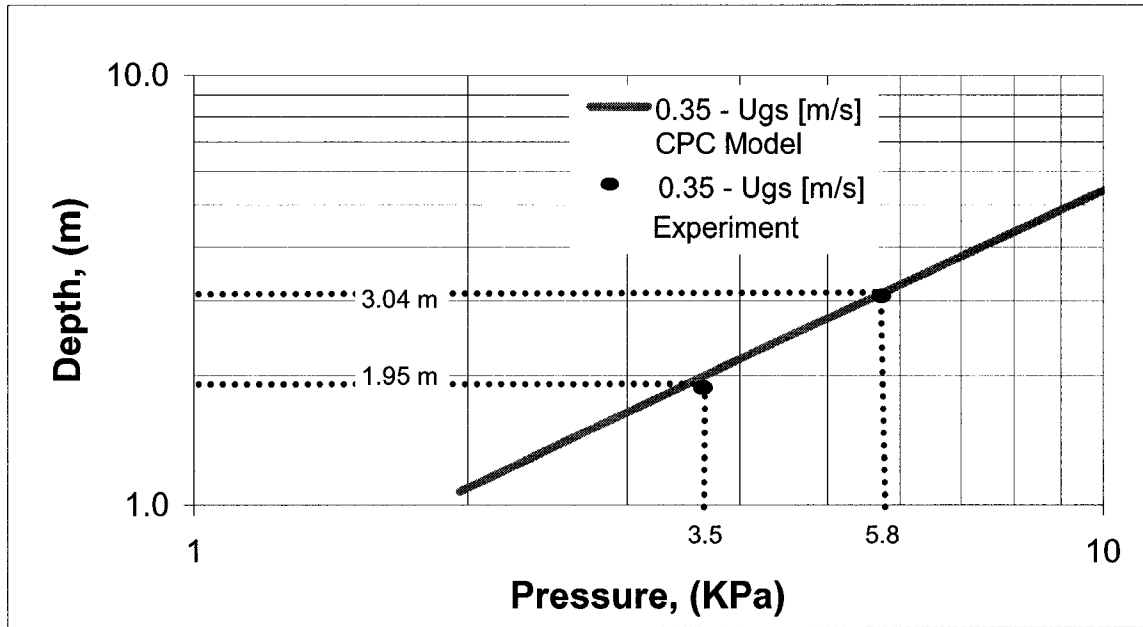


**Figure 5.7** Calculated (CPC Model) critical depth ( $L_{CPC}$ ) versus critical depth measured at three variable reservoir pressures (12mm diameter tubing-air injection rate corresponding to 0.35 and 0.93 m/s- water-methanol/air system).

For both tubing diameters, the maximum error occurred at the higher gas injection velocities; also mainly due to the higher flow instabilities.

### 5.3.3 CPC field application

The CPC model can be used as a rapid calculation tool to assess the feasibility of liquid transport with small diameter pipes under existing gas and liquid flow rate and bottom hole pressure (or submergence conditions).

An example of the possible use of this model is presented in Figure 5.7, which is an extrapolation of the results obtained from the model predictions with the 12 mm ID riser and a water/ air system.

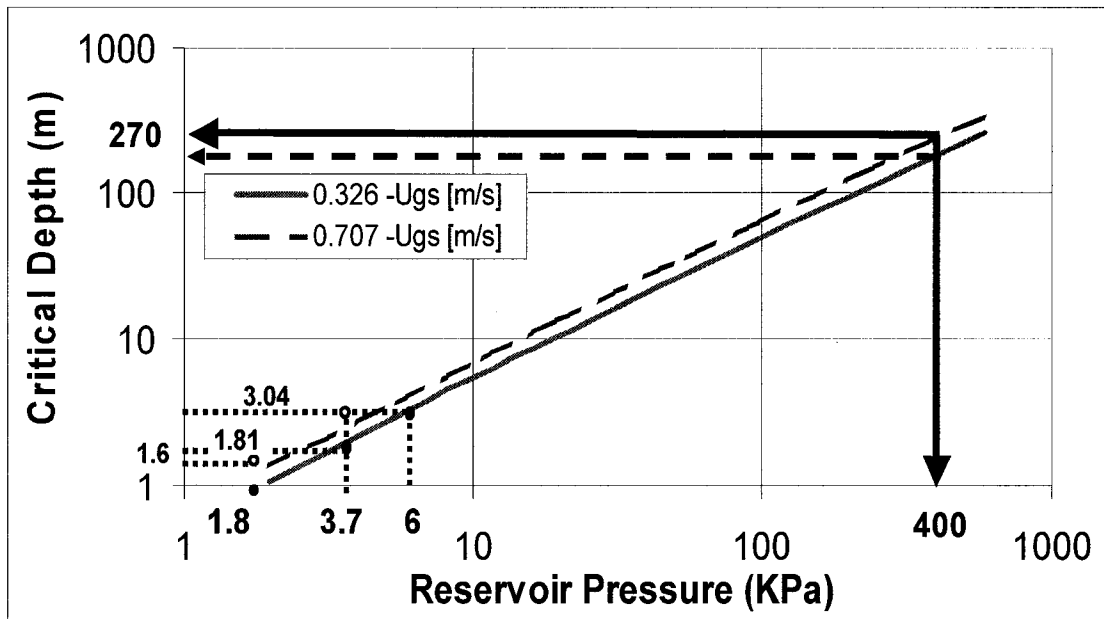


**Figure 5.8** CPC model prediction of critical depth ( $L_{CPC}$ ) versus reservoir pressure (12 mm diameter tubing), extrapolation to field conditions

As shown in Figure 5.8, for a reservoir pressure of 400 KPa (equivalent to water column height of 40 m) and a specific gas injection rate of 0.707 m/s, the model predicted a critical depth of  $L_{CPC}=270$  m. The calculated submergence for this example was 12.5%, much lower than the 50% limit suggested as the critical (minimum) submergence value required for unloading water from conventional wells with larger diameter ( $D>1$  inch) tubing. Note that increasing the gas injection velocity from 0.326 m/s to 0.707 m/s did increase the critical depth from 200m to 270m (35% increment). The critical depth will increase with increments of gas velocity until the frictional pressure drop becomes significantly larger than the static pressure and act to reducing the  $L_{CPC}$  with any increment of injected gas.

To improve the CPC model prediction accuracy, a modification of the described CPC version was attempted. The new CPC model (named SDP) took into consideration the thickness of liquid falling back around the T-D bubble as a function of the liquid surface tension.

## 5.4 Small diameter pipe model (SDP)

The SDP model followed the same principles as the CPC model. The assumptions of the SDP model are as follows:

- a) The liquid will be transported in a unique liquid slug unit, similarly to a lump slug flow.
- b) The void fraction at the bottom of the riser will be calculated according to the drift flux model. The void fraction at the top is assumed to be close to 1.0
- c) The thickness of liquid falling back is modeled as a function of the liquid surface tension.
- d) The void fraction increases while the liquid slug travels to the top as a consequence of the liquid falling back effect; the void fraction will be assumed as a function of the risers' length.

### 5.4.1 SDP Model formulation

Similar to the CPC model, the SDP model considers two critical levels: the bottom hole (inlet) and the wellhead (outlet).

The Input data include: liquid and gas physical properties such as density, viscosity, liquid surface tension, liquid and gas flow rates at the inlet and outlet conditions, riser diameter and length, and liquid level at static conditions.

The INLET:

The inlet conditions were determined by using Equations 5.2 to 5.7 as described for the CPC model. A numerical value of the  $\alpha_{in}$  is estimated.

The OUTLET:

The outlet conditions are known (the pressure and temperature found at the top of the riser or separator). These conditions were used to determine the liquid and gas physical properties at the wellhead level.

The void fraction at the top of the riser is expected to be less than 1.0 since some production is expected.

In order to determine the void fraction distribution along the riser it is necessary to calculate the void fraction at any intermediate point along the riser. Hence, the intermediate void fraction,  $\alpha_i$ , is expressed as a function of the length of the riser and the inlet void fraction:  $\alpha_i = f(L, \alpha_{in})$ .

Assuming the riser will be divided into “n” equal sized segments, the void fraction corresponding to inlet of the first section will be,  $\alpha_1$ , and the void fraction at the outlet of the first section will be,  $\alpha_2$  (Figure 5.9). The void fraction  $\alpha_2$  will be the inlet void fraction of the second section located just above the first one and so on.

Figure 5.9 shows the expected evolution of the liquid slug while travels within one section from point 1 to point 2. The volume of the liquid slug will be reduced by the action of the liquid fall back; the void fraction at both cross-sections (i.e. point 1 to 2) will be different.

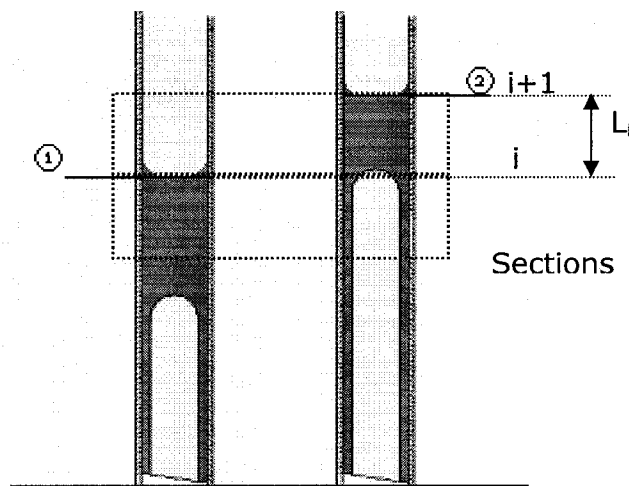


**Figure 5.9** Evolution of the liquid slug while travels from point 1 (position i) to point 2 (position i+1)

Assuming  $L_T$  as the total length of the riser (m), the length of each section,  $L_i$ , is:

$$L_i = \frac{L_T}{n} \quad 5.18$$

$\alpha_1$  is calculated by assuming the inlet conditions at the bottom of the riser in Equations 5.2 –5.7. It is very important to notice that in Nicklin's Drift Flux Equation (Equation 5.5), used for the void fraction calculation, the distribution coefficient ( $C_0$ ) was assumed 1.2 as demonstrated by Taylor and Dumitrescu to conventional diameter pipes. However, this approximation should be revisited for small diameter pipes since authors (Mishima and Hibiki [22]) have calculated variation in this value for smaller diameter pipes (4 mm tubes).

The void fraction at the point 2 is:

$$\alpha_2 = \alpha_1 + \Delta\alpha \quad 5.19$$

Where  $\Delta\alpha$  can be calculated using the general expression for the void fractions:

$$\Delta\alpha = \frac{V_{g2}}{V_{g2} + V_{L2}} - \frac{V_{g1}}{V_{g1} + V_{L1}} \quad 5.20$$

Where  $V_L$  and  $V_g$  are the liquid and the gas volume in the slug unit ( $m^3$ ), and the subscripts 1 and 2 represents the location in the riser.

Assuming the liquid is incompressible and isothermal conditions exist, a volumetric balance equation for the liquid slug can be written as follows:

$$V_{L2} = V_{L1} + V_{L\text{ add}} - V_{FB} \quad 5.21$$

$V_{L1}$  is the volume of the liquid column measured under static conditions at the bottom of the riser,  $V_{L\text{ add}}$  is the volume of liquid that enters the system while traveling from point 1 to point 2,  $V_{FB}$  is the volume of liquid falling back ( $m^3$ ) while traveling from point 1 to point 2, and  $V_{L2}$  is the volume of liquid measured at point 2. By substituting  $V_{L1}$  and  $V_{L\text{ add}}$  for its mathematical expressions, the Equation 5.21 is written as follows:

$$V_{L2} = \frac{\pi D^2}{4} L_T s + Q_L t - V_{FB} \quad 5.22$$

where  $D$  is the internal diameter of the tube (m), and  $s$  is the submergence value,  $Q_L$  is the liquid flow rate ( $\text{m}^3/\text{s}$ ), and  $t$  is the traveling time (s) from point 1 to 2.

$V_{FB}$  can be expressed as function of the liquid falling back flow rate,  $Q_{FB}$ , and time as follows:

$$V_{FB} = Q_{FB} t \quad 5.23$$

where

$$t = \frac{L_i}{U_m} \quad 5.24$$

and  $U_m$  (m/s) is the mixture velocity (Equation 5.4).

The liquid falling back flow rate is defined as:

$$Q_{FB} = U_{LTD} A_F \quad 5.25$$

$U_{LTD}$  is the velocity of the liquid falling back that surrounds the T-D bubble (m/s) and  $A_F$  ( $\text{m}^2$ ) is the cross section area of this liquid film.

$U_{LTD}$  can be determined from Equation 5.26, proposed by Brotz [55] and also used by Ansari [51] in his model.

$$U_{LTD} = \sqrt{196.7 g \delta_L} \quad 5.26$$

The liquid film thickness,  $\delta_L$ , is given by the Equation 5.27 [34]. It relates the film thickness to the capillary number and indirectly to the liquid surface tension.

$$\delta_L = 0.32D(3Ca)^{2/3} \quad 5.27$$

where Ca is the capillary number:

$$Ca = \frac{\mu U_{T-D}}{\sigma} \quad 5.28$$

$\mu$  is the dynamic viscosity and  $U_{T-D}$  is the T-D bubble velocity, which is approximated to the  $U_g$  (Equation 5.5) since it is assumed that all the gas is contained into the T-D bubble.

By combining Equations 5.21 - 5.28, the volume of the liquid slug at the point 2,  $V_{L2}$ , can be calculated.

The last parameters needed to calculate the void fraction at point 2 are the gas volumes. From the void fraction general equation,

$$\alpha_1 = \frac{V_{g1}}{V_{g1} + V_{L1}} \quad 5.29$$

By solving the Equation 5.29 for  $V_{g1}$  (m/s) the following mathematical expression is obtained:

$$V_{g1} = \frac{\alpha_1 V_{L1}}{(1 - \alpha_1)} \quad 5.30$$

Finally, the volume of gas at the point 2,  $V_{g2}$  (m/s), can be calculated from Equation 5.31, which is a volumetric balance equation for the gas assuming isothermal conditions and no expansion effect.

$$V_{g2} = V_{g1} + Q_g t \quad 5.31$$

The results obtained from the model assumed no expansion effect because the minimum difference in pressure for the short airlift system (3.0 m).

Now the void fraction at point 2,  $\alpha_2$ , can be calculated by introducing values of all the variables in Equations 5.19 and 5.20.

Once all parameters are estimated, it is possible to calculate the void fraction for the next section at point 3 and so on until reaching the top of the riser.

The average void fraction will be calculated by taking the instantaneous void fractions,  $\alpha_i$ , over the total length of the riser and divided by the total length of the riser,  $L_T$ .

$$\bar{\alpha}_{ave} = \frac{\int_0^{L_T} \alpha_i(L) dL}{L_T} \cong \frac{\sum_{i=1}^n (\alpha_{i+1} + \alpha_i)(L_{i+1} - L_i)}{2L_T} \quad 5.33$$

The  $\bar{\alpha}_{ave}$  can be assessed numerically as the sum of the area below the curve (i.e. void fraction vs. length) divided by the total length. In the Equation 5.33, the area was calculated using the trapezoidal method.

Once  $\bar{\alpha}_{ave}$  is calculated for the specified input conditions, it should be compared to the void fraction calculated by using the pressure balance equation (Equation 5.14).

If the values of void fraction from both methods are equal, it means the input data are correct. Otherwise, it is necessary to change one of the parameters and run the model again.

#### 5.4.2 SDP model verification

The SDP model was verified by using the data obtained from the experiments with the water/air and water-methanol / air systems using 12.0 and 7.8 mm risers and 20.1% (63.5 cm) and 12.5% (38.1 cm) submergence values.

This verification uses the SDP and Ansari's models to calculate the risers' length (Calculated Depth) at which the experimentally measured liquid and gas flowrates can be produced (i.e. The gas and liquid flowrate experimentally measured in the present work are input conditions for the models. The Calculated Depth is determined when the flowing bottom hole pressure is equal to the available reservoir pressure).

This validation was carried out for water, which is illustrated in Figures 5.10 and 5.11, and for water-methanol, which is shown in Figures 5.12 and 5.13.

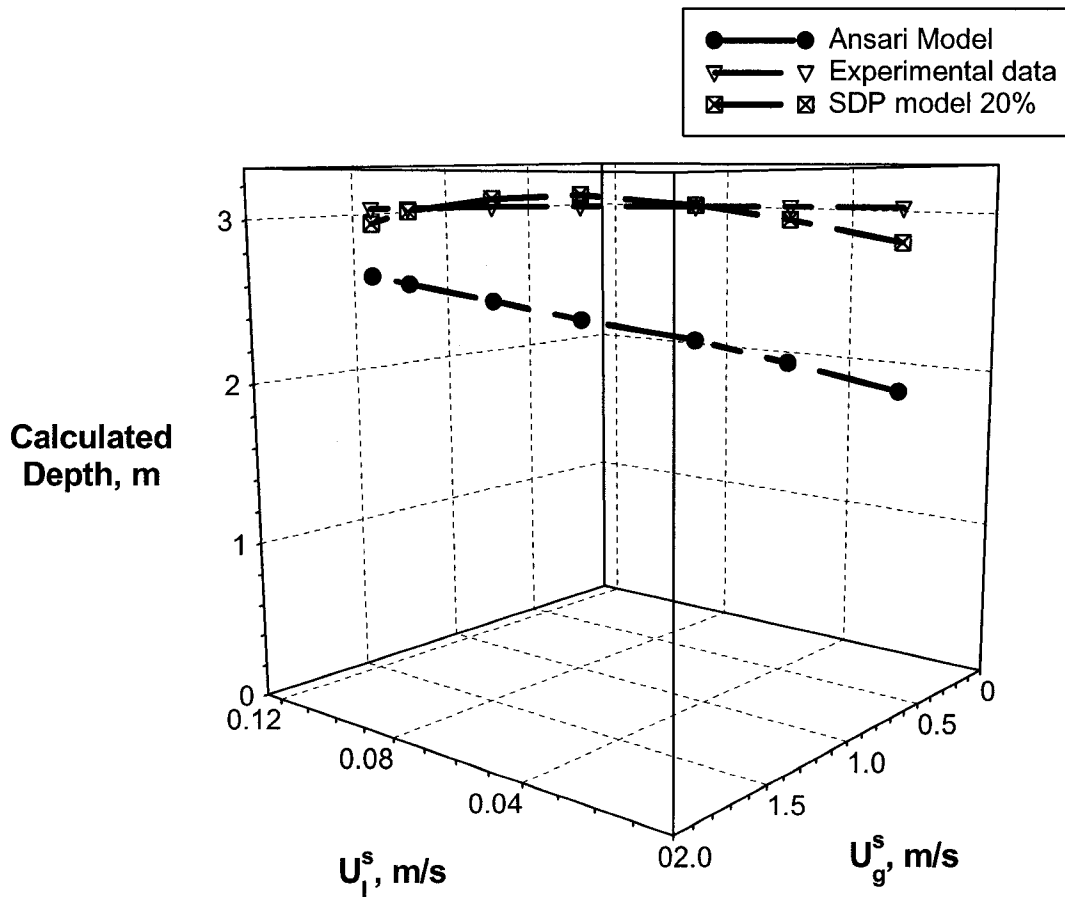


**Figure 5.10** Prediction (SDP and Ansari's models) of the riser's length (well depth) for a certain liquid production (laboratory measured) and injected gas flowrate (Note – the depth used in the laboratory is 3.04 m) for a 12 mm riser: 63.5 cm of water.

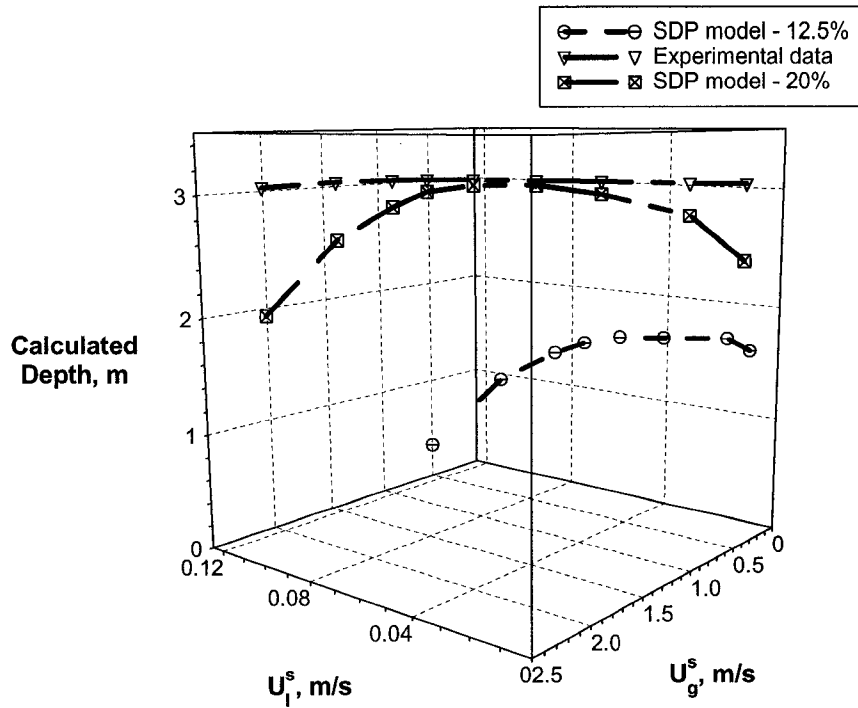


**Figure 5.11** Prediction (SDP Model) of the riser's length (well depth) for a certain liquid production (laboratory measured) and injected gas flowrate (Note – the depth used in the laboratory is 3.04 m) for a 7.8 mm riser: 63.5 and 38.1 cm of water.

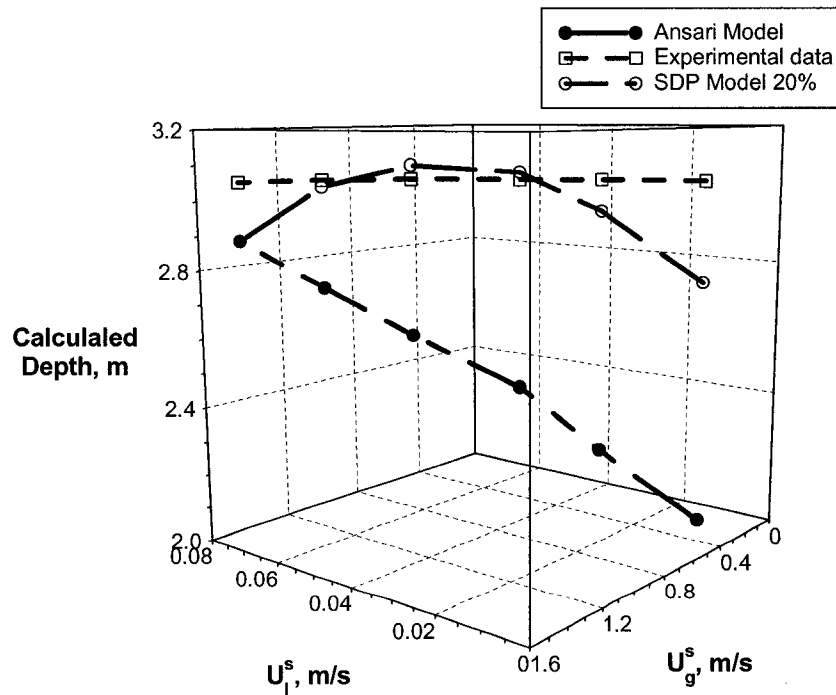


**Figure 5.12** Prediction (SDP and Ansari's models) of the riser's length (well depth) for a certain liquid production (laboratory measured) and injected gas flowrate (Note – the depth used in the laboratory is 3.04 m) for a 12 mm riser: 63.5 cm of water/methanol.

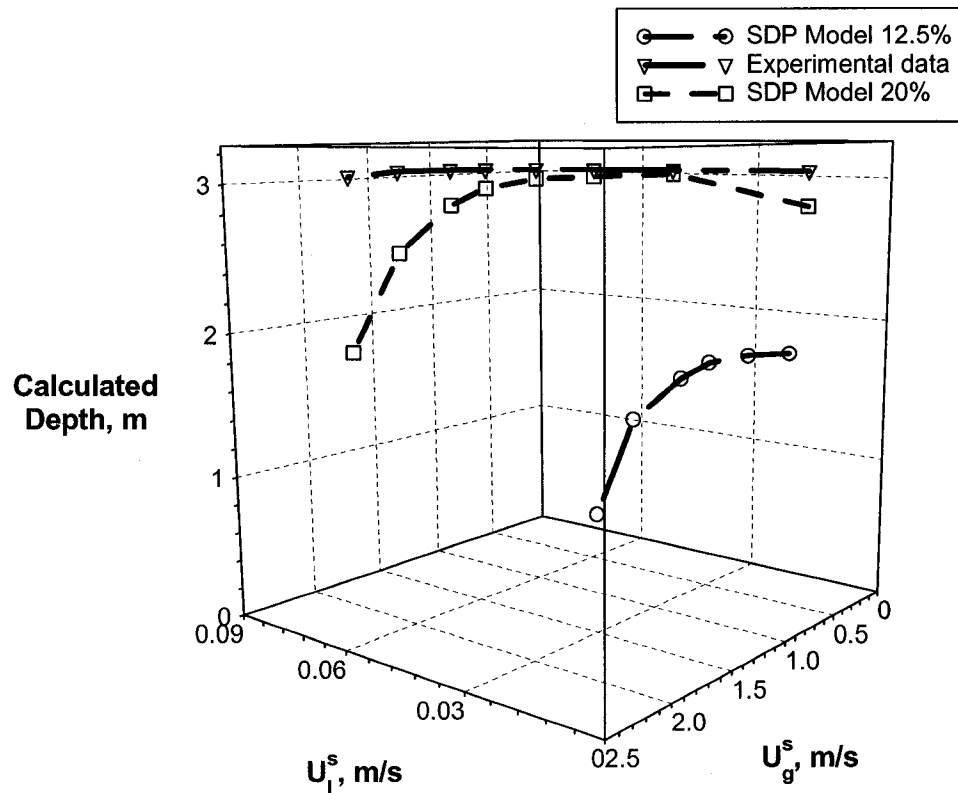


**Figure 5.13** Prediction (SDP Model) of the riser’s length (well depth) for a certain liquid production (laboratory measured) and injected gas flowrate (Note – the depth used in the laboratory is 3.04 m) for a 7.8 mm riser: 63.5 and 38.1 cm of water/methanol.

Figure 5.10, a 3D graph, shows the SDP and Ansari’s models predictions of “Calculated Depth” at 63.5 cm of water level (20.1% submergence) in a 12.0 mm riser, using as input data the experimental values for water and air production rates. The riser’s length predictions made by the SDP model matched pretty well the experimental data (3.04 m) showing errors no more than 9.5 %. The Ansari’s model predictions shows an ascending trend as increments in gas velocity. The maximum and minimum errors were 62 and 13% at 0.4 and 1.7 m/s gas superficial velocities, respectively.

Figure 5.11 shows the SDP model predictions for the 7.8 mm riser in air-water system. A parabolic shape is more evident for both submergences. For the 63.5 cm water level, the SDP model matches the experimental data for the air superficial velocity range form 0.5 to 1.0 m/s approximately. When the superficial gas velocity is very low or very high, the

SDP model under-estimated the experimental data within an error less than 32%. For the 38.1 cm water level the maximum depths appeared within the same air superficial velocity range. The maximum error observed was 60.6%.

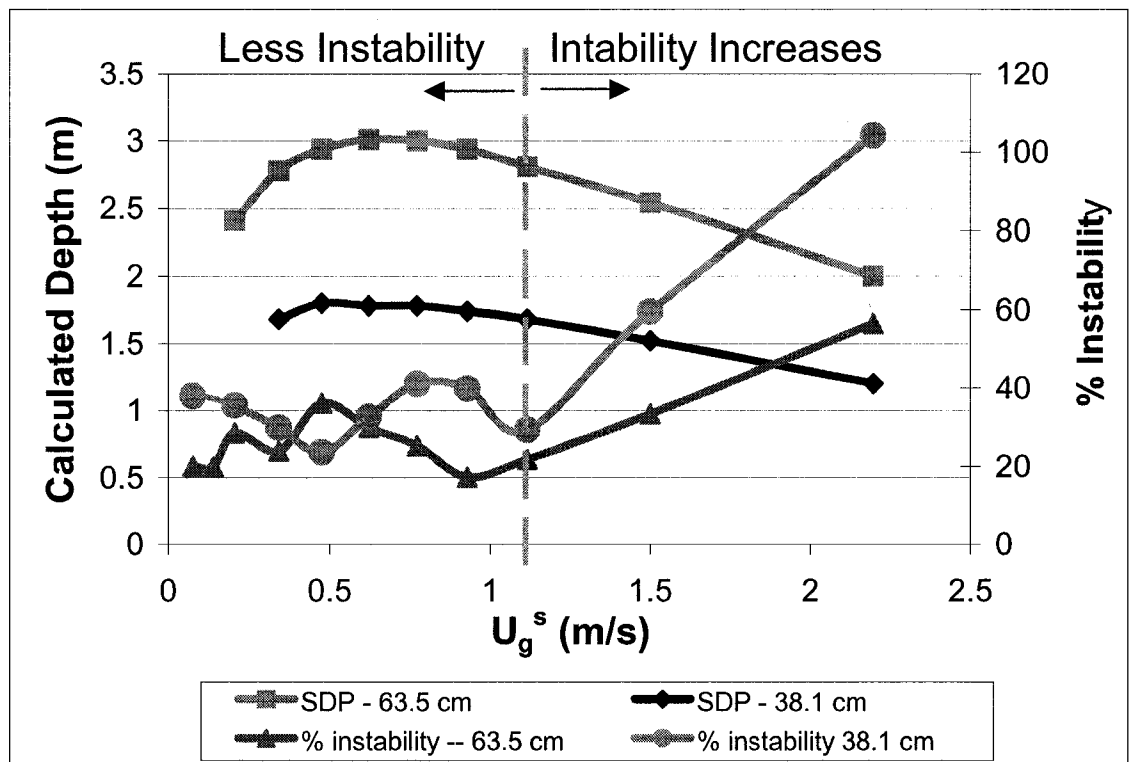
The water-methanol system also was evaluated with the SDP and Ansari's models. Figure 5.12 shows the results for 12.0 mm riser. Similarly as observed with water, the SDP model matches the experimental data very well; the maximum error was 11 %. Ansari's model again has a better matching with experimental data at higher gas superficial velocities. The maximum and minimum error observed for Ansari's model predictions were 38 and 5 %, respectively.

Figure 5.13 shows the SDP model predictions for the water/methanol-air system in a 7.8 mm riser. At the higher submergence (63.5 cm of liquid column) the calculated depth matched the experimental depth for range of 0.4 to 0.8 m/s gas superficial velocity. Above 0.8 m/s the calculated depth (SDP model) shows an increased under prediction; the maximum error (41%) appears at the maximum gas superficial velocity.

It is evident that the predictions made by the SDP model represented the experimental values for the 20% submergence, but it fails when predicted maximum riser's length especially for low submergences (Less than 20%) and very high air flow rates. The difference in surface tension did not contribute to better length predictions at the lower submergences. It is clear that another parameter is interfering with the liquid production and the correct riser's length predictions. As mentioned before, the possible cause for such marked difference could be the presence of instabilities during the whole experiment, especially at low submergence values.

#### **5.4.3 SDP model predictions and instabilities**

In order to understand better the instability effect, the pressure instabilities observed for the 7.8 mm riser in the air/water system were plotted in the same graph with the maximum riser's length prediction made for both submergences (Figure 5.14).



**Figure 5.14** SDP Model Length prediction for a 7.8 mm riser: 63.5 and 38.1 cm of water compared against its respective percentage of instability

The percentage of instability was calculated as the pressure difference between the maximum and minimum registered BHP divided into the equivalent hydrostatic reservoir pressure measured from the gas injection point.

The percentage of instabilities was considerably higher for small submergences especially at high superficial gas velocities (higher than 1.0 m/s). It was observed that the higher instability value, the higher percent error in the riser's length prediction. This behaviour is consistently repeated for the two tested risers' diameter and liquids.

Even though it is not possible to affirm that the considerable difference in length prediction is caused only by the instability effect, indeed this phenomenon eventually can produce a benefice on liquid production or, in this case, on the maximum reached riser's length.

#### 5.4.4 SDP model and liquid production

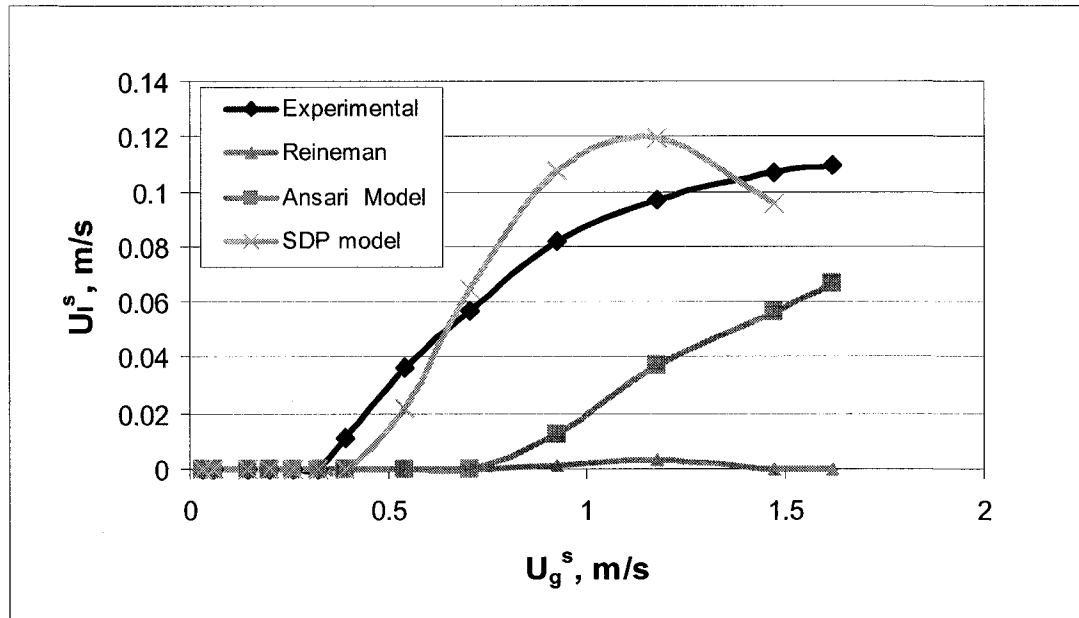


**Figure 5.15** Liquid production vs. gas injected, comparison between Ansari, Reinemann and SDP models and the Experimental data - 12 mm riser, 63.5 cm liquid level (20.1 % submergence).

Figure 5.15 is an example of the liquid production predictions for SDP, Ansari and Reinemann models. The SDP model correctly predicted the critical production condition. On the other hand, the estimated liquid production increased rapidly while increasing the gas injection rate to a maximum point at  $U_g^s = 1.2$  m/s where there is a clear over estimation of the liquid production, + 20%. Beyond this point, the liquid production fell quickly intersecting the experimental curve at  $U_g^s = 1.4$  m/s and falling into a region of considerable under prediction of the liquid production. This region is dominated by the frictional pressure losses and it is very sensitive to small changes in gas velocity. This excessive frictional pressure losses effect was not observed during the experiments for this riser.

Even though the SDP model did better liquid production predictions than the Ansari's and Reinemann's models, it still failed in simulating the soft increment in production represented by the experimental curve.

It is important to point out that the inclusion of the liquid fall back effect as well as the assumption of a unique slug unit traveling along the riser in the SDP model produced a remarkable difference in liquid production prediction compared to the Reinemann model that did not include them. The very modest prediction of the Reinemann model at low submergence values were widely overcome by the SDP model.

#### **5.4.5 Limitations of the SDP model**

1. The model was validated for isothermal short lift systems where the gas expansion is negligible. For longer risers a correction for gas expansion should be done.
2. The SDP model considered a single liquid slug traveling from the bottom to the top of the riser; eventual corrections caused by instabilities are not included.
3. The SDP model predicted reasonable accurate values for liquid production, critical production conditions and maximum risers lengths for the higher submergence value (20.1%). For the smaller submergences, still some corrections should be done in order to include instabilities effects. Therefore, this model is not suitable when submergence is less than 20%.
4. Another limiting factor is the tube diameter. Simulations with the 4.0 mm diameter riser did not show any satisfactory results with errors around 100%. This model predicted a rapid increment in frictional pressure losses. Therefore, at small gas velocities the liquid production quickly vanished. The best results were obtained for the 12 mm diameter riser under 20.1% submergence.

## CHAPTER 6

### CONCLUSIONS AND RECOMENDATIONS

---

#### 6.1 Conclusions

- 1 Replacing conventional large diameter tubing ( $D > 1$  inch) with small-diameter tubing ( $D < 1$  inch) offers potential advantages for unloading water and resuming production from gas wells with low reservoir pressure.
- 2 An experimental and a numerical modeling study have been conducted to investigate advantages and limitations of using small-diameter tubes for extreme gas lifting conditions.
- 3 An experimental apparatus was designed and operated to produce salient proof of the concept of gas lifting using small diameter tubing. Experiments have been conducted to measure liquid production with air lifting when water-air and water-methanol/air flow take place in small diameter pipes (4 mm, 7.8 mm, 12 mm).
- 4 Within the range of experimental conditions, it was seen that the elongated bubble pattern was the most common flow pattern observed with small diameter pipes. The elongated bubble flow pattern observed with water-air system was altered when the liquid surface tension was reduced. An increased number of small bubbles are formed in the liquid slug when the surface tension was reduced.
- 5 Experiments with 4 mm riser showed increased liquid production at very low air flowrates at which larger diameter pipes did not indicated production conditions.

- 6 The surface tension affected the T-D bubble velocity in small diameter pipes. It was seen that when the surface tension is reduced, the upward gas velocity increased – and, implicitly, the overall void fraction decreased.
- 7 Laboratory tests were able to identify and quantify the occurrence of flow instabilities reflected through significant oscillations of bottom hole pressure. It appears (for laboratory conditions) that instabilities do not negatively affect the average liquid production.
- 8 Experimental data have been further used to introduce a new effectiveness concept (Critical Production Condition- CPC). A numerical model using the CPC concept was designed and validated with laboratory data to assess critical conditions of the process in the field applications. Laboratory validation of the CPC model indicates a range of errors under 18%.
- 9 The CPC model was further used to determine limiting depth condition for liquid transport for various field conditions including low reservoir pressures and gas-liquid flowrates. The results indicated that small diameter pipes could be practically used in the field to unload gas wells with very low reservoir pressures.
- 10 An extension of the CPC model (Small Diameter Pipe – SDP model) was completed to better capture the liquid surface tension effect, particularly on the thickness and flowrate of the liquid film fall-back. Validated with laboratory experiments, the SDP model predicted the liquid production and the maximum riser length within a range of errors (depending on flow regime) between 8 and 20%. While the margin of error was not significantly reduced, as compared with CPC model (designed for assessing extreme length minimal reservoir conditions only), by introducing the fall back effect, the SPD model is better suited for further improvements.

## 6.2 Recommendations for future works

- 1 To improve our understanding on the effects of liquid film fallback and improve the confidence required for designing field operations, additional laboratory work needs to be performed with both conventional and small-diameter tubes using liquid mixtures of various interfacial tensions.
- 2 To validate the observations made in the lab as well as the data predicted by the CPC and the SDP models, experiments should be conducted with longer risers ( $L > 40$  ft) under field conditions.
- 3 Unloading liquid from the 4mm diameter riser at very low air flow rates should be studied in detail since it offers the best performance of liquid recovery at the lower submergence values ( $< 10\%$ ).
- 4 Following the observations in this study (Chapter #4) indicating a linear correlation between maximum production condition point (MPC) and submergence, a numerical and experimental investigation aiming to exploit this linearity in a possible new/improved model is suggested.
- 5 Additional methods and field strategies aiming at improvement of efficiency observed with small diameter pipes through decreasing the liquid fall back should be investigated.
- 6 Continuation of direct observations on T-D bubble velocity (tracking), particularly performed during instabilities occurring at very low submergence values is warmly suggested. A high-speed (professional) movie camera (rather than a popular digital model) is suggested for better results.
- 7 A study of flow instabilities should be conducted to improve our understanding of instability influence on liquid production. Two pressure transducers with

similar or better response and accuracy of the one used for present experiments (0.25% Full Scale accuracy, 3000 Hz) should be installed at the bottom and in an intermediate position for a better and more accurate description of instabilities source and magnitude.

- 8 The improvement of the SDP model using results obtained from the instabilities study is suggested in view of reducing the present margin of errors for predictions of liquid production. Additionally, the pressure and temperature effects, particularly for field (depth) conditions, should be introduced in the SDP model.

## REFERENCES

---

1. Libson, T. N., James H. R., "CASE HISTORIES: IDENTIFICATION OF AND REMEDIAL ACTION FOR LIQUID LOADING IN GAS WELLS – INTERMEDIATE SHELF GAS PLAY", SPE 7467, JPT, April 1980, pp. 685-693.
2. MacDonald M. R., "FLUID LOADING IN LOW PERMEABILITY GAS WELLS IN THE COTTON VALLEY SANDS OF EAST TEXAS". SPE 9855, SPE/DOE Low Permeability Symposium, Denver - Colorado, U.S.A. May 27-29, 1981, 8 p.
3. Arthur, D., Langhus, B., Raw-Schatzinger, V., "COALBED NATURAL GAS RESOURCES AND PRODUCED WATER MANAGEMENT". Gas TIPS, A Publication of Gas Technology Institute, the U.S. Department of Energy and Hart Publications, Inc., V 9, N 3, pp. 21-24, Summer 2003.
4. Neves, T.R., Brimhall, R.M., "ELIMINATION OF LIQUID LOADING IN LOW-PRODUCTIVITY GAS WELLS". SPE 18833, SPE Production Operations Symposium, Oklahoma City, Oklahoma, March 13-14, 1989, 8 p.
5. Turner, R.G., Hubbard, M.G., Duckler, A. E., "ANALYSIS AND PREDICTION OF MINIMUM FLOWRATE FOR CONTINUOUS REMOVAL OF LIQUIDS FROM GAS WELLS". SPE 2198, JPT, November 1969, pp. 1475-1482.
6. Putra, S. A., "DEVELOPMENT OF A MECHANISTIC TWO-FLUID CHURN FLOW MODEL AND DESIGN OF TUBING-COLLAR INSERTS FOR ENHANCING LIQUID LIFTING TO PREVENT LIQUID LOAD-UP IN GAS WELLS". Colorado School of Mines. PhD. Thesis, November 3, 2000.
7. Alves, I. N., Caetano, E. F., Minami, K., Shoham, O, "MODELING ANNULAR FLOW BEHAVIOR FOR GAS WELLS", Annual Mtg. of ASME, Chicago, November 27, 1988, pp. 87-97.
8. Saleh, S., Al-Jamae'y, M., "FOAM-ASSISTED LIFTING IN LOW PRESSURE GAS WELLS". SPE 37425, SPE Production Operations Symposium, Oklahoma City, Oklahoma, 9-11 March, 1997, pp. 317-323.
9. Bernadiner, M. G., "FOAMED GAS LIFT". SPE 21639, SPE Production Operations Symposium, Oklahoma City, Oklahoma, 7-9 April 1991, pp. 75-82.
10. Stephenson, G.B., Rouen, R.P., Rosenzweig M.H., "GAS WELL DEWATERING: A COORIDNATED APPROACH". SPE 58984. International Petroleum Conference and Exhibition, Villahermosa –Mexico, 1-3 February 2000, 9 p.

11. Corlew, Ed., Rochelle J, "AIR PULSE SYSTEM FOR ARTIFICIAL LIFT REDUCES COST". Petroleum Technology Digest, Supplement to World Oil Magazine, September, 2000.
12. Song, F.Y., Islam, M.R., "THE APPLICATION OF FOAMS IN GAS LIFTING SYSTEMS". Unsolicited SPE paper, SPE 27413, June 1993, 12 p.
13. Hinze J.O., "FUNDAMENTALS OF THE HYDRODYNAMIC MECHANISM OF SPLITTING IN DISPERSION PROCESSES", A.I.Ch.E. Journal, September 1955, V 1, No. 3, pp. 289-295.
14. Ahsan J., Scott S.L: "INVESTIGATION OF NEW TOOL TO UNLOAD LIQUIDS FROM STRIPPER-GAS WELLS", SPE 84136, SPE Annual Technical Conference and Exhibition, Denver, Colorado, U.S.A, 5-8 October 2003, 12 p.
15. Toma P., Korpany G., Harris P., Alberta Research Council; Landry R., Reber K., West Petro Investment: " A NOVEL GASLIFT TOOL FOR IMPROVING PRODUCTION IN MARGINAL WELLS". JCPT, September 1994, V 34, No. 4, pp. 50-57.
16. Mingaleeva, G.R., "ON THE MECHANISM OF A HELICAL MOTION OF FLUIDS IN REGIONS OF SHARP PATH BENDING", Tech. Phys. Lett. , October 2003, V 28, No. 8, pp. 657 – 659.
17. Kirkpatrick, C.V., "PETROLEUM ENGINEERING HANDBOOK", Chapter 5: Gas Lift, Society of Petroleum Engineers, Richardson, TX, U.S.A., 1987, pp. 5-1 – 5-52.
18. Eicher Jr., H. V., "THE HISTORY OF GAS LIFT AND ITS MODERN APPLICATION TO THE PETROLEUM INDUSTRY", The Petroleum Engineer, January 1952, pp. B-36 – B-40.
19. Taitel Y. and Barnea D and Duckler, A.E., " MODELLING FLOW PATTERN TRANSITIONS FOR STEADY UPWARD GAS-LIQUID FLOW IN VERTICAL TUBES". AIChE Journal, May 1980, V 26, No. 3, pp. 345-354.
20. Nicklin D. J., Wilkes J. O., and Davidson J. F.: "TWO-PHASE FLOW IN VERTICAL TUBES". Trans. Inst. of Chem. Engrs., 1962, V 40. pp. 61.
21. Harmathy, T.Z.: "VELOCITY OF LARGE DROPS AND BUBBLES IN MEDIA OF INFINITE OR RESTRICTED EXTENT" AIChE J., June 1960, V. 6, No. 2, pp. 281-288.

22. Mishima K. and Hibiki T., "SOME CHARACTERISTICS OF AIR-WATER TWO-PHASE FLOW IN SMALL DIAMETER VERTICAL TUBES". *Int. J. of Multiphase Flow*, 1996, V 22. No.4. pp. 703-771.
23. Brauner N., "THE PREDICTION OF DISPERSED FLOWS BOUNDARIES IN LIQUID – LIQUID AND GAS-LIQUID SYSTEMS". *Int. J. of Multiphase Flow*, 2001, V 27, pp. 885-910.
24. Kolmogorov, A.N., "ON THE BRAKING OF DROPS IN TURBULENT FLOW". *Dokady Akad. Nauk.* , 1949, V 66, pp. 825-828.
25. Hughamark, G.A., "DROP BREAKUP IN TURBULENT PIPE FLOW", 1971, *AIChE J.*, V4, pp. 1000.
26. Clay, P.H., "THE MECHANISM OF EMULSION FORMATION IN TURBULENT FLOW, PART I," *Proc. Roy. Acad. Sci. (Amsterdam)*, 1940, V 43, pp. 852.
27. Sevik, M., and S. H. Park, "THE SPLITTING OF DROPS AND BUBBLES BY TURBULENT FLUID FLOW". *Trans. ASME, J. Fluid Engr.*, 1973, V 95, 53.
28. Brodkey, R.S, "THE PHENOMENA OF FLUID MOTIONS", Addison-Wesley Press, Don Mills, Ontario, Canada, 1967, pp. 565-605.
29. Wallis, G. B., "ONE DIMENSIONAL TWO-PHASE FLOW", McGraw-Hill Book Co., New York, 1969.
30. Govier, G.W., Aziz, K., "THE FLOW OF COMPLEX MIXTURES IN PIPES", Chapter 8: The vertical flow of gas-liquid and liquid-liquid mixtures in pipes, Van Nostrand Reinhold Co., Toronto, Canada, 1972, pp. 322-323.
31. Nicklin D. J., Wilkes J. O., and Davidson J. F.: " TWO-PHASE FLOW IN VERTICAL TUBES". *Trans. Inst. of Chem. Engrs.* V 40, pp. 61, 1974.
32. Barnea, D., Luninski, Y., Taitel, Y., " FLOW PATTERN IN HORIZONTAL AND VERTICAL TWO PHASE FLOW IN SMALL DIAMETER PIPES". *Canadian Journal of Chemical Engineering*, October 1983, V 61, pp. 617-620.
33. Mishima, K & Ishii, M., " FLOW REGIME TRANSITION CRITERIA FOR UPWARD TWO PHASE FLOW IN VERTICAL TUBES". *Int. J. Mass Heat Transfer*, V 27. pp. 723-737, 1984.
34. Stark, J., Manga, M., "THE MOTION OF LONG BUBBLES IN NETWORK OF TUBES". *Int. J. of Transport in Porous Media*, 2000, V 40, pp. 201-218.

35. Coleman, J. W., Garimella, S., "CHARACTERIZATION OF TWO-PHASE FLOW PATTERNS IN SMALL DIAMETER ROUND AND RECTANGULAR TUBES". *Int. J. Mass and Heat Transfer*, 1999, V 42, pp. 2869-2881.
36. Kariwasaki, A., Fukano, T., Ousaka, A. & Kagawa, M., "ISOTHERMAL AIR-WATER TWO PHASE UP- AND DOWNWARD FLOWS IN A VERTICAL CAPILLARY TUBE". (1<sup>st</sup> report, Flow pattern and void fraction). *Trans., JSME (Ser. B)*, 1991, V 58, pp. 4036-4043.
37. Yang, C-Y., Shieh, C-C., "FLOW PATTERN OF AIR-WATER AND TWO-PHASE R-134A IN SMALL CIRCULAR TUBES". *Int. J. Multiphase Flow*, 2001, V. 27, pp. 1163-1171.
38. Toma, P., "MULTIPHASE FLOW IN PIPES", Graduate Course. Handouts from the vertical flow chapter, University of Alberta, Canada. September 2002.
39. Dumitrescu, D.T., "STROMUNG AN EINER LUFTBLASE IM SENKRECHTEN ROHR", *Z. Angew. Math. Mech.* 23, 3, Jun.1943, pp. 139-149.
40. Barnea, D., Shoham, O., Taitel, Y. "FLOW PATTERN TRANSITION FOR GAS-LIQUID FLOW IN HORIZONTAL AND INCLINED PIPES". *Int. Multiphase Flow*, 1980, V 6, pp. 217-225.
41. Hasan A. R.: "VOID FRACTION IN BUBBLY AND SLUG FLOW IN DOWNWARD VERTICAL AND INCLINED SYSTEMS", *SPE Production and Facilities*, August 1995, SPE 26522. pp. 172-176.
42. Reinemann D. J., Parlange J. Y. and Timmons M. B. "THEORY OF SMALL-DIAMETER AIRLIFT PUMPS", *Int. J. Multiphase Flow*, 1990, V16 No. 1, pp. 112-122.
43. Nickens, H. V. & Yanitell, D. W., "THE EFFECTS OF SURFACE TENSION AND VISCOSITY ON THE RISE VELOCITY OF A LARGE GAS BUBBLE IN A CLOSED, VERTICAL LIQUID-FILLED TUBE", *Int. J. Multiphase Flow*, 1987, V. 13, pp. 57-69.
44. White, E. T. & Beardmore, R. H. "THE VELOCITY OF RISE OF SINGLE CYLINDRICAL AIR BUBBLES THROUGH LIQUIDS CONTAINED IN VERTICAL TUBES". *Chem. Eng. Sci.*, 1962, V 17, pp. 351-361.
45. Tung, K. W. & Parlange, J. Y. "NOTE ON THE MOTION OF LONG BUBBLES IN CLOSED TUBES-INFLUENCE OF SURFACE TENSION", *Acta mech.*, 1976, V24, pp. 313-317.
46. Kouremenos, D.A., Staicos, J. "PERFORMANCE OF A SMALL AIR -LIFT PUMP". *Int. J. Heat and Fluid Flow*, September 1985, V 6, No. 3, pp.217-222.

47. De Cachard, F., Delhay, J. M., "A SLUG-CHURN FLOW MODEL FOR SMALL-DIAMETER AIRLIFT PUMPS". *Int. Multiphase Flow*, 1996, V. 22, No. 4, pp. 627-649.
48. Lawniczak, F., Francois, P., Scrivener, O., Kastrinakis E. G., Nychas S. G., "THE EFFICIENCY OF SHORT AIRLIFT PUMPS OPERATING AT LOW SUBMERGENCE RATIOS". *The Canadian Journal of Chemical Engineering*, February 1999V. 77, pp. 3-9.
49. Guet, S., Ooms G., Oliemans, R. V. A., Mudde, R. F., "BUBBLE INJECTOR EFFECT ON THE GASLIFT EFFICIENCY". *AIChE Journal*, September 2003, V. 49, No. 9, pp. 2242-2252.
50. Fernandes, C. R., "EXPERIMENTAL AND THEORETICAL STUDIES OF ISOTHERMAL AND UPWARD GAS-LIQUID FLOWS IN VERTICAL TUBES". PhD. Thesis, Department of Chemical Engineering, August 1981, University of Houston.
51. Ansari, A.M., Sylvester, N.D., Sarica, C., Shoham, O., Brill, J.P., "A COMPREHENSIVE MECHANISTIC MODEL FOR UPWARD TWO-PHASE FLOW IN WELLBORES". *SPE Production and Facilities*, May 1994, pp. 143-150.
52. Nakoriakov, V.E., Kashinsky, O.N. & Kozmenko, B.K., "EXPERIMENTAL STUDY OF GAS-LIQUID SLUG FLOW IN A SMALL DIAMETER VERTICAL PIPE". *Int. J. Multiphase Flow*, 1986, V. 12, pp. 337-355.
53. Yamasaki, Y. & Yamaguchi, K., "CHARACTERISTICS OF COCURRENT TWO-PHASE DOWNFLOW IN TUBES; VOID FRACTION AND PRESSURE DROP". *J. Nuclear Sci. & Tech*, April 1979, V. 161, pp. 245.
54. Vo D.T. and Shoham O.: "A NOTE ON THE EXISTENCE OF A SOLUTION FOR TWO-PHASE SLUG FLOW IN VERTICAL PIPES", *ASME J. Energy Resources Tech.*, 1989, No. 111, pp. 64.
55. Brotz, W.: "UBER DIE VORAUSBERECHNUNG DER ABSORPTIONSGESCHWINDIGKEIT CON GASEN IN STROMENDEN FLUSSIGKEITSSCHICHTEN", *Chem. Ing. Tech.*, 1954, No. 26, pp 470.
56. Brown, R.A.S., "THE MECHANICS OF LARGE GAS BUBBLES IN TUBES", *Can. J. Chem. Eng.*, 1965, V 43, pp. 217.
57. Liao, Q., Zhao, T.S., "MODELING OF TAYLOR BUBBLE RISING IN A VERTICAL MINI NONCIRCULAR CHANNEL FILLED WITH A STAGNANT LIQUID", *Int. J. Multiphase Flow*, 2003, V 29, pp. 411-434.

58. De Cachard, F., Delhaye, J.M., "STABILITY OF SMALL DIAMETER AIRLIFT PUMPS", *Int. J. Multiphase Flow*, 1998, V 24, No. 1, pp. 13-34.
59. Iguchi, M., Terauchi, Y., "RISING BEHAVIOR OF AIR-WATER TWO-PHASE FLOWS IN VERTICAL PIPE OF POOR WETABILITY", *ISIJ International*, 2000, V 40, No. 6, pp. 567-571.
60. Perry & Chilton, "CHEMICAL ENGINEERS' HANDBOOK", Mc. Graw-Hill, Fifth Edition, 1973, pp. 3-247.
61. Aziz, K., Govier, G. and Fogorasi, M. "PRESSURE DROP IN WELLS PRODUCING OIL AND GAS", *J. Can. Pet. Techn.*, July-Sept. 1972, V 11, pp. 38.
62. Brill J., Mukhrerjee, H., "MULTIPHASE FLOW IN WELLS", *SPE Monograph*, 1999, V17, pp. 39.
63. Beggs, H. and Brill, J. "A STUDY OF TWO PHASE FLOW IN INCLINED PIPES". *Int. Journal Pet. Tech.*, May 1973, pp. 607-617.
64. Shoham, J. "FLOW PATTERN TRANSITION AND CHARACTERIZATION IN GAS-LIQUID TWO PHASE FLOW IN INCLINED PIPES". Ph. D. dissertation, Tel- Aviv Univ., 1982 Ramat-Aviv, Israel.
65. American Institute of Chemical Engineers, "THE 100 MOST CITED ARTICLES IN AICHE JOURNAL HISTORY", *AIChE Journal*, January 2004, No. 1, V 50, pp. 4 – 6.

## APPENDIX A

### EXPERIMENTAL DATA FOR CONVENTIONAL DIAMETER PIPES

---

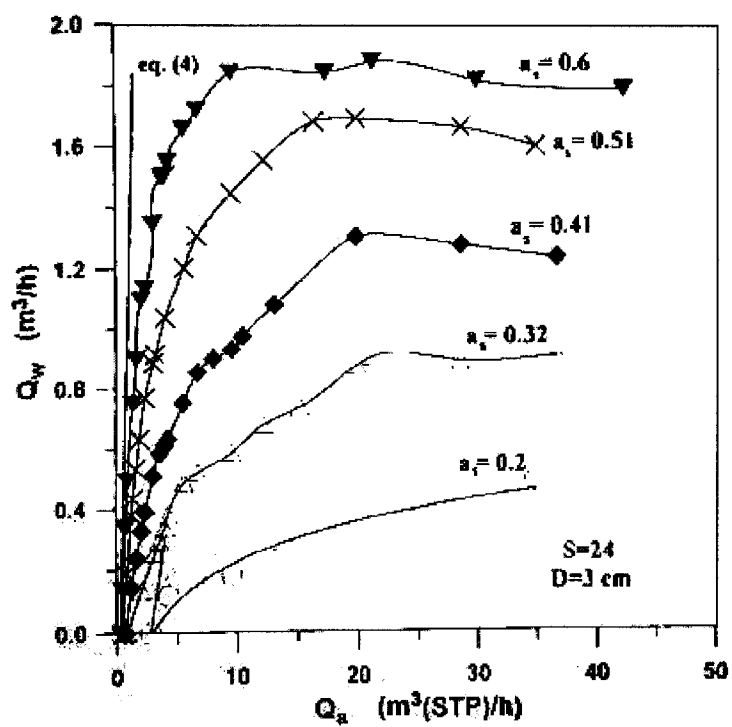


Figure A.1 Water rate as function of air flow rate. [48]

Theoretical Results of the Slug Flow Model (Part B) And Comparison with their corresponding Experimental Data													
$U_g^s$ (m/s)	$U_l^s$ (m/s)	$\beta$	$\beta_{exp}$ (%)	$\beta / \beta_{exp} * 100$ (%)	$\alpha_{T-D}$ (%)	$\alpha_{T-D exp.}$ (%)	$\alpha_{T-D} / \alpha_{T-D exp.} * 100$ (%)	$\alpha_{LS}$ (%)	$\alpha_{LS exp.}$ (%)	$\alpha_{LS} / \alpha_{LS exp.} * 100$ (%)	$\alpha_{SU}$ (%)	$\alpha_{SU exp.}$ (%)	$\alpha_{SU} / \alpha_{SU exp.} * 100$ (%)
0.51	0	0.6	0.63	-4.8	87.9	83.5	5.3	29.6	27.3	8.4	64	63	1.6
0.99	0	0.74	0.73	1.4	87	84.8	2.6	26.8	26.9	-0.4	72	69	4.3
1.14	0	0.77	0.79	-2.5	86.8	85.1	2.0	26.1	25.5	2.4	73	73	0.0
0.38	0.0161	0.49	0.54	-9.3	88.1	83.5	5.5	30.5	27.5	10.9	59	58	1.7
1	0.0161	0.73	0.73	0.0	87	84.2	3.3	26.7	26.2	1.9	71	69	2.9
0.55	0.049	0.56	0.61	-8.2	87.7	83.2	5.4	28.8	27.4	5.1	62	61	1.6
1.09	0.049	0.72	0.72	0.0	86.8	86.2	0.7	26.1	25.2	3.6	70	69	1.4
1.43	0.049	0.77	0.74	4.1	86.4	85	1.6	24.9	25.7	-3.1	72	70	2.9
0.42	0.099	0.42	0.38	10.5	87.8	84.2	4.3	29.2	27.7	5.4	54	49	10.2
0.67	0.099	0.56	0.6	-6.7	87.4	83.7	4.4	27.8	28	-0.7	61	61	0.0
0.99	0.099	0.66	0.72	-8.3	86.9	84.5	2.8	26.2	26.8	-2.2	66	68	-2.9
0.51	0.121	0.46	0.51	-9.8	87.6	84	4.3	28.5	28.1	1.4	56	56	0.0
0.67	0.121	0.54	0.55	-1.8	87.3	85.2	2.5	27.6	28.7	-3.8	60	60	0.0
0.83	0.121	0.6	0.56	7.1	87.1	84	3.7	26.8	28.9	-7.3	63	60	5.0
1.32	0.121	0.71	0.71	0.0	86.4	85.2	1.4	24.9	27.7	-10.1	69	69	0.0
0.68	0.222	0.47	0.48	-2.1	87.1	86.1	1.2	26.9	26.7	0.7	55	55	0.0
0.91	0.222	0.55	0.62	-11.3	86.8	86.2	0.7	25.9	28.1	-7.8	60	64	-6.3
1.4	0.222	0.67	0.66	1.5	86.2	84.6	1.9	24.2	29.9	-19.1	66	66	0.0
0.76	0.322	0.44	0.45	-2.2	86.8	85.2	1.9	26	27.2	-4.4	53	53	0.0
1.08	0.322	0.55	0.51	7.8	86.4	86.7	-0.3	24.8	28.7	-13.6	58	58	0.0
1.41	0.322	0.62	0.62	0.0	86	87.2	-1.4	23.9	27.6	-13.4	62	64	-3.1
1.17	0.49	0.49	0.5	-2.0	86.1	86.2	-0.1	24	26.6	-9.8	55	56	-1.8
1.5	0.49	0.57	0.59	-3.4	85.8	86.4	-0.7	23.2	28.7	-19.2	59	63	-6.3
1.16	0.61	0.45	0.48	-6.2	86	84	2.4	23.5	26.3	-10.6	51	54	-5.6

**Table A.1** Experimental data, Fernandes experiment for slug flow [50].

## APENDIX B APPARATUS DESIGN

Figure B.1 is a detailed description of the apparatus including parts, dimensions and special fittings.

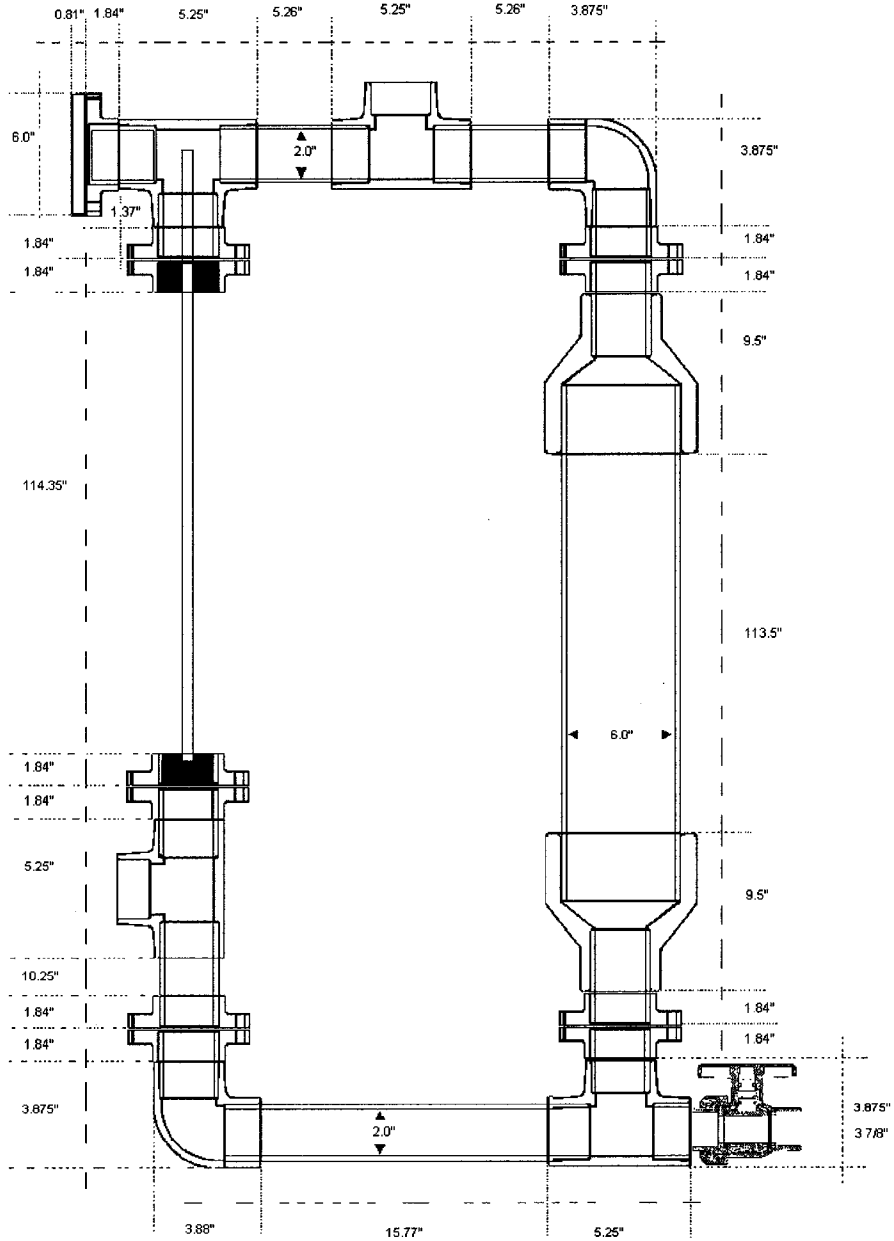


**Figure B.1** Apparatus dimensions.

Some designing criteria took into consideration the liquid and gas flow rate expected to be produced. Since the only available model for small diameter pipes was the Reinemann et al. [42], most of the data used for the design were based on Reinemann's model predictions. Data presented in Table B.1 re-generated from the graphs and model presented in reference [42].

Diam.	Ql	Qg	BHP		Submergence		Ql	Qg	Um	Efficiency
			Kpa	psi	Calculated	Real				
25	0.0001623	0.0002352	126.34	18.33	0.60	0.6	9.738	0.847	0.809702	0.45
25	0.0000029	0.0000635	126.40	18.34	0.60	0.6	0.173	0.229	0.135214	0.03
25	0.0006042	0.0002352	141.05	20.47	0.90	0.9	36.254	0.847	1.709979	0.28
25	0.0002125	0.0000400	141.54	20.54	0.91	0.9	12.753	0.144	0.514437	0.52
9.53	0.0000133	0.0000190	125.71	18.24	0.59	0.6	0.795	0.068	0.452034	0.49
9.53	0.0000004	0.0000042	125.74	18.25	0.59	0.6	0.025	0.015	0.065084	0.07
9.53	0.0000472	0.0000190	140.96	20.46	0.90	0.9	2.833	0.068	0.92824	0.27
9.53	0.0000149	0.0000027	141.38	20.52	0.91	0.9	0.892	0.010	0.24686	0.55
6	0.0000014	0.0000013	126.26	18.3216	0.60	0.6	0.085	0.005	0.096929	0.72
6	0.0000058	0.0000066	126.26	18.3222	0.60	0.6	0.349	0.024	0.440669	0.58
6	0.0000151	0.0000066	140.97	20.4568	0.90	0.9	0.905	0.024	0.767945	0.25
6	0.0000010	0.0000001	141.00	20.4616	0.90	0.9	0.058	0.00048	0.038951	0.805
3.18	0.00000162	0.00000543	124.84	18.1164	0.57	0.57	0.097	0.020	0.886902	0.23
3.18	0.00000025	0.00000027	124.89	18.1229	0.57	0.57	0.015	0.001	0.065696	0.695
3.18	0.00000306	0.00000543	138.41	20.0848	0.85	0.85	0.184	0.020	1.069218	0.11
3.18	0.00000102	0.00000027	138.38	20.0804	0.85	0.85	0.061	0.001	0.162237	0.66

**Table B.1** Data from Reinemann's model [42] in 3.18 mm, 6 mm, 9.53 mm and 25 mm risers.

The real submergence value was the data read from graphs [42] and the calculated submergence value was the data obtained from the model.

### Section #1: Storage tank

Design criterion: Transition time 3 minutes.

According to the predicted flow rate, the maximum flow rate expected is 0.79 L/min for a 9.53 mm diameter riser under a submergence of 60%. Assuming 8 tubes producing in parallel the total flow rate will be 6.24 L/min. The number of parallel pipes, 8, was obtained from the cross sectional area ratio between a 1.0 inch pipe (25.4 mm diameter) and 9.5 mm diameter (i.e.  $\text{Area}_{25.4 \text{ mm}} / \text{Area}_{9.5 \text{ mm}} = 7.14$ , was approximated to 8 for designing purposes).

After three minutes flowing at maximum flow rate, the volume passing through the pipe will be  $3 \times 6.24$  litres = 18.72 litres. This volume will define the diameter of the storage tank. It is assumed an average submergence of 15%. The maximum pipe length in clear PVC was 10 ft (3.05 m). The sequences of calculations were shown in table B.2.

<b>Volume to be Circulated</b>	<b>Equivalent Height, 15% submergence</b>	<b>Height below the gas Injection point</b>	<b>Total height</b>	<b>Area = Vol./Total height</b>	<b>Diameter Storage Tank</b>	<b>Diameter Storage Tank</b>
liters	m	m	m	m <sup>2</sup>	m	in
18.72	0.475	0.305	0.8	0.0234	0.172	6.79

**Table B.2** Calculations for the storage tank diameter

The nearest commercial pipe diameter available was 6 inches. This diameter (Cross sectional area =  $0.0058 \text{ m}^2$ ) allowed a maximum possible liquid velocity of 0.053 m/s under maximum production of 18.72 L/min or  $0.000312 \text{ m}^3/\text{s}$ . For a single riser the velocity could be as low as 0.0067 m/s.

### Section 2: Bottom loop section

The pipe diameter used to transport the liquid from the storage tank to the gas injection point was designed to minimize the frictional pressure losses. The commercial availability for the reduction couplings from 6 inches to the designed diameter was an important constraint to be considered. The cost and real functionality played an important role on the pipe selection. Table B.3, shows the predicted frictional pressure losses for three possible pipe diameters.

<b>Reduction ID in x ID in</b>	<b>Tube Diameter ID in</b>	<b>Max. Liquid flow rate L/min</b>	<b>Liquid velocity m/s</b>	<b>Reynolds Number N<sub>Re</sub></b>	<b>f</b>	<b>Frictional Pressure Losses, Pa/m</b>
6x4	4	0.78	0.00503	511.299	0.000360	0.0000449
6x3	3	0.78	0.00895	681.732	0.000270	0.0001419
6x2	2	0.78	0.02015	1022.598	0.000180	0.0007184

**Table B.3** Bottom loop pipe selection - Frictional pressure losses for 4, 3 and 2 inches pipe diameter.

The pressure losses even for the smallest calculated diameter were expected to be very low (around  $1.0E-7$  psi) then all diameters were considered suitable to be implemented. The selection was made based on the cost of the pipe; therefore the selected pipe was a 2.0 in (50.8mm ID) clear PVC pipe.

### Section 3: Air injection

Figure B.2 shows a schematic of the gas injector section.

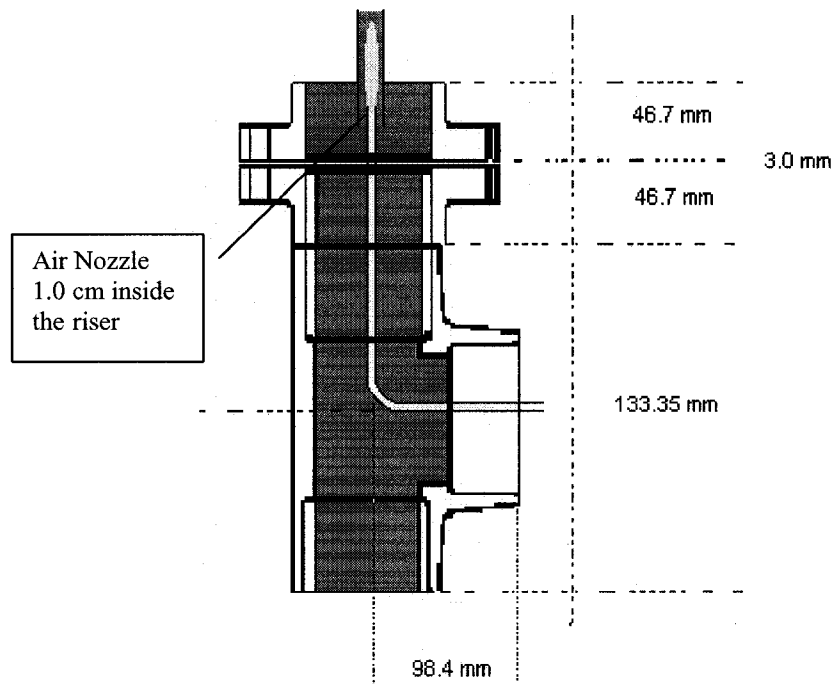


**Figure B.2.** The air injection section

The air nozzle was inserted coaxially into the riser penetrating it 1.0 cm from the bottom. Because the air is released inside the tubing, the possible pressure losses caused by the reduction in pipe diameter can be avoided.

The calculated value of external cross sectional area of the nozzle to the internal cross section area of the tubing ratio, Equation B.1 [48], are known in table B.4.

$$A_s = \frac{(\text{Nozzle OD})^2}{(\text{Tubing ID})^2} \quad \text{B.1}$$

Nozzle	OD, mm	ID, mm	As 12 mm riser	As 7.8 mm riser	As 4.0 mm riser
1	1.6	N/A	----	----	6.25
2	6.3	4.35	3.51	1.53	----

**Table B.4** Cross sectional area (As) ratio used during the experiments

The cross sectional area ratio (As) could also be optimized with respect to the liquid production rate, but in this set of experiments this factor was left out of the scope of this research.

#### Section 4: Riser

Three tube diameters were selected for the experiment under low submergence conditions: 4mm, 7.8 mm and 12mm ID risers.

The sections were designed to be removable using a system of flanges and special metallic fittings. Maximum riser's length was 10 ft.

#### Section 5: Air/Liquid separator

The separator was designed for a mixture flow rate of 0.01 m/s under full flow conditions. Table B.5 details the steps used to calculate the minimum separator diameter.

Maximum Liquid flow rate L/min	Expected Velocity m/s	Calculated cross Section area m <sup>2</sup>	Recommended Length m	Diameter cm
0.000107	0.01	0.0107	0.5	2.14

**Table B.5** Calculations for determining the diameter of the separator

Even though the diameter calculated was 1.0 inch, a pipe of 2.0 inches ID was suggested to be placed instead. A separator with bigger diameter would increase the flow capacity and the retention time facilitating the gas-liquid separation.

A third factor was considered to improve the liquid flow. A small ( $2^\circ$ ) tilt was applied to the separator section in order to facilitate the liquid drainage towards the storage tank (Figure B.3).

A vent was located at the middle upper part of the separator to release the gas (air). At high gas flow rates, some micro droplets can be carried with the gas stream so a convenient sponge or stainless steel wool could be placed just above the top of the riser or in the vent orifice to trap the liquid.

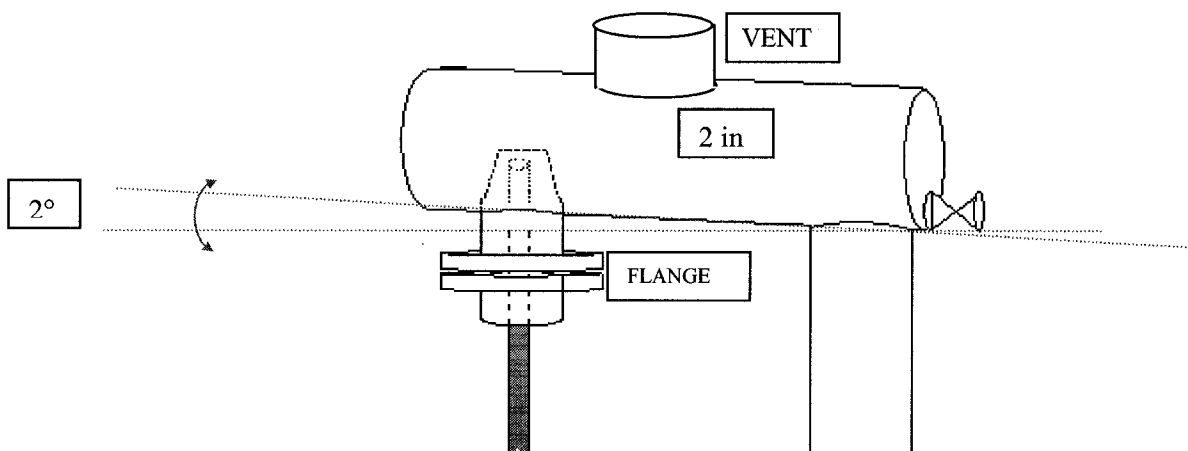


**Figure B.3** Separator design: Angle applied to allow the liquid flow toward the storage tank.

## APPENDIX C

### EXPERIMENTAL RESULTS FOR THE WATER/AIR GAS LIFT SYSTEM

#### C.1. 12 mm riser's experimental data

##### C.1.1 20.1% Submergence

SUBMERGENCE 20.1%											
① Atmospheric Conditions		② Column of water static cond.	③ Pressure Static Conditions	④ BHP Flowing Conditions	⑤ Differential Pressure ③-④	⑥ Air Flow rate	⑦ Liquid Mass	⑧ Liquid Production Average	Observed Pattern	Max reached Height E bubble	Max reached Height "Foam"
T °C	P Kpa	in	psi	psi	psi	l/min	Kg	l/min	(in)	(in)	(in)
20	100	25	0.904	0.92	-0.016	0.2	0	0.0000	Bubble	32.0	35.0
20	100	25	0.904	0.92	-0.016	0.5	0	0.0000	E Bubble	43.0	54.5
20	100	25	0.904	0.93	-0.026	1	0	0.0000	E Bubble	55.0	68.0
20	100	25	0.904	0.93	-0.026	1.4	0	0.0000	E Bubble	73.0	76.0
20	100	25	0.904	0.93	-0.026	1.8	0	0.0000	BB-SL-	92.0	---
20	100	25	0.904	0.93	-0.026	2.2	0	0.0000	E bubble	112.5	---
20	100	25	0.904	0.93	-0.026	2.7	0.1	0.0758	E bubble	120.0	---
20	100	25	0.904	0.93	-0.026	3.7	0.2	0.2468	E bubble	120.0	---
20	100.1	25	0.904	0.93	-0.026	4.8	0.4	0.3869	E bubble	120.0	---
20	100.1	25	0.904	0.94	-0.036	6.3	0.4	0.5554	E bubble	120.0	---
20	100.1	25	0.904	0.95	-0.046	8	0.5	0.6575	S-instability	120.0	---
20	100.1	25	0.904	0.98	-0.076	10	0.5	0.7248	S-instability	120.0	---
20	103.2	25	0.904	0.99	-0.086	11	0.5	0.7422	S- instability	120.0	---

**Table C.1** First repeatability data for 12 mm ID riser, submergence 20.1%

The test was repeated three times in different days. The recorded data and repeatability percentage are presented in table C.2.

Air Injection l/min	Produced water, l/min			Error First/Second	Error Second /Third	Error First/Third
	First	Second	Third			
0.2	0.0000	0.0000	0.0000	---	---	---
0.5	0.0000	0.0000	0.0000	---	---	---
1	0.0000	0.0000	0.0000	---	---	---
1.4	0.0000	0.0000	0.0000	---	---	---
1.8	0.0000	0.0000	0.0000	---	---	---
2.2	0.0000	0.0000	0.0000	---	---	---
2.7	0.0758	0.0792	0.0739	-4.57	6.68	2.41
3.7	0.2468	0.2542	0.2419	-3.00	4.82	1.97
4.8	0.3869	0.4065	0.3882	-5.07	4.52	-0.33
6.3	0.5554	0.5579	0.5452	-0.46	2.27	1.83
8	0.6575	0.6664	0.6550	-1.34	1.70	0.38
10	0.7248	0.7277	0.7243	-0.41	0.48	0.07
11	0.7422	0.7501	0.7387	-1.06	1.51	0.47

**Table C.2** Percentage of repeatability for three sets of data for the 12 mm riser at 20.1% submergence

### C.1.2 16.67% Submergence

SUBMERGENCE 16.67% THIRD REPEATABILITY											
① Atmospheric Conditions		② Column of water	③ Pressure Static	④ BHP Flowing	⑤ Differential Pressure	⑥ Air Flow rate	⑦ Liquid Mass	⑧ Liquid Production	Observed Pattern	Max reached Height	Max reached Height
T °C	P Kpa	static cond. in	Conditions psi	Conditions psi	③-④ psi	l/min	Kg	Average l/min		E bubble (in)	"Foam" (in)
21	102	20	0.723	0.75	-0.027	0.2	0	0.0000	Bubble	27.0	28.5
21	102	20	0.723	0.76	-0.037	0.5	0	0.0000	E. Bubble	30.5	55.0
21	102	20	0.723	0.76	-0.037	1	0	0.0000	E. Bubble	39.0	79.0
21	102	20	0.723	0.77	-0.047	1.4	0	0.0000	E Bubble	51.0	105.0
21	102	20	0.723	0.78	-0.057	1.8	0	0.0000	E bubble	70.5	80.5
21	102	20	0.723	0.77	-0.047	2.2	0	0.0000	E bubble	87.5	---
21	102	20	0.723	0.77	-0.047	2.7	0	0.0000	E bubble	110.0	---
21	102.1	20	0.723	0.77	-0.047	3.7	0.1	0.0818	E bubble	120	---
21	102.1	20	0.723	0.76	-0.037	4.8	0.2	0.1973	E bubble	120	---
21	100.6	20	0.723	0.77	-0.047	6.3	0.3	0.3284	E bubble	120.0	---
21	102.1	20	0.723	0.79	-0.067	8	0.4	0.4066	E bubble	120.0	---
21	102.1	20	0.723	0.83	-0.107	10	0.5	0.4557	+ - instable	120.0	---
21	102.1	20	0.723	0.84	-0.117	11	0.5	0.4795	+ - instable	120.0	---

**Table C.3** Third repeatability data for 12 mm ID riser, submergence 16.67%

The test was repeated three times to obtain repeatability data. The recording data and repeatability percentage are presented in table C.4.

Air Injection l/min	Produced water, l/min			Error First/Second	Error Second /Third	Error First/Third
	First	Second	Third			
0.2	0.0000	0.0000	0.0000	---	---	---
0.5	0.0000	0.0000	0.0000	---	---	---
1	0.0000	0.0000	0.0000	---	---	---
1.4	0.0000	0.0000	0.0000	---	---	---
1.8	0.0000	0.0000	0.0000	---	---	---
2.2	0.0000	0.0000	0.0000	---	---	---
2.7	0.0000	0.0000	0.0000	---	---	---
3.7	0.0756	0.0874	0.0818	-15.66	6.39	-8.27
4.8	0.1899	0.1992	0.1973	-4.94	0.98	-3.92
6.3	0.3309	0.3224	0.3284	2.56	-1.84	0.77
8	0.4108	0.4122	0.4066	-0.34	1.36	1.02
10	0.4643	0.4600	0.4557	0.94	0.93	1.86
11	0.4901	0.4867	0.4795	0.69	1.48	2.16

**Table C.4** Repeatability for three sets of data for the 12 mm riser at 16.67% submergence

### C.1.3 12.5% Submergence

SUBMERGENCE 12.5% SECOND REPEATABILITY											
① Atmospheric Conditions		② Column of water static cond.	③ Pressure Static Conditions	④ BHP Flowing Conditions	⑤ Differential Pressure ③-④	⑥ Air Flow rate	⑦ Liquid Mass	⑧ Liquid Production Average	Observed Pattern	Max reached Height E bubble (in)	Max height Reached "Foam" (in)
T °C	P Kpa	in	psi	psi	psi	l/min	Kg	l/min			
20	102.7	15	0.542	0.57	-0.028	0.2	0	0.0000	Bubble	21.5	22.5
20	102.7	15	0.542	0.57	-0.028	0.5	0	0.0000	E Bubble	23.0	37.0
20	102.7	15	0.542	0.58	-0.038	1	0	0.0000	E Bubble	29.0	60.0
20	102.7	15	0.542	0.58	-0.038	1.4	0	0.0000	E Bubble	38.0	57.0
20	102.6	15	0.542	0.58	-0.038	1.8	0	0.0000	E bubble	53.0	---
20	102.6	15	0.542	0.58	-0.038	2.2	0	0.0000	E bubble	62.0	---
20	102.6	15	0.542	0.58	-0.038	2.7	0	0.0000	E bubble	81.0	---
20	102.6	15	0.542	0.58	-0.038	3.7	0	0.0000	E bubble	104.0	---
20	102.6	15	0.542	0.59	-0.048	4.8	0.03	0.0276	E bubble	120.0	---
20	102.6	15	0.542	0.6	-0.058	6.3	0.1	0.1142	E bubble	120.0	---
20	102.6	15	0.542	0.62	-0.078	8	0.2	0.1797	Instability	120.0	---
20	102.6	15	0.542	0.64	-0.098	10	0.2	0.2247	Instability	120.0	---
20	102.6	15	0.542	0.66	-0.118	11	0.2	0.2356	Instability	120.0	---

**Table C.5** Second repeatability set of data for 12 mm ID riser, submergence 12.5%

The test was repeated three times to obtain repeatability data. The recorded data and repeatability percentage are presented in table C.6.

Air Injection l/min	Produced water, l/min			Error First/Second	Error Second /Third	Error First/Third
	First	Second	Third			
0.2	0.0000	0.0000	0.0000	---	---	---
0.5	0.0000	0.0000	0.0000	---	---	---
1	0.0000	0.0000	0.0000	---	---	---
1.4	0.0000	0.0000	0.0000	---	---	---
1.8	0.0000	0.0000	0.0000	---	---	---
2.2	0.0000	0.0000	0.0000	---	---	---
2.7	0.0000	0.0000	0.0000	---	---	---
3.7	0.0000	0.0000	0.0000	---	---	---
4.8	0.0340	0.0276	0.0291	18.90	-5.60	14.36
6.3	0.1221	0.1142	0.1202	6.46	-5.27	1.53
8	0.1849	0.1797	0.1764	2.79	1.86	4.61
10	0.2176	0.2247	0.2292	-3.25	-2.02	-5.34
11	0.2510	0.2356	0.2287	6.11	2.95	8.88

**Table C.6.** Repeatability for three sets of data for the 12 mm riser at 12.5% submergence

## C.2 7.8 mm riser's experimental data

### C.2.1 20.1% Submergence

SUBMERGENCE 20.1% FOURTH REPEATABILITY										
① Atmospheric Conditions		② Column of water static cond.	③ Pressure Static Conditions	④ BHP Flowing Conditions	⑤ Differential Pressure ③-④	⑥ Air Flow rate	⑦ Liquid Mass	⑧ Liquid Production Average	Observed Pattern	Max reached Height E bubble (in)
T °C	P Kpa	in	psi	psi	psi	l/min	Kg	l/min		
22	100	25	0.904	0.92	-0.016	0.2	0	0.0000	E BB	67
22	100	25	0.904	0.92	-0.016	0.4	0	0.0000	E BB	118
22	100	25	0.904	0.928	-0.024	0.6	0.05	0.0201	E BB	120-max
22	100	25	0.904	0.92	-0.016	1	0.1	0.0646	E BB	120-max
22	100	25	0.904	0.936	-0.032	1.4	0.2	0.1472	E BB	120-max
22	100	25	0.904	0.92	-0.016	1.8	0.3	0.2064	E BB	120-max
22	100	25	0.904	0.904	0.000	2.2	0.4	0.2643	E BB	120-max
22	100	25	0.904	0.896	0.008	2.7	0.5	0.3029	E BB	120-max
22	100	25	0.904	0.888	0.016	3.1	0.5	0.3224	E BB	120-max
22	100	25	0.904	0.896	0.008	4.1	0.5	0.3408	E BB	120-max
22	100	25	0.904	0.912	-0.008	6.3	0.5	0.3253	E BB	120-max

**Table C.7** Fourth repeatability data for 7.8 mm ID riser, submergence 20.1%

The test was repeated three times in different days. The recorded data and repeatability percentage are presented in table C.8.

Air Injection l/min	Produced water, l/min			% Variation First/Second	% Variation Second /Third	% Variation First/Third
	First	Second	Third			
0.22	0.0000	0.0000	0.0000	---	---	---
0.4	0.0000	0.0053	0.0076	---	-44.75	---
0.59	0.0129	0.0239	0.0285	-85.65	-19.22	-121.33
0.97	0.0561	0.0635	0.0746	-13.10	-17.42	-32.80
1.36	0.1407	0.1429	0.1319	-1.56	7.69	6.25
1.78	0.2029	0.2069	0.2099	-1.95	-1.49	-3.46
2.21	0.2669	0.2655	0.2658	0.53	-0.13	0.40
2.66	0.3067	0.3064	0.3090	0.09	-0.86	-0.76

**Table C.8** Percentage of repeatability to obtain sets of data for the 7.8 mm riser at 20.1% submergence

### C.2.2 16.67% Submergence

SUBMERGENCE 16.7% - FOURTH REPEATABILITY										
① Atmospheric Conditions		② Column of water static cond. in	③ Pressure Static Conditions psi	④ BHP Flowing Conditions psi	⑤ Differential Pressure ③-④ psi	⑥ Air Flow rate l/min	⑦ Liquid Mass Kg	⑧ Liquid Production Average l/min	Observed Pattern	Max reached Height E bubble (in)
T °C	P Kpa									
23	103	20	0.723	0.744	-0.021	0.2	0	0.0000	E BB	60
23	103	20	0.723	0.736	-0.013	0.6	0	0.0000	E BB	118
22	103	20	0.723	0.744	-0.021	1	0.05	0.0204	E BB	120-max
22	102.9	20	0.723	0.744	-0.021	1.4	0.05	0.0750	E BB	120-max
22	102.9	20	0.723	0.744	-0.021	1.8	0.1	0.1370	E BB	120-max
22	102.9	20	0.723	0.744	-0.021	2.2	0.2	0.1775	E BB	120-max
22	102.9	20	0.723	0.728	-0.005	2.7	0.2	0.2119	E BB	120-max
22	102.9	20	0.723	0.72	0.003	4.1	0.2	0.2439	E BB	120-max
22	102.9	20	0.723	0.768	-0.045	6.3	0.2	0.2238	E BB	120-max

**Table C.9** Fourth repeatability data for 7.8 mm ID riser, submergence 16.67%

The test was repeated three times to obtain repeatability data. The recorded data and repeatability percentage are presented in table C.10.

Air Injection l/min	Produced water, l/min			% Variation First/Second	% Variation Second /Third	% Variation First/Third
	First	Second	Third			
0.22	0.0000	0.0000	0.0011	---	---	---
0.59	0.0000	0.0115	0.0212	---	-84.51	---
0.97	0.0171	0.0271	0.0219	-58.75	19.17	-28.31
1.36	0.0612	0.0648	0.0762	-5.91	-17.64	-24.60
1.78	0.1294	0.1340	0.1415	-3.52	-5.58	-9.30
2.21	0.1762	0.1866	0.1857	-5.88	0.44	-5.41
2.66	0.2169	0.2135	0.2152	1.56	-0.77	0.79

**Table C.10** Repeatability for three sets of data for the 7.8 mm riser at 16.67% submergence

### C.2.3 12.5% Submergence

SUBMERGENCE 12.5% FOURTH REPEATABILITY										
① Atmospheric Conditions		② Column of water static cond.	③ Pressure Static Conditions	④ BHP Flowing Conditions	⑤ Differential Pressure ③-④	⑥ Air Flow rate	⑦ Liquid Mass	⑧ Liquid Production Average	Observed Pattern	Max reached Height E bubble (in)
T °C	P Kpa	in	psi	psi	psi	l/min	Kg	l/min		
20	101.9	15	0.542	0.56	-0.018	0.2	0	0.0000	E BB	53
20	101.9	15	0.542	0.56	-0.018	0.6	0	0.0000	E BB	99
20	101.9	15	0.542	0.544	-0.002	0.8	0.005	0.0028	E BB	120-max
20	102.4	15	0.542	0.552	-0.010	1	0.01	0.0020	E BB	120-max
20	102.4	15	0.542	0.544	-0.002	1.4	0.02	0.0135	E BB	120-max
20	102.4	15	0.542	0.56	-0.018	1.8	0.05	0.0636	E BB	120-max
20	102.4	15	0.542	0.56	-0.018	2.2	0.1	0.0955	E BB	120-max
20	102.4	15	0.542	0.56	-0.018	2.7	0.2	0.1231	E BB	120-max
20	102.4	15	0.542	0.56	-0.018	4.1	0.2	0.1452	E BB	120-max
20	102.4	15	0.542	0.584	-0.042	6.3	0.2	0.1313	E BB	120-max

**Table C.11** Fourth repeatability set of data for 7.8 mm ID riser, submergence 12.5%

The test was repeated three times to obtain repeatability data. The recorded data and repeatability percentage are presented in table C.12.

Air Injection l/min	Produced water, l/min			% Variation First/Second	% Variation Second /Third	% Variation First/Third
	First	Second	Third			
0.22	0.0000	0.0000	0.0000	---	---	---
0.59	0.0000	0.0000	0.0000	---	---	---
0.77	0.0000	0.0000	0.0043	---	-100.00	-100.00
0.97	0.0019	0.0034	0.0043	-33.88	-20.69	-54.57
1.36	0.0130	0.0141	0.0052	-20.59	172.74	152.15
1.78	0.0532	0.0524	0.0581	1.53	-9.96	-8.43
2.21	0.0993	0.1045	0.1017	-5.16	2.83	-2.33
2.66	0.1202	0.1294	0.1280	-7.20	1.14	-6.05

**Table C.12** Repeatability for three sets of data for the 7.8 mm riser at 12.5% submergence

### C.2.4 8.33 % Submergence

SUBMERGENCE 8.3% FOURTH REPEATABILITY										
① Atmospheric Conditions		② Column of water static cond.	③ Pressure Static Conditions	④ BHP Flowing Conditions	⑤ Differential Pressure ③-④	⑥ Air Flow rate	⑦ Liquid Mass	⑧ Liquid Production Average	Observed Pattern	Max reached Height E bubble (in)
T °C	P Kpa	in	psi	psi	psi	l/min	Kg	l/min		
21	102.2	10	0.362	0.368	-0.006	0.2	0	0.0000	E BB	58
21	102.2	10	0.362	0.36	0.002	0.6	0.005	0.0055	E BB	113
21	102.2	10	0.362	0.36	0.002	1	0.005	0.0031	E BB	120-max
21	102.2	10	0.362	0.376	-0.014	1.4	0	0.0000	E BB	120-max
21	102.1	10	0.362	0.384	-0.022	1.8	0.005	0.0044	E BB	120-max
21	102.1	10	0.362	0.368	-0.006	2.2	0.05	0.0298	E BB	120-max
21	102.1	10	0.362	0.384	-0.022	2.7	0.05	0.0441	E BB	120-max
21	102.1	10	0.362	0.392	-0.030	4.1	0.05	0.0549	E BB	120-max
21	102.1	10	0.362	0.416	-0.054	6.3	0.05	0.0433	E BB	120-max

**Table C.13** Second repeatability set of data for 7.8 mm ID riser, submergence 8.33%

The test was repeated three times to obtain repeatability data. The recorded data and repeatability percentage are presented in table C.14.

Air Injection l/min	Produced water, l/min			% Variation First/Second	% Variation Second /Third	% Variation First/Third
	First	Second	Third			
0.22	0.0000	0.0000	0.0000	---	---	---
0.59	0.0000	0.0000	0.0000	---	---	---
0.97	0.0036	0.0000	0.0000	100.00	---	100.00
1.36	0.0000	0.0000	0.0000	---	---	---
1.78	0.0023	0.0035	0.0044	-54.95	-20.16	-48.48
2.21	0.0262	0.0251	0.0285	4.34	-12.10	-8.11
2.66	0.0444	0.0428	0.0447	3.47	-4.29	-0.85

**Table C.14** Repeatability for three sets of data for the 7.8 mm riser at 8.33% submergence

### C.2.4 6.25% Submergence

SUBMERGENCE 6.25% FOURTH REPEATABILITY										
① Atmospheric Conditions		② Column of water static cond. in	③ Pressure Static Conditions psi	④ BHP Flowing Conditions psi	⑤ Differential Pressure ③-④ psi	⑥ Air Flow rate l/min	⑦ Liquid Mass Kg	⑧ Liquid Production Average l/min	Observed Pattern	Max reached Height E bubble (in)
T °C	P Kpa									
21	101.8	7.5	0.271	0.288	-0.017	0.2	0	0.0000	E BB	55
21	101.8	7.5	0.271	0.272	-0.001	0.6	0	0.0000	E BB	100
21	101.8	7.5	0.271	0.28	-0.009	1	0	0.0000	E BB	120
21	101.8	7.5	0.271	0.288	-0.017	1.4	0	0.0000	E BB	120-max
21	101.8	7.5	0.271	0.296	-0.025	1.8	0	0.0000	E BB	120-max
21	102	7.5	0.271	0.304	-0.033	2.2	0.001	0.0002	E BB	120-max
21	102	7.5	0.271	0.304	-0.033	2.7	0.01	0.0085	E BB	120-max
21	102	7.5	0.271	0.32	-0.049	4.1	0.02	0.0154	E BB	120-max
21	102	7.5	0.271	0.36	-0.089	6.3	0.01	0.0079	E BB	120-max

**Table C.15** Second repeatability set of data for 7.8 mm ID riser, submergence 4.16%

The test was repeated three times to obtain repeatability data. The recorded data and repeatability percentage are presented in table C.16.

Air Injection l/min	Produced water, l/min			% Variation	% Variation	% Variation
	First	Second	Third	First/Second	Second /Third	First/Third
0.22	0.0000	0.0000	0.0000	---	---	---
0.59	0.0000	0.0000	0.0000	---	---	---
0.97	0.0000	0.0000	0.0000	---	---	---
1.36	0.0000	0.0000	0.0000	---	---	---
1.78	0.0000	0.0000	0.0000	---	---	---
2.21	0.0004	0.0002	0.0002	60.10	-18.26	104.84
2.66	0.0071	0.0068	0.0074	3.95	-8.08	-4.30

**Table C.16** Liquid production at 6.25% submergence in a 7.8 mm riser - % Variation in three sets of data

### A.2.3 4.0 mm riser's experimental data

#### C.3.1 20.1% Submergence

SUBMERGENCE 20.1% SECOND REPEATABILITY												
① Atm. conditions		② Column of water static cond. in	③ Pressure, Static cond. psi	④ Pressure Transducer volts	⑤ Pressure Though Nozzle psi	⑥ BHP Dynamic Conditions psi	⑦ Differential Pressure ⑧-③ psi	⑧ Q air l/min	⑨ Liquid mass Kg	⑩ Water Density kg/m <sup>3</sup>	⑪ Time sec	⑫ Q liquid Average l/min
T °C	P Kpa											
22	101.64	25	0.904	1.140	0.248	0.664	-0.240	0.22	0.05	1000.43	115	0.0262
21	101.64	25	0.904	1.800	0.704	0.736	-0.168	0.59	0.05	1000.54	130	0.0233
21	101.61	25	0.904	3.010	1.680	0.728	-0.176	0.97	0.05	1000.54	46	0.0618
21	101.61	25	0.904	4.870	3.270	0.626	-0.278	1.36	0.05	1000.54	44	0.0707
21	101.61	25	0.904	8.290	5.960	0.672	-0.232	1.78	0.1	1000.54	99	0.0608
21	101.61	25	0.904	10.500	7.610	0.79	-0.114	2.2	0.1	1000.54	110	0.0547

**Table C.17** Second repeatability data for 4.0 mm ID riser, submergence 20.1%

The test was repeated three times in different days. The recorded data and repeatability percentage are presented in table C.18.

Air Injection l/min	Produced water, l/min			% Variation	% Variation	% Variation
	First	Second	Third	First/Second	Second /Third	First/Third
0.22	0.0000	0.0000	0.0000	---	---	---
0.4	0.0000	0.0053	0.0076	---	-44.75	---
0.59	0.0129	0.0239	0.0285	-85.65	-19.22	-121.33
0.97	0.0561	0.0635	0.0746	-13.10	-17.42	-32.80
1.36	0.1407	0.1429	0.1319	-1.56	7.69	6.25
1.78	0.2029	0.2069	0.2099	-1.95	-1.49	-3.46
2.21	0.2669	0.2655	0.2658	0.53	-0.13	0.40
2.66	0.3067	0.3064	0.3090	0.09	-0.86	-0.76

**Table C.18** Percentage of repeatability for three sets of data for the 4.0 mm riser at 20.1% submergence

### C.3.2 16.67% Submergence

SUBMERGENCE 16.67% THIRD REPEATABILITY												
① Atm. conditions		② Column of water static cond. in	③ Pressure, Static cond. psi	④ Pressure Transducer volts	⑤ Pressure Though Nozzle psi	⑥ BHP Dynamic Conditions psi	⑦ Differential Pressure ③-④ psi	⑧ Q air l/min	⑨ Liquid mass Kg	⑩ Water Density kg/m <sup>3</sup>	⑪ Time sec	⑫ Q liquid Average l/min
T °C	P Kpa											
19	100.98	20	0.723	1.010	0.248	0.56	0.163	0.22	0.05	1000.75	142	0.0212
19	100.98	20	0.723	1.620	0.704	0.592	0.131	0.59	0.05	1000.75	162	0.0177
18	100.91	20	0.723	2.780	1.680	0.544	0.179	0.97	0.1	1000.85	134	0.0445
18	100.91	20	0.723	4.630	3.270	0.434	0.289	1.36	0.1	1000.85	116	0.0517
18	100.91	20	0.723	8.000	5.960	0.44	0.283	1.78	0.1	1000.85	134	0.0454
18	100.86	20	0.723	10.900	7.610	1.11	-0.387	2.21	0.1	1000.85	147	0.0399

**Table C.19** Third repeatability data for 4.0 mm ID riser, submergence 16.67%

The test was repeated three times to obtain repeatability data. The recorded data and repeatability percentage are presented in table C.20.

Air Injection l/min	Produced water, l/min			% Variation	% Variation	% Variation
	First	Second	Third	First/Second	Second /Third	First/Third
0.22	0.0000	0.0000	0.0011	---	---	---
0.59	0.0000	0.0115	0.0212	---	-84.51	---
0.97	0.0171	0.0271	0.0219	-58.75	19.17	-28.31
1.36	0.0612	0.0648	0.0762	-5.91	-17.64	-24.60
1.78	0.1294	0.1340	0.1415	-3.52	-5.58	-9.30
2.21	0.1762	0.1866	0.1857	-5.88	0.44	-5.41
2.66	0.2169	0.2135	0.2152	1.56	-0.77	0.79

**Table C.20** Repeatability for three sets of data for the 4.0 mm riser at 16.67% submergence

### C.3.3 12.5% Submergence

SUBMERGENCE 12.5% - SECOND REPEATABILITY												
① Atm. conditions		② Column of water static cond.	③ Pressure, Static cond.	Pressure Transducer	Pressure Though Nozzle	④ BHP Dynamic Conditions	⑤ Differential Pressure ③-④	⑥ Q air	⑦ Liquid mass	⑧ Water Density	⑨ Time	⑩ Q liquid Average
T °C	P Kpa	in	psi	volts	psi	psi	psi	l/min	Kg	kg/m <sup>3</sup>	sec	l/min
16	101.97	15	0.542	0.710	0.248	0.32	0.222	0.22	0.02	1001.03	86	0.0137
16	101.91	15	0.542	1.330	0.704	0.36	0.182	0.59	0.01	1001.03	53	0.0110
16	101.91	15	0.542	2.590	1.680	0.392	0.150	0.97	0.05	1001.03	103	0.0287
17	101.91	15	0.542	4.070	3.270	-0.014	0.556	1.36	0.05	1000.94	85	0.0349
17	101.91	15	0.542	8.000	5.960	0.44	0.102	1.78	0.05	1000.94	98	0.0305
18	101.91	15	0.542	10.600	7.610	0.87	-0.328	2.21	0.05	1000.85	121	0.0214

**Table C.21** Second repeatability set of data for 4.0 mm ID riser, submergence 12.5%

The test was repeated three times to obtain repeatability data. The recorded data and repeatability percentage are presented in table C.22.

Air Injection l/min	Produced water, l/min			% Variation	% Variation	% Variation
	First	Second	Third	First/Second	Second /Third	First/Third
0.22	0.0000	0.0000	0.0000	---	---	---
0.59	0.0000	0.0000	0.0000	---	---	---
0.77	0.0000	0.0000	0.0043	---	-100.00	-100.00
0.97	0.0019	0.0034	0.0043	-33.88	-20.69	-54.57
1.36	0.0130	0.0141	0.0052	-20.59	172.74	152.15
1.78	0.0532	0.0524	0.0581	1.53	-9.96	-8.43
2.21	0.0993	0.1045	0.1017	-5.16	2.83	-2.33
2.66	0.1202	0.1294	0.1280	-7.20	1.14	-6.05

**Table C.22** Repeatability for three sets of data for the 4.0 mm riser at 12.5% submergence

### C.3.4 8.33 % Submergence

SUBMERGENCE 8.33% SECOND REPEATABILITY												
① Atm. conditions		② Column of water static cond.	③ Pressure, Static cond.	④ Pressure Transducer	⑤ Pressure Though Nozzle	⑥ BHP Dynamic Conditions	⑦ Differential Pressure ③-④	⑧ Q air	⑨ Liquid mass	⑩ Water Density	⑪ Time	⑫ Q liquid Average
T °C	P Kpa	in	psi	volts	psi	psi	psi	l/min	Kg	kg/m <sup>3</sup>	sec	l/min
18	101.58	10	0.362	0.510	0.248	0.16	0.202	0.22	0.01	1000.85	73	0.0082
18	101.58	10	0.362	0.970	0.704	0.072	0.290	0.59	0.01	1000.85	136	0.0045
18	101.58	10	0.362	2.330	1.680	0.184	0.178	0.97	0.02	1000.85	91	0.0134
17	101.72	10	0.362	4.340	3.270	0.202	0.160	1.36	0.02	1000.94	65	0.0183
17	101.72	10	0.362	7.690	5.960	0.192	0.170	1.78	0.02	1000.94	80	0.0152
17	101.72	10	0.362	10.070	7.610	0.446	-0.084	2.21	0	1000.94	100	0.0000

**Table C.23** Second repeatability set of data for 4.0 mm ID riser, submergence 8.33%

The test was repeated three times to obtain repeatability data. The recorded data and repeatability percentage are presented in table C.24.

Air Injection l/min	Produced water, l/min			% Variation First/Second	% Variation Second /Third	% Variation First/Third
	First	Second	Third			
0.22	0.0000	0.0000	0.0000	---	---	---
0.59	0.0000	0.0000	0.0000	---	---	---
0.97	0.0036	0.0000	0.0000	100.00	---	100.00
1.36	0.0000	0.0000	0.0000	---	---	---
1.78	0.0023	0.0035	0.0044	-54.95	-20.16	-48.48
2.21	0.0262	0.0251	0.0285	4.34	-12.10	-8.11
2.66	0.0444	0.0428	0.0447	3.47	-4.29	-0.85

**Table C.24** Repeatability for three sets of data for the 4.0 mm riser at 8.33% submergence

### C.3.4 4.16% Submergence

SUBMERGENCE 4.16% SECOND REPEATABILITY											
① Atm. conditions		② Pressure, Static cond.	③ Pressure Transducer	④ Pressure Though Nozzle	⑤ BHP Dynamic Conditions	⑥ Differential Pressure ②-③	⑦ Q air	⑧ Liquid mass	⑨ Water Density	⑩ Time	⑪ Q liquid Average
T °C	P Kpa	psi	volts	psi	psi	psi	l/min	Kg	kg/m <sup>3</sup>	sec	l/min
18	101.37	0.181	0.250	0.248	0.048	0.133	0.22	0.005	1000.85	125	0.0023
18	101.37	0.181	0.920	0.704	0.032	0.149	0.59	0	1000.85	100	0.0000
18	101.46	0.181	2.240	1.680	0.112	0.069	0.97	0	1000.85	100	0.0000
19	101.46	0.181	4.150	3.270	0.05	0.131	1.36	0.01	1000.75	254	0.0024
19	101.46	0.181	7.630	5.960	0.144	0.037	1.78	0	1000.75	100	0.0000
19	101.46	0.181	9.790	7.610	0.222	-0.041	2.21	0	1000.75	100	0.0000

**Table C.25** Second repeatability set of data for 4.0 mm ID riser, submergence 4.16%

The test was repeated three times to obtain repeatability data. The recorded data and repeatability percentage are presented in table C.26.

Air Injection l/min	Produced water, l/min			% Variation First/Second	% Variation Second /Third	% Variation First/Third
	First	Second	Third			
0.22	0.0024	0.0023	0.0026	1.50	-10.00	-8.35
0.59	0.0000	0.0000	0.0000	---	---	---
0.97	0.0000	0.0000	0.0000	---	---	---
1.36	0.0023	0.0024	0.0026	-3.01	-8.76	-12.04
1.78	0.0000	0.0000	0.0000	---	---	---
2.21		0.0000	0.0000	---	---	---

**Table C.26** Liquid production at 4.16% submergence in a 4.0 mm riser - % Variation in three sets of data

## APPENDIX D

### COMPARATIVE EXPERIMENTAL RESULTS FOR THE WATER-AIR AND WATER/METHANOL -AIR GAS LIFT SYSTEMS

#### D.1 12 mm riser's experimental data water –air system

Pipe Diameter [mm]	12
Ac [m <sup>2</sup> ]	0.0001131
T	18°C
% Submergence	20.1
Column of water [cm]	63.5
BHP static, [psi]	0.904

Q air [L/min]	BHP [psi]			Av. t <sub>T-D</sub> [s]	Av. U <sub>T-D</sub> [m/s]	Q liquid [L/min]	Um=U <sub>Ls</sub> +U <sub>gs</sub> [m/s]	U <sub>T-D∞</sub> [m/s]	U <sub>g-20.1%</sub> [m/s]
	Max	Min	Diff						
0.22	0.994	0.889	0.105			0.0000	0.0324	0.0206	0.0595
0.4	0.971	0.882	0.089			0.0000	0.0589	0.0206	0.0913
0.98	0.989	0.888	0.101			0.0000	0.1444	0.0206	0.1939
1.36	1.015	0.872	0.143			0.0000	0.2004	0.0206	0.2611
1.78	1.015	0.876	0.139			0.0000	0.2623	0.0206	0.3354
2.21	1.012	0.881	0.131			0.0000	0.3257	0.0206	0.4114
2.66	1.008	0.872	0.136	1.10	0.55	0.0758	0.4032	0.0206	0.5044
3.7	1	0.866	0.134	0.84	0.71	0.2468	0.5816	0.0206	0.7185
4.8	1.004	0.867	0.137	0.64	0.94	0.3869	0.7644	0.0206	0.9378
6.3	1.021	0.834	0.187	0.44	1.35	0.5554	1.0102	0.0206	1.2329
8	1.044	0.832	0.212			0.6575	1.2758	0.0206	1.5516
10	1.091	0.788	0.303			0.7248	1.5805	0.0206	1.9172
11	1.085	0.767	0.318			0.7422	1.7304	0.0206	2.0971

**Table D.1** Data for a 12 mm riser with 63.5 cm of water, submergence 20.1%.

Pipe Diameter [mm]	12
A [m <sup>2</sup> ]	0.0001131
Temperature	20°C
% Submergence	12.5
Column of water [cm]	38.1
BHP static, [psi]	0.542

Q air [L/min]	BHP [psi]			Av. $t_{T-D}$ [s]	Av. $U_{T-D}$ [m/s]	Q liquid [L/min]	Um= $U_{Ls}+U_{gs}$ [m/s]	$U_{T-D \infty}$ [m/s]	$U_g-12.5\%$ [m/s]
	Max	Min	Diff						
0.22	0.614	0.524	0.09			0	0.0324	0.0206	0.0595
0.59	0.604	0.516	0.088			0	0.0869	0.0206	0.1249
0.98	0.642	0.516	0.126			0	0.1444	0.0206	0.1939
1.36	0.662	0.499	0.163			0	0.2004	0.0206	0.2611
1.78	0.625	0.506	0.119			0	0.2623	0.0206	0.3354
2.21	0.637	0.52	0.117			0	0.3257	0.0206	0.4114
2.66	0.642	0.508	0.134			0	0.3920	0.0206	0.4910
3.7	0.654	0.511	0.143			0	0.5453	0.0206	0.6749
4.8	0.679	0.493	0.186	0.68	0.89	0.028	0.7114	0.0206	0.8743
6.3	0.682	0.474	0.208	0.48	1.25	0.114	0.9452	0.0206	1.1549
8	0.727	0.356	0.371	0.39	1.54	0.1797	1.2054	0.0206	1.4671
10	0.714	0.385	0.329			0.2247	1.5068	0.0206	1.8287
11	0.748	0.362	0.386			0.2356	1.6557	0.0206	2.0075

**Table D.2** Data for a 12 mm riser with 38.1 cm of water, submergence 12.5%.

### D.2 7.8 mm riser's experimental data water –air system

Pipe Diameter [mm]	7.8
A [m <sup>2</sup> ]	4.7784E-05
Temperature	20°C
% Submergence	20.1
Column of water [cm]	63.5
BHP static, [psi]	0.904

Q air [L/min]	BHP [psi]			Av. $U_{T-D}$ [m/s]	Q liquid [L/min]	Um= $U_{Ls}+U_{gs}$ [m/s]	$U_{T-D \infty}$ [m/s]	$U_g-20.1\%$ [m/s]
	Max	Min	Diff					
0.22	1.072	0.891	0.181		0.0000	0.077	0.013	0.105
0.4	1.059	0.879	0.18		0.0000	0.140	0.013	0.181
0.59	1.018	0.76	0.258		0.0201	0.213	0.013	0.269
0.98	1.01	0.794	0.216		0.0646	0.364	0.013	0.451
1.36	1.022	0.695	0.327	0.59	0.1472	0.526	0.013	0.644
1.78	1.006	0.735	0.271	0.89	0.2064	0.693	0.013	0.845
2.21	0.987	0.758	0.229	1.13	0.2643	0.863	0.013	1.049
2.66	0.966	0.81	0.156	1.26	0.3029	1.033	0.013	1.254
3.2	0.973	0.776	0.197	1.56	0.3224	1.229	0.013	1.488
4.3	0.991	0.689	0.302	2.09	0.3408	1.619	0.013	1.956
6.3	0.993	0.482	0.511		0.3253	2.311	0.013	2.786
8	1.039	0.402	0.637					
10			0					
11			0					

**Table D.3** Data for a 7.8 mm riser with 63.5 cm of water, submergence 20.1%.

Pipe Diameter [mm]	7.8
A [m <sup>2</sup> ]	4.7784E-05
Temperature	20°C
% Submergence	12.5
Column of water [cm]	38.1
BHP static, [psi]	0.542

Q air [L/min]	BHP [psi]			Av. U <sub>T-D</sub> 12.5% [m/s]	Q liquid [L/min]	Um=U <sub>LS</sub> +U <sub>qs</sub> [m/s]	U <sub>T-D∞</sub> [m/s]	U <sub>q</sub> -12.5% [m/s]
	Max	Min	Diff					
0.22	0.725	0.519	0.206		0	0.0767	0.0134	0.1055
0.59	0.694	0.501	0.193		0	0.2058	0.0134	0.2603
0.98	0.684	0.522	0.162		0.002	0.3425	0.0134	0.4244
1.36	0.657	0.529	0.128	0.57	0.0135	0.4791	0.0134	0.5883
1.78	0.675	0.498	0.177	0.75	0.0636	0.6430	0.0134	0.7850
2.21	0.644	0.421	0.223	1.03	0.0955	0.8041	0.0134	0.9784
2.66	0.682	0.466	0.216	1.33	0.1231	0.9707	0.0134	1.1783
3.2	0.629	0.47	0.159	1.66	0.13	1.1615	0.0134	1.4072
4.3	0.651	0.328	0.323	2.47	0.1452	1.5505	0.0134	1.8739
6.3	0.681	0.116	0.565		0.1313	2.2432	0.0134	2.7052

Table D.4 Data for a 7.8 mm riser with 38.1 cm of water, submergence 12.5%.

### D.3 12 mm riser's experimental data water/methanol 60:40 –air system

Pipe Diameter [mm]	12
A [m <sup>2</sup> ]	0.0001131
Temperature	20°C
% Submergence	20.1
Column of water [cm]	63.5
BHP static, [psi]	0.856
Density [g/cm <sup>3</sup> ]	0.947

Q air [L/min]	BHP [psi]			Av. U <sub>T-D</sub> 20.1% [m/s]	Q liquid [L/min]	Um=U <sub>LS</sub> +U <sub>qs</sub> [m/s]	U <sub>T-D∞</sub> [m/s]	U <sub>q</sub> -20.1% [m/s]
	Max	Min	Diff					
0.22	0.947	0.851	0.096		0.0000	0.0324	0.0206	0.0595
0.59	0.964	0.852	0.112		0.0000	0.0869	0.0206	0.1249
0.98	1.01	0.846	0.164		0.0000	0.1444	0.0206	0.1939
1.36	0.976	0.836	0.14		0.0000	0.2004	0.0206	0.2611
1.78	0.957	0.851	0.106		0.0000	0.2623	0.0206	0.3354
2.21	0.946	0.848	0.098		0.0000	0.3257	0.0206	0.4114
2.66	0.961	0.847	0.114	0.60	0.0365	0.3974	0.0206	0.4974
3.7	0.946	0.86	0.086	0.86	0.1625	0.5692	0.0206	0.7036
4.8	0.979	0.841	0.138	1.05	0.2565	0.7452	0.0206	0.9148
6.3	0.958	0.831	0.127	1.60	0.3817	0.9846	0.0206	1.2022
8	0.985	0.839	0.146		0.4636	1.2472	0.0206	1.5173
10	1.062	0.853	0.209		0.5137	1.5494	0.0206	1.8798
11	1.069	0.841	0.228		0.5245	1.6983	0.0206	2.0586

Table D.5 Data 12.0 mm riser with 63.5 cm of water/methanol, submergence 20.1%.

Pipe Diameter [mm]	12
A [m <sup>2</sup> ]	0.0001131
Temperature	20°C
% Submergence	12.5
Column of water [cm]	63.5
BHP static, [psi]	0.514
Density [g/cm <sup>3</sup> ]	0.947

Q air] [L/min]	BHP [psi]			Av. U <sub>T-D</sub> 12.5%	Q liquid [L/min]	Um=U <sub>Ls</sub> +U <sub>gs</sub> [m/s]	U <sub>T-D∞</sub> [m/s]	U <sub>g</sub> -12.5% [m/s]	U <sub>gs</sub> -12.5% [m/s]
	Max	Min	Diff	[m/s]					
0.22	0.611	0.5	0.111		0.0000	0.0324	0.0206	0.0595	0.032
0.59	0.698	0.494	0.204		0.0000	0.0869	0.0206	0.1249	0.087
0.98	0.56	0.497	0.063		0.0000	0.1444	0.0206	0.1939	0.144
1.36	0.638	0.495	0.143		0.0000	0.2004	0.0206	0.2611	0.200
1.78	0.6	0.492	0.108		0.0000	0.2623	0.0206	0.3354	0.262
2.21	0.584	0.492	0.092		0.0000	0.3257	0.0206	0.4114	0.326
2.66	0.593	0.492	0.101		0.0000	0.3920	0.0206	0.491	0.392
3.7	0.6	0.508	0.092		0.0000	0.5453	0.0206	0.6749	0.545
4.8	0.598	0.506	0.092	1.04	0.0000	0.7074	0.0206	0.8694	0.707
6.3	0.638	0.505	0.133	1.34	0.0000	0.9284	0.0206	1.1347	0.928
8	0.677	0.481	0.196	1.62	0.0270	1.1829	0.0206	1.4401	1.179
10	0.722	0.485	0.237		0.0740	1.4846	0.0206	1.8021	1.474
11	0.738	0.393	0.345		0.0814	1.6330	0.0206	1.9802	1.621

**Table D.6** Data 12 mm riser with 38.1 cm of water/methanol, submergence 12.5%.

#### D.4 7.8 mm riser's experimental data water/methanol 60:40 –air system

Pipe Diameter [mm]	7.8
A [m <sup>2</sup> ]	4.7784E-05
Temperature	20°C
% Submergence	20.1
Column of water [cm]	63.5
BHP static [psi]	0.856
Density [g/cm <sup>3</sup> ]	0.947

Q air [L/min]	BHP [psi]			Av. $U_{T-D}$ 20.1% [m/s]	Q liquid [L/min]	$U_m=U_{L_s}+U_{g_s}$ [m/s]	$U_{T-D\infty}$ [m/s]	$U_g-20.1\%$ [m/s]
	Max	Min	Diff					
0.22	1	0.846	0.154		0.000	0.0729	0.0137	0.1013
0.59	0.97	0.849	0.121		0.000	0.1956	0.0137	0.2485
0.98	0.972	0.839	0.133		0.0316	0.3354	0.0137	0.4162
1.36	0.973	0.835	0.138	0.68	0.1140	0.4887	0.0137	0.6002
1.78	0.925	0.824	0.101	0.92	0.1611	0.6436	0.0137	0.7861
2.21	0.924	0.815	0.109	1.25	0.1932	0.7968	0.0137	0.9699
2.66	0.923	0.799	0.124	1.62	0.2192	0.9547	0.0137	1.1593
3.2	0.934	0.743	0.191		0.2296	1.1371	0.0137	1.3783
4.3	0.947	0.71	0.237		0.2338	1.5033	0.0137	1.8177
6.3	0.986	0.506	0.48		0.1949	2.1535	0.0137	2.5980
8	0.991	0.652	0.339					
10								

**Table D.7** Data 7.8 mm riser with 63.5 cm of water/methanol, submergence 20.1%.

<b>Pipe Diameter [mm]</b>	<b>7.8</b>
<b>A [m<sup>2</sup>]</b>	<b>4.7784E-05</b>
<b>Temperature</b>	<b>20°C</b>
<b>% Submergence</b>	<b>12.5</b>
<b>Column of water [cm]</b>	<b>38.1</b>
<b>BHP static [psi]</b>	<b>0.514</b>
<b>Density [g/cm<sup>3</sup>]</b>	<b>0.947</b>

Q air [L/min]	BHP [psi]			Av. $U_{T-D}$ 12.5% [m/s]	Q liquid [L/min]	$U_m=U_{L_s}+U_{g_s}$ [m/s]	$U_{T-D\infty}$ [m/s]	$U_g-12.5\%$ [m/s]
	Max	Min	Diff					
0.22	0.67	0.505	0.165		0	0.077	0.013	0.105
0.59	0.671	0.503	0.168		0	0.206	0.013	0.260
0.98	0.656	0.502	0.154		0	0.342	0.013	0.424
1.36	0.626	0.484	0.142	0.66	0	0.474	0.013	0.583
1.78	0.623	0.492	0.131	0.88	0.0245	0.629	0.013	0.769
2.21	0.601	0.499	0.102	1.14	0.0412	0.785	0.013	0.956
2.66	0.608	0.472	0.136	1.63	0.0556	0.947	0.013	1.150
3.2	0.603	0.414	0.189		0.0602	1.137	0.013	1.378
4.3	0.612	0.285	0.327		0.0626	1.522	0.013	1.839
6.3	0.658	0.344	0.314		0.0292	2.208	0.013	2.662

**Table D.8** Data 7.8 mm riser with 38.1 cm of water/methanol, submergence 12.5%.



Among the assessed parameters are the superficial liquid and gas velocities, void fractions, flow pattern, and pressure losses along the pipe. This spreadsheet used a macro function programmed in Visual Basic to perform iterative calculations.

## E.2 Ansari's Model [51]

SLUG PATTERN MODEL				MACRO: CTRL + A			
				Note: Change only the red numbers.			
<b>According to Ansari Model.</b>							
<b>Well Conditions:</b>							
		<b>INPUT</b>	<b>Units</b>			<b>INPUT</b>	<b>Units</b>
<b>Depth</b>	3.04	m		<b>Tubing diam</b>	0.157480315	in	0.00400
<b>BHP</b>	15.601	Psi	107.5	<b>Area</b>	0.019	in <sup>2</sup>	0.000125664
<b>BH Temp</b>	68	grad F	20.0	<b>Gradient of T</b>	0.01	gradF/ft	0.01867
<b>WHP</b>	14.7	psi	101.3				
<b>WH Temp</b>	68	grad F	20.0				
		CFD	10.17136136				
<b>Fluid Flow rates @ standard conditions:</b>			m <sup>3</sup> /d	L/min	m <sup>3</sup> /hr	<b>Gas Type</b>	
<b>Q Water</b>	1.0114624	BPD	0.268	3.18	0.012	1-5	Methane
<b>Q Gas</b>	0.112385395	Mcf/d	3.18	2.21	0.1328	3	Nitrogen
<b>Q water(l/min)</b>	0.20800	<b>Q air (L/min)</b>	2.21				Air
<b>GWR</b>	11.05						Vap H <sub>2</sub> O
							CO <sub>2</sub>
<b>Submergence</b>							
<b>Fluid Level</b>	0.633	m	Note: Fluid level is measured from the bottom to top				
<b>Gas injection point</b>	3.04	m					
<b>Surface Level</b>	0	m					
<b>Submergence</b>	0.21	NOT POSSIBLE GAS LIFTING				MACRO	
						Note: Run it with CTRL + A	
						DATA:	
						LENGTH INT: 40 cm	
						0.40	
<b>PROPERTIES</b>							
DEN L	999.90	Kg/m <sup>3</sup>					
DEN G	1.66	Kg/m <sup>3</sup>					
PIPE DIAM	0.004	m					
VISC KIN G	5.55E-06	m <sup>2</sup> /s					
VISC KIN L	1.16566E-06	m <sup>2</sup> /s					
INTER TENS	72.4	dyne/cm					
	0.07	N/m					
VISC DYN G	0.009208252	cP					
VISC DYN L	1.164371594	cP					

Table E.2 Input data Ansari's model.

Ansari's model implemented a system of eight equations to calculate all the parameters in a slug flow, Table E.3. This model includes the liquid falling back film for void fraction calculations. Similar to Hasan's model, this model was enhanced using a macro programmed in Visual Basic to develop iterative calculations at every interval depth. The input data, Table E.2, corresponds to the bold numbers; the output table is located at the bottom of the spreadsheet in a results table, table E.4.

	Depth increm m	Pressure Kpa	Temperature grad C	U <sub>sg</sub> m/s	U <sub>sl</sub> m/s	Um m/s
	0.404474719	138.7	20.04	2.17142	0.2652572	2.437
<b>Development of the Ansari's et al. Model</b>						
He recommend to use a step by step procedure. SPE V17, pg50						
<b>1. First Step:</b>						
Velocity of Taylor-Dumitrescu Bubble.			$U_{TB} =$	2.993		m/s
Gas Hold up in the slug zone:			$H_{gLS} =$	0.316		
Liquid Hold up in the slug zone:			$H_{lLS} =$	0.684		
Velocity of gas in slug zone:			$U_{gLS} =$	3.129		m/s
<b>2. Second Step:</b>						
Here it is necessary to apply solver in order to find the value $H_{LTB}$ , Hold up in T-D bubble.						
Assume a Value for TD liquid Holdup=			$H_{LTB}$ assumed=	0.122		
According to Vo and Shoham the original problem with eight unknowns for this slug pattern could be combined algebraically to give:						
					0.000	
					2.568	2.394
<b>SOLVER:</b> By changing HLTD (E69), making F73 = 0.000						
<b>3. Third Step:</b>						
Find the value for $U_{LTB}$ , Liquid velocity in the TD bubble.						
			$U_{LTB} =$	0.493		m/s
<b>4. Fourth Step:</b>						
Liquid Velocity in Liquid Slug Zone:			$U_{LLS} =$	2.372		m/s
<b>5. Fifth Step:</b>						
			$U_{gls} =$	3.129		m/s
<b>6. Sixth Step:</b>						
Velocity of gas in TD bubble zone:			$U_{gTB} =$	3.042		m/s
<b>7. Seventh Step:</b>						
Find the value for $\beta$ .						
			$\beta =$	0.703		
From equation 4.186.						
$\beta =$	$L_{TB}/L_{SU}$		If we assume a = LLS=30d, then:			
$L_{TB} =$	Length of the Taylor Bubble, m	$L_{TB} =$	0.28			m
$L_{SU} =$	Length of Slug body, m	$L_{SU} =$	0.40			m
$LLS =$	Length of the Liquid slug, m	$L_{LS} =$	0.120			m

**Table E.3** Model calculations for a specific flowing condition. Punctual results.

Column depth m	Depth increment m	Pressure Kpa	Temperature grad C	U <sub>sg</sub> m/s	U <sub>sl</sub> m/s	$\frac{\rho}{\text{Length ratio}}$	$\rho_{L,S}$	Static Press drop Above IP Kpa	Kin. Visc. SL m <sup>2</sup> /s	$N_{Re,LS}$	f	Fric. Press Kpa	Total P Loss Kpa	Annular U <sub>ga</sub>	Bubble U <sub>ba</sub>	$m_{SL}$
2.831323035	0.404474719	136.7	20.04	2.2	0.2652672	0.703	684.26	0.610	0.000001698	8337.595	0.030	4.55643526	5.367	S	S	0.711136057
Column depth m	Depth increment m	Pressure Kpa	Temperature grad C	U <sub>sg</sub> m/s	U <sub>sl</sub> m/s	$\frac{\rho}{\text{Length ratio}}$	$\rho_{L,S}$	Static Press drop Above IP Kpa	Kin. Visc. SL m <sup>2</sup> /s	$N_{Re,LS}$	f	Fric. Press Kpa	Total P Loss Kpa	Annular U <sub>ga</sub>	Bubble U <sub>ba</sub>	$m_{SL}$
0.404	0.404	101.3	20.0	2.97265	0.26526	0.74401	699.6	0.7	0.0000016950	1072.5	0.029	6.417955539	7.1	S	S	0.7405
0.809	0.404	108.4	20.0	2.77763	0.26526	0.73595	672.5	0.7	0.0000016940	1046.1	0.029	5.948322238	6.7	S	S	0.7348
1.213	0.404	115.1	20.0	2.61712	0.26526	0.72854	675.1	0.7	0.0000016931	9990.1	0.029	5.566002210	6.3	S	S	0.7294
1.618	0.404	121.4	20.0	2.48127	0.26526	0.72165	677.6	0.8	0.0000016923	9396.0	0.030	5.251460814	6.0	S	S	0.7245
2.022	0.404	127.4	20.0	2.36426	0.26526	0.71519	679.9	0.8	0.0000016915	8696.3	0.030	4.985311576	5.8	S	S	0.7198
2.427	0.404	133.1	20.0	2.26198	0.26526	0.70910	682.2	0.8	0.0000016908	8646.9	0.030	4.756262636	5.5	S	S	0.7154
2.831	0.404	136.7	20.0	2.17142	0.26526	0.70332	684.3	0.8	0.0000016901	8337.6	0.030	4.558435264	5.4	S	S	0.7111

Table E.4 Ansari's model Table of Results.

### E.3 Reinemann's Model [42]

Theory of Small-Diameter Airlift Pumps, D.J. Reinemann, J.Y. Parlange and M.B. Timmons. Int. J. Multiphase Flow Vol. 16. No. 1. Pp, 113-122, 1990.												
Air lift performance on small diameter tubes, 3-25 mm. The model was based on the drift flux model and a simple approximation to the slug flow. The accuracy of the model was very well established and in most of the cases the theoretical and experimental values of efficiency was pretty close. The maximum efficiencies appeared at higher submergences, more than 60%, and diameters less than 6mm.												
INPUT DATA:				Q <sub>g</sub> (l/min)	Useful data							
Dimensionless Gas flow (Q <sub>g</sub> ):	0.74			0.59	Sup. Tension:	0.074 N/m						
Efficiency: (n)	0.04			0.01	Kin. Visc. Liquid:	1.04235E-06 m <sup>2</sup> /s						
					Density of Liquid:	997.85 kg/m <sup>3</sup>						
					Area=	0.00004778 m <sup>2</sup>						
Q <sub>l</sub> m <sup>3</sup> /s	Q <sub>g</sub> m <sup>3</sup> /s	Diam. mm	Dynamic m <sup>2</sup> /s	Re	f	Inv. Eotvos Σ	VTS	Q <sub>l</sub>	ε	α	Efficiency n	
1.67E-07	9.83333E-06	7.8	1.04235E-06	1566.03841	0.0502327	0.132780941	0.111707205	0.013034699	0.729298408	0.2745975	0.0462853	
0.01	0.59											
L/min	L/min											
Expected Bottom Hole Pressure, P <sub>0</sub> :												
Total Length m	ZL m	P <sub>0</sub> Kpa	psi	liquid level exp. 25								
3.048	2.211026678	109.5436798	15.896298	15.74404167								
Diam. mm	Q <sub>l</sub> m <sup>3</sup> /s	Q <sub>g</sub> m <sup>3</sup> /s	P <sub>0</sub> Kpa	psi	Submerg.	Efficiency	U <sub>m</sub> m/s					
7.8	1.66867E-07	9.83333E-06	109.5436798	15.90	0.27	0.046285346	0.209276717					

Table E.5 Reinemann's model spread sheet

This spreadsheet calculates superficial velocities, pressure losses, submergence, efficiency and BHP for a short air lift system, depth smaller than 10 m. Its accuracy depends of the submergence value. It is recommended to be run only with liquid levels over 60% submergence. This model is applicable for elongated bubble flow in small diameter pipes flowing in a low pressure system. The gas expansion was not considered.

## E.4 Critical Production Condition Model (CPC Model)

This model predicted the critical production depth for given conditions of submergence, liquid and gas flowrates. This model considered a long T-D bubble transporting the liquid to the top of the riser in a single liquid slug unit. The void fraction at the top of the riser was assumed to be equal 1.0. Table E.6 showed the CPC model, input data.

1. Properties		IFT dyne/cm	LIQ Density kg/m <sup>3</sup>	Gas Density kg/m <sup>3</sup>	Liq. Visc cP				
Water	100%	72.4	999	1.254978762	1				
Water/Methanol	60/40 %	38	947	1.254978762	1.71				
2. Input flow rates									
Qgas L/min	Qliq L/min	Drift Flux Coefficient Co							
11	0.7422	1.2							
3. Qg correction by gas expansion - average gas density for pressure losses calculatons									
Gas Density Kg/m3	Flow rate m3/s	Pressure Pa	Temperature K						
1.2	0.000183333	101300	293.15						
Gas Density Kg/m3	Flow rate m3/s	Pressure Pa	Temperature K	Qg (U/min)					
Entrance	1.273	0.000	107523.121	293.245	10.367				
Exit	1.237	0.000	101300.000	293.150	11.000				
Average	1.255				10.683				
4. Pipe Diameter & Flow									
Liquid l/min	Gas l/min	ID mm	A m <sup>2</sup>	U(GS) m/s	U(LS) m/s	Um m/s	Re (-)	f (-)	
Entrance	0.7422	10.3667	12	1.1E-04	1.528	0.109	1.637	19625.2	0.025
Exit	0.7422	11.0000	12	1.1E-04	1.621	0.11	1.730	20744.0	0.025
5. Void Fraction and Pressure Losses									
ALPHA (-)	AVG DENS kg/m <sup>3</sup>	Dp/L Pa/m	DP/L m <sub>LIQ</sub> /m	U <sub>T-D</sub> m/s	U <sub>G</sub> m/s				
Entrance	0.785	214.22	606	0.062	0.1201	2.085			
Exit	<b>0.788</b>	213.00	664.30	0.06778	0.1201	2.197			
Average	0.7866								
6. Elements of Pressure Balance at Production Limit (CPC Model)									
Voids (Average) Limit (No Prod) Average Void 0.8287	Res. Press								
	H m	h m	Water Level In	L=h+H m					
	2.225	0.635	75	2.86					
DIFF VOID FRAC 0.042	***								

Table E.6 CPC model spreadsheet

The difference in void fraction presented in section 6, Table E.6, corresponded to the difference between the theoretical value of void fraction calculated from the pressure losses equation and the average void fraction calculated from the drift flux equation.

The idea in this model was to change the riser's depth, the blue number in the section 6, until making this difference equal to zero. This process was done used a Solver function in the excel spreadsheet. The critical depth also can be calculated from equation 5.17.

### E.5 Small Diameter Pipe Model (SDP Model)

The objective of this model was to determine the liquid production rate or the maximum risers length for specific liquid and gas flow conditions. The SDP model included the negative effect of the liquid falling back. The instabilities were not considered in this model.

The SDP model came from a modification of the CPC model therefore the input data from sections 1 to 6 in table E.6 were used. Note that in section 5, Table E.7, the exit void fraction, ALPHA, is less than 1.0, because for the SDP model was designed to consider only flowing conditions with liquid production.

5. Void Fraction and Pressure Losses						
	ALPHA (-)	AVG DENS kg/m <sup>3</sup>	Dp/L Pa/m	DP/L m <sub>Liq</sub> /m	U <sub>T-D</sub> m/s	U <sub>G</sub> m/s
Entrance	0.735	263.29	222	0.023	0.0968	0.820
Exit	<b>0.740</b>	260.85	243.36	0.02483	0.0968	0.863
Average	0.7374					

**Table E.7** SPD Model – Void Fraction.

The sections 7 to 9, table E.8, are used to calculate the film falling back thickness and velocity using the capillary number, the volumes for the liquid slug, T-D bubble and liquid fall back, and the void fraction in points #1 and #2.

SDP MODEL									
7. Calculations - Film (flowback) for the SDP model									
	Ca	From Ca No	Re <sub>F</sub>	Assumed	Calculated	Static	Total Dp/dl	Res Press	
	(-)	δ (mm)	(-)	U <sub>F</sub>	U <sub>F</sub>	Dp/dl	Pa/m	Pa/m	Pa/m
				m/s	m/s	Pa/m			
Entrance	0.0113245	0.263	187.2	0.712	0.712	1878.819	2101	6223.12065	
Exit	0.0119167	0.272	197.0	0.725	0.725				
8. VOID FRACTION RELATIVE TO AN INITIAL VOID FRACTION									
Volumes									
α 1	LT	Submergence	VL1	VG1	time (t)	VG2			
Alpha 1	m	s	m <sup>3</sup>	m <sup>3</sup>	s	m <sup>3</sup>			
0.739819927	3.05	0.208196721	3.43246E-05	9.76016E-05	4.778362426	0.0002394			
0									
Volumes									
VFB	VL2	α 2	From (6)		SDP model	VOID FRACTION			
m <sup>3</sup>	m <sup>3</sup>	Void fraction	Predicted		DIFF				
2.11266E-07	3.41133E-05	0.875258982	Average α						
			0.6093		0.2680				
9. Determination of Average void fraction									
L Total	3.05	m	Number sections	40					
Li	α	Suma alpha	Average alpha						
[m]			void fraction						
			0.827235						
1	0.076	0.816	0.062						
2	0.153	0.818	0.062						
3	0.229	0.820	0.063						
4	0.305	0.822	0.063						
5	0.381	0.824	0.063						
6	0.458	0.826	0.063						
7	0.534	0.828	0.063						
8	0.610	0.830	0.063						
9	0.686	0.831	0.063						
10	0.763	0.833	0.064						
11	0.839	0.835	0.064						
12	0.915	0.837	0.064						
13	0.991	0.838	0.064						
14	1.068	0.840	0.064						
15	1.144	0.842	0.064						
16	1.220	0.843	0.064						
17	1.296	0.845	0.064						
18	1.373	0.846	0.065						
19	1.449	0.848	0.065						
20	1.525	0.849	0.065						
21	1.601	0.851	0.065						
22	1.678	0.852	0.065						
23	1.754	0.854	0.065						
24	1.830	0.855	0.065						
25	1.906	0.857	0.065						
26	1.983	0.858	0.065						
27	2.059	0.859	0.066						
28	2.135	0.860	0.066						
29	2.211	0.862	0.066						
30	2.288	0.863	0.066						
31	2.364	0.864	0.066						
32	2.440	0.865	0.066						
33	2.516	0.867	0.066						
34	2.593	0.868	0.066						
35	2.669	0.869	0.066						
36	2.745	0.870	0.066						
37	2.821	0.871	0.066						
38	2.898	0.872	0.067						
39	2.974	0.873	0.067						
40	3.050	0.874							

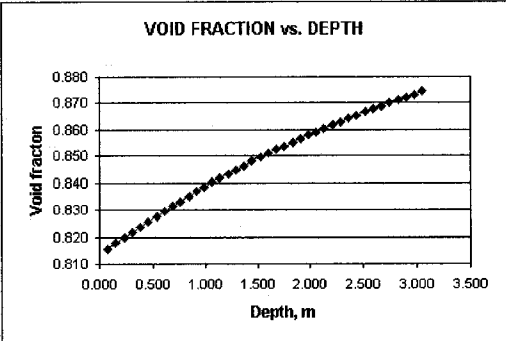


Table E.8 SDP model spreadsheet

The section 9 (Determination of average void fraction) in table E.8 was used to determine the maximum risers length reached for specific liquid and gas flow rates. The Length  $L_T$  is varied until the SDP model differential void fraction is equal to zero. The differential void fraction is calculated as the difference between the average void fraction calculated from section 9 and the predicted average void fraction from section 6.

Even the model was corrected using an average gas density to calculate the frictional and static pressure losses at the entrance and exit, the model is not suitable for long risers until a correct step by step gas density correction will be done.